AD-A135009

REPORT DOCUMENTATION PAGE		READ INSTRUCTIONS BEFORE COMPLETING FORM
1. REPORT NUMBER Technical Report 1	2. GOVT ACCESSION NO. AD·A135009	3. RECIPIENT'S CATALOG NUMBER
4. TITLE (and Subtitle) BROADBAND DISCRIMINATION STUDIES		5. TYPE OF REPORT & PERIOD COVERED Semi-Annual Technical 01 Oct 1977 - 31 Mar 1978
		6. PERFORMING ORG. REPORT NUMBER
7. AUTHOR(s) T. V. McEvilly L. R. Johnson		8. CONTRACT OR GRANT NUMBER(s) AFOSR-78-3481
9. PERFORMING ORGANIZATION NAME AND ADDRESS Seismographic Station University of California Berkeley, California 94720		10. PROGRAM ELEMENT, PROJECT, TASK AREA & WORK UNIT NUMBERS A03291-11 62701E 3291
11. CONTROLLING OFFICE NAME AND ADDRESS DARPA 1400 Wilson Boulevard Arlington, Virginia 22209		12. REPORT DATE 24 July 1978
		13. NUMBER OF PAGES 166
14. MONITORING AGENCY NAME & ADDRESS(if different from Controlling Office) AFOSR Bolling Air Force Base Washington, D.C. 20332		15. SECURITY CLASS. (of this report) Unclassified
		15a. DECLASSIFICATION/DOWNGRADING SCHEDULE

16. DISTRIBUTION STATEMENT (of this Report)

Approved for public release; distribution unlimited.

17. DISTRIBUTION STATEMENT (of the abstract entered in Block 20, if different from Report)

18. SUPPLEMENTARY NOTES

DTIC
ELECTE
NOV 28 1983
S   E

19. KEY WORDS (Continue on reverse side if necessary and identify by block number)

seismology
wave propagation
anelasticity
attenuation

20. ABSTRACT (Continue on reverse side if necessary and identify by block number)

A formulation is presented which incorporates linear anelastic attenuation into plane layer models in an exact manner. Several examples of body wave propagation in absorbing media are presented. The formulation is extended to both Love and Rayleigh wave propagation. Eigenvalue and surface displacement calculations for a high loss soil structure indicate that Rayleigh waves are more strongly affected by attenuation than are Love waves.

DD FORM 1 JAN 73 1473   EDITION OF 1 NOV 65 IS OBSOLETE

83 11 28 083

Wave Propagation in Anelastic Media
with Applications to Seismology

By

Walter Joseph Silva, Jr.

A.B. (University of California) 1971
M.A. (University of California) 1975

DISSERTATION

Submitted in partial satisfaction of the requirements for the degree of

DOCTOR OF PHILOSOPHY

in

Geophysics

in the

GRADUATE DIVISION

of the

UNIVERSITY OF CALIFORNIA, BERKELEY

Approved:

..... *Lane Johnson* ....

..... *J.V. McEvilly* ....

....

Committee in Charge

....

WAVE PROPAGATION IN ANELASTIC
MEDIA WITH APPLICATIONS TO SEISMOLOGY

by

Walter Silva

Department of Geology and Geophysics

University of California, Berkeley, California, U.S.A.

ABSTRACT

A formulation is presented which incorporates
linear anelastic attenuation into plane layer models
in an exact manner. Several examples of body wave
propagation in absorbing media are presented. Surface
time histories are compared between predicted acceler-
ation records using the plane-layered model and data
recorded by a vertical array. Spectral ratios between
the surface and bedrock, computed for the horizontal
components, show fair agreement with the model pre-
dictions. In particular, the importance of attenuation
in predicting ground motion in soils is demonstrated.
It is further shown that converted waves are of minor
importance while lateral propagation can be significant.

The formulation is extended to both Love and
Rayleigh wave propagation. Eigenvalue and surface
displacement calculations for a high loss soil structure
indicate that Rayleigh waves are more strongly affected

WAVE PROPAGATION IN ANELASTIC
MEDIA WITH APPLICATIONS TO SEISMOLOGY

by

Walter Silva

Department of Geology and Geophysics

University of California, Berkeley, California, U.S.A.

ABSTRACT

A formulation is presented which incorporates linear anelastic attenuation into plane layer models in an exact manner. Several examples of body wave propagation in absorbing media are presented. Surface time histories are compared between predicted acceleration records using the plane-layered model and data recorded by a vertical array. Spectral ratios between the surface and bedrock, computed for the horizontal components, show fair agreement with the model predictions. In particular, the importance of attenuation in predicting ground motion in soils is demonstrated. It is further shown that converted waves are of minor importance while lateral propagation can be significant.

The formulation is extended to both Love and Rayleigh wave propagation. Eigenvalue and surface displacement calculations for a high loss soil structure indicate that Rayleigh waves are more strongly affected

by attenuation than are Love waves. Inverse calculations for upper mantle and crustal structures, with both synthetic and real data, reveal a significant dependence of surface wave attenuation upon the velocity structure. Use of this information can greatly aid in velocity inversions and demonstrates the incompatibility of conventionally extracted attenuation data with respect to phase data. Further indications are that, for the overdetermined case, the same layering (number and thickness) may not be optimum for both the velocity and attenuation inversion parameters. In addition, the same layering is probably not optimum for both Love and Rayleigh wave inversions.

TABLE OF CONTENTS

TABLE OF CONTENTS (continued)

INTRODUCTION

Recently there has been a greater appreciation of
the effects of anelastic attenuation in the earth. The
recent upsurge in interest is primarily due to a recog-
nition that the velocity dispersion accompanying atten-
uation can be significant (Liu and Archambeau, 1976).
In view of this much effort has been directed towards
dispersion corrections to free oscillation data which
is then inverted to obtain corrected earth models
(Hart et al., 1977). The results have been very
encouraging in that body wave and free oscillation earth
models have largely been reconciled. In light of this
realization it now appears that attenuation will receive
much more consideration. It is the effort of this
thesis that this consideration be in terms of exact,
rather than approximate, theory.

In Chapter 1 the Haskell-Thompson propagation
matrix technique is extended to include anelastic
attenuation in an exact manner. In order to demon-
strate the effect of attenuation (as compared to purely
elastic propagation) on body waves, several examples
are presented. In particular, transfer functions are
calculated for typical soil and crustal structures.
In addition, an example is shown demonstrating the
effect of an attenuating boundary layer above the
core-mantle boundary on reflected pulses.

As a means of estimating the suitability of the plane-layer model in predicting ground motion comparisons are made between the predicted surface motion and data recorded at a vertical array. The array is located in a soil section and demonstrates the effect of low velocity surficial material on wave motion.

In Chapter 2 the formulation is applied to both Love and Rayleigh wave propagation. In this section a soil and an upper mantle model are considered which demonstrate the effects of attenuation on surface wave propagation. In addition, an inversion scheme is presented by which depth dependent velocity and attenuation may be estimated simultaneously from surface wave phase and amplitude data. The inversion scheme is demonstrated using synthetic data and is then applied to real data suitable for upper mantle structures.

CHAPTER 1

BODY WAVES

I. FORMULATION

In both the body wave and surface wave analysis
the matrizant technique (see Haskell, 1953, for first
seismological application) is employed as the compu-
tational algorithm. In this approach the medium
properties are assumed piecewise constant. The equations
of motion are integrated analytically and the solutions
propagated by matching boundary conditions at the layer
interfaces. The main disadvantage of this method over
direct numerical integration of the equations of motion
(Gilbert and Backus, 1966) is, of course, that it is
possible only for plane geometry. To overcome this
shortcoming, various earth stretching transformations
have been developed (Schwab and Knopoff, 1972) which are
used in this treatise where appropriate. The following
paper extends the matrizant method to include anelastic
attenuation in an exact manner and forms the basis for
this thesis.

BODY WAVES IN A LAYERED ANELASTIC SOLID

By W. Silva

ABSTRACT

A formulation extending the Haskell-Thompson matrix method to include the effects of anelastic attenuation is presented. The formulation is exact in that no low-loss approximations are made. Consideration is given to nonparallel propagation and attenuation directions with corresponding velocity anisotropy. Examples are presented for models representing soils, the crust, and the core-mantle boundary.

INTRODUCTION

With the increase in the number of stations and the higher degree of standardiza [...] recent years, more use is being made of seismic amplitude data. This has contribute [...] increased regionalization of structure down to the core-mantle boundary. In ord [...] accurately represent this fine structure in applying corrections or to resolve it in inverting data, more use is being made of the higher frequencies where the attenuation effects are most significant. It is therefore becoming increasingly important to consider nongeometrical attenuation exactly. Past approximations in dealing with loss (Knopoff, 1964) must be replaced with exact formulations (Lockett, 1962; Cooper, 1967; Borcherdt, 1971; Buchen, 1971).

In order to consider the effects of a vertical variation in attenuation as well as velocity and density on body waves, an extension of the Haskell-Thompson (Haskell, 1953) matrix formulation using an exact theory is presented. In particular, the restricted problem of anelastic layers on an elastic half-space is considered, but the formulation can easily be extended to include an attenuating half-space. Previous consideration of the problem (Kanai, 1950) dealt with normally incident homogeneous waves with viscoelasticity of the Voigt type. The present treatment considers incident P or SV waves at arbitrary angles and a general constitutive relation.

FORMULATION

The most general form of a linear constitutive relation is Boltzman's superposition principle (Gurtin and Sternberg, 1962) which, written in terms of the tensorial relaxation function $r(t)$ is

$$P_{ij}(t) = \int^t \, r_{ijkl}(t-\tau)\, d\varepsilon_{kl}(\tau)$$
$$= r_{ijkl}(t) * d\varepsilon_{kl}(t) \tag{1}$$

where $P_{ij}(t)$ and $\varepsilon_{ij}(t)$ are the time-dependent stress and strain tensors and the symbol $*$ denotes the Stieltjes convolution.

Assuming the medium to be isotropic and homogeneous, equation (1) may be broken up into bulk and shear components and written as

$$P_{ij}(t) = 2\mu(t) * d\varepsilon_{ij}(t) \qquad\qquad i \ne j$$

$$P_{kk}(t) = 3\kappa(t) * d\varepsilon_{kk}(t) \tag{2}$$

where $\mu(t)$ and $\kappa(t)$ are the relaxation functions in shear and bulk. Assuming that the

particle displacements u_i are infinitesimal, the strain can be written

$$\varepsilon_{ij} = \tfrac{1}{2}[u_{i,j} + u_{j,i}]$$

and, neglecting body forces, the linear momentum equation is

$$P_{ij,j}(t) = \rho \ddot{u}_i \tag{3}$$

where ρ is the medium density. Substituting equation (2) into equation (3) yields the equation of motion.

$$[\kappa(t) + \tfrac{4}{3}\mu(t)] * [\nabla(\nabla \cdot d\mathbf{u})] - [\mu(t) * [\nabla \times (\nabla \times d\mathbf{u})] = \rho \ddot{\mathbf{u}}. \tag{4}$$

Since the convolutions make the time-domain representation quite intractable, it is customary to take the Fourier transform of equation (4). Restated in terms of transformed variables, equation (4) becomes

$$[\bar{\kappa} + \tfrac{4}{3}\bar{\mu}]\nabla(\nabla \cdot \bar{\mathbf{u}}) - [\bar{\mu}]\nabla \times (\nabla \times \bar{\mathbf{u}}) = -\rho \omega^2 \bar{\mathbf{u}} \tag{5}$$

where

$$\bar{\kappa} = i\omega\int_{-\infty}^{\infty} \kappa(t)e^{-i\omega t}\,dt, \qquad \bar{\mu} = i\omega\int_{-\infty}^{\infty} \mu(t)e^{-i\omega t}\,dt$$
$$\bar{\mathbf{u}} = \int_{-\infty}^{\infty} \mathbf{u}e^{i\omega t}\,dt.$$

At this point it is convenient to introduce the transformed P and S displacement potentials in terms of Helmholtz's relation

$$\bar{\mathbf{u}} = \nabla\bar{\phi} + \nabla \times \bar{\psi}, \qquad \nabla \cdot \bar{\psi} \equiv 0. \tag{6}$$

Substituting equation (6) into equation (5) results in the familiar Helmholtz equations for the P and S potentials $\bar{\phi}$ and $\bar{\psi}$.

$$[\nabla^2 + K_P{}^2]\bar{\phi} = 0, \qquad [\nabla^2 + K_S{}^2]\bar{\psi} = 0 \tag{7}$$

where

$$K_P{}^2 = \frac{\omega^2}{\bar{\alpha}^2} = \omega^2 \frac{\rho}{\bar{\kappa}(\omega) + \tfrac{4}{3}\bar{\mu}(\omega)}$$
$$K_S{}^2 = \frac{\omega^2}{\bar{\beta}^2} = \omega^2 \frac{\rho}{\bar{\mu}(\omega)}. \tag{8}$$

Note that the terms $\bar{\alpha}^2$ and $\bar{\beta}^2$ are in general frequency-dependent in both real and imaginary parts.

MEDIUM PARAMETERIZATION

Let us now consider, for demonstration purposes, the case of S waves. A general solution for $\bar{\psi}$ in equation (7) is

$$\bar{\psi} = \bar{\psi}(\omega)\exp(-i\mathbf{K}_S \cdot \mathbf{X}) \tag{9}$$

where $\mathbf{K}_S$ is a complex vector with the real and imaginary parts having different directions in general.

$$\mathbf{K}_S = \mathbf{P}_S - i\mathbf{A}_S \tag{10}$$

$$K_S{}^2 = \mathbf{K}_S \cdot \mathbf{K}_S = |\mathbf{P}_S|^2 - |\mathbf{A}_S|^2 - i2\mathbf{P}_S \cdot \mathbf{A}_S \tag{11}$$

$$\mathbf{P}_S \cdot \mathbf{A}_S = |\mathbf{P}_S|\,|\mathbf{A}_S|\cos(\gamma_s). \tag{12}$$

$\mathbf{P}_S$ is the propagation vector such that $\omega/|\mathbf{P}_S|$ is the phase velocity and $\mathbf{A}_S$ the attenuation vector such that $\exp(-\mathbf{A}_S \cdot \mathbf{X})$ represents the spatial decay of the potential. The nonzero γ_s gives rise to the inhomogeneous waves (Borcherdt 1971, Buchen 1971, Cooper 1967, Lockett 1962) whose amplitude varies (monotonically) along a wave front. It becomes necessary now to specify the three parameters $|\mathbf{P}_S|$, $|\mathbf{A}_S|$, and γ_s in terms of material properties and medium geometry.

Writing the transformed shear modulus $\mu(\omega)$ in equation (8) in terms of a real part, $\mu_R(\omega)$, and an imaginary part, $\mu_I(\omega)$, the quality factor Q_s for shear waves is defined as

$$Q_s^{-1} = \frac{\mu_I(\omega)}{\mu_R(\omega)} = \frac{1}{2\pi}\frac{\Delta E}{E} \tag{13}$$

where E is the peak energy density stored and ΔE is the energy lost, both per cycle (Borcherdt, 1971, 1973). K_S^2 may be written in the following form

$$K_S^2 = \frac{\omega^2}{v_s^2}\frac{2}{1+\sqrt{1+Q_s^{-2}}}\left(1 - \frac{i}{Q_s}\right) \tag{14}$$

where v_s is the homogeneous wave velocity of the medium. Using (14) to invert (11) and (12) we arrive at convenient expressions for $|\mathbf{P}_S|$ and $|\mathbf{A}_S|$

$$|\mathbf{P}_S|^2 = \frac{\omega^2}{v_s^2}\frac{1}{1+\sqrt{1+Q_s^{-2}}}(1 + \sqrt{1+Q_s^{-2}\cos^{-2}(\gamma_s)}) \tag{15}$$

$$|\mathbf{A}_S|^2 = \frac{\omega^2}{v_s^2}\frac{1}{1+\sqrt{1+Q_s^{-2}}}(-1 + \sqrt{1+Q_s^{-2}\cos^{-2}(\gamma_s)}) \tag{16}$$

with similar expressions for P waves using the P parameters. In the low-loss approximation for homogeneous waves ($\gamma_s = 0$, $Q_s \gg 1$) equation (16) reduces to the well-known expression

$$|\mathbf{A}| = \frac{\omega}{2v_s Q_s}$$

When dealing with highly dissipative materials the vectorial nature of $\mathbf{A}$ must be considered. The problem is that for a given incident wave (direction of both $\mathbf{P}$ and $\mathbf{A}$ specified) onto a plane boundary between two viscoelastic media, the direction of both P and A must be determined for the P and SV reflected and transmitted waves. These directions can be uniquely determined by applying the usual boundary conditions at a welded interface (or free surface for half-space problems). This results in an extended form of Snell's law in that A_x as well as P_x must be continuous (Borcherdt 1973, Lockett 1962). In the restricted case considered in this paper where the incident medium is elastic, A_x is zero everywhere. This enables elastic layers to be interbedded with absorbing media.

Extension of the Haskell-Thompson Formulation for Layered Media

The following development follows closely that of Haskell (1953, 1962). However, displacement potentials are used here. Referring to Figure 1 for coordinate reference, we can write the solutions to equation (7) in the usual form

$$\phi = [A_p \exp(iK_{P_z}Z) + B_p \exp(-iK_{P_z}Z)]\exp(-iK_{P_x}X)$$

$$\psi = \psi_y = [A_s \exp(iK_{S_z}Z) + B_s \exp(-iK_{S_z}Z)]\exp(-iK_{S_x}X) \tag{17}$$

where A, B are complex and in general frequency-dependent amplitudes. From equation (10)

$$K_z = P_z - iA_z; \quad K_x = P_x - iA_x.$$

In the simple case we are considering (incident elastic wave) we have $A_x \equiv 0$, and from the boundary conditions A_x must be zero everywhere. Thus K_x remains a real quantity. If the incident medium were anelastic, the incident attenuation direction would have to be specified along with the propagation direction, and then A_z in each layer would adjust itself to be consistent with a continuous A_x and a specified $K_{P,S}^2$ for that layer (see equation 14). Choosing A_P and A_S as upgoing potentials (negative z direction) we can write for each layer

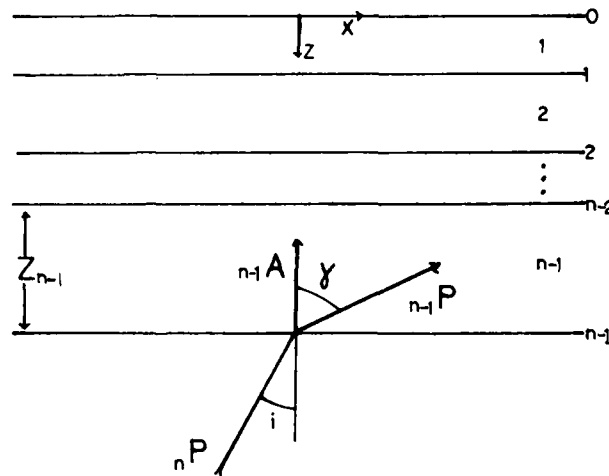$$K_z = \text{principal value } (K^2 - K_x^2)^{1/2}. \tag{18}$$

FIG. 1. The problem is uniquely specified given V_p, V_s, Q_P, Q_S, ρ, and Z for each layer and given $_nA_{P,S}$ (incident P- or S-wave potential amplitude) in the elastic half-space. For an anelastic half-space, the direction of the incident-wave attenuation vector must also be specified.

Using equations (2), (3), (6), (17), the displacements and stresses for layer m can be put in the following matrix form

$$
\begin{bmatrix} u \\ w \\ P_{zx} \\ P_{zz} \end{bmatrix}_m =
\begin{bmatrix}
-iK_{Px}C_P & K_{Sz}S_S & K_{Px}S_P & -iK_{Sz}C_S \\
-K_{Pz}S_P & -iK_{Sx}C_S & iK_{Pz}C_P & K_{Sx}S_S \\
i2\bar{\mu}K_{Px}K_{Pz}S_P & -\bar{\mu}\Omega C_S & 2\bar{\mu}K_{Pz}K_{Px}C_P & -i\bar{\mu}\Omega S_S \\
\bar{\mu}\Omega C_P & i2\bar{\mu}K_{Sz}K_{Px}S_S & i\bar{\mu}\Omega S_P & 2\bar{\mu}K_{Sz}K_{Sx}C_S
\end{bmatrix}_m \times
$$

$$
\begin{bmatrix}
A_P + B_P \\
A_S + B_S \\
A_P - B_P \\
A_S - B_S
\end{bmatrix}_m
$$

where

$$C_P = \cos(K_{Pz}Z_m) \qquad C_S = \cos(K_{Sz}Z_m)$$

$$S_P = \sin(K_{Pz}Z_m) \qquad S_S = \sin(K_{Sz}Z_m).$$

$$\Omega = K_{Px}^2 - K_{Sz}^2.$$

This result (which is equivalent to equation (3 20) of Grant and West, 1965) can be conveniently written as

$$X_m = D_m(Z_m)C_m. \tag{19}$$

Thus we see that Z_m (layer thickness) is the phase factor which propagates the potentials across the mth layer and that D_m may be thought of as a form of propagator matrix with C_m the coefficient matrix. With this in mind and with the idea of eliminating C_m we can write (Haskell, 1953)

$$X_{m-1} = D_m(0)C_m; \qquad C_m = D_m^{-1}(0)X_{m-1}. \tag{20}$$

Then applying the usual boundary conditions

$$X_m = (D_m(Z_m)D_m^{-1}(0))(D_{m-1}(Z_{m-1})D_{m-1}^{-1}(0))X_{m-2}$$

$$= a_m a_{m-1} \dots a_1 X_0. \tag{21}$$

and for $n-1$ layers where layer n is an elastic half-space and interface 0 is a free surface

$$C_n = D_n^{-1}(0)a_{n-1}a_{n-2}\dots a_1 X_0$$

$$= J X_0 \tag{22}$$

with the following matrix elements.

$$(-_m K_S^2)D_m(0)^{-1} = \begin{vmatrix} -2iK_{Px} & 0 & 0 & 1/\bar{\mu} \\ 0 & -i2K_{Px} & -1/\bar{\mu} & 0 \\ 0 & -i\Omega/K_{Pz} & -K_{Px}/(\bar{\mu}K_{Pz}) & 0 \\ i\Omega/K_{Sz} & 0 & 0 & -K_{Px}/(\bar{\mu}K_{Sz}) \end{vmatrix}_m \tag{23}$$

$$X_0 = \begin{vmatrix} u_0 \\ w_0 \\ 0 \\ 0 \end{vmatrix} \qquad C_n = \begin{vmatrix} A_P + B_P \\ A_S + B_S \\ A_P - B_P \\ A_S - B_S \end{vmatrix} \tag{24}$$

The elements of

$$(-_m K_S^2)a_m$$

are given by

$$a_{11} = \Omega C_S - 2K_{Px}^2 C_P$$

$$a_{12} = -iK_{Px}[2K_{Sz}S_S + (\Omega/K_{Pz})S_p]$$

$$a_{13} = -\bar{\mu}^{-1}[K_{Sz}S_S + (K_{Px}^2/K_{Pz})S_p]$$

$$a_{14} = -iK_{Px}\bar{\mu}^{-1}[C_P - C_S]$$

$$a_{21} = iK_{Px}[2K_{Pz}S_P + (\Omega/K_{Sz})S_S]$$

$$a_{22} = \Omega C_P - 2K_{Px}^2 C_S$$

$$a_{23} = a_{14}$$

$$a_{24} = -\bar{\mu}^{-1}[K_{Pz}S_P + (K_{Px}^2/K_{Sz})S_S]$$

$$a_{31} = \bar{\mu}[4K_{Px}^2 K_{Pz}S_P + (\Omega^2/K_{Sz})S_S]$$

$$a_{32} = -i2\bar{\mu}K_{Px}\Omega[C_P - C_S]$$

$$a_{33} = a_{11}$$

$$a_{34} = a_{21}$$

$$a_{41} = a_{32}$$

$$a_{42} = \bar{\mu}[4K_{P_x}^2 K_{S_z} S_S + (\Omega^2 / K_{P_z}) S_P]$$

$$a_{43} = a_{12}$$

$$a_{44} = a_{22}.$$

C_n therefore becomes the input matrix and choosing $A_{P,S}$ in the upgoing $(-z)$ direction and considering incident P, we can invert equation (22) to give the surface displacements u_0 and w_0 in terms of the incident potential $(_nA_p)$, K_x, and the layering.

$$u_0 = -2[J_{22} + J_{42}]_n A_p/R$$

$$w_0 = 2[J_{21} + J_{41}]_n A_p/R$$

$$R = [J_{21} + J_{41}][J_{12} + J_{32}] - [J_{22} + J_{42}][J_{11} + J_{31}]. \tag{26}$$

APPLICATIONS

In order to illustrate the effects of attenuation, three models which represent soils, the crust, and the core-mantle boundary are considered. The structures are listed in Table 1. With the exception of the low-velocity layer of the upper mantle, these appear to be the three regions where nongeometrical attenuation is most pronounced and therefore may have some effect on observational interpretation. Also, knowledge of the Q structure of these regions will be valuable in interpreting materials and structure mechanisms when an acceptable theory is found relating state variables, material properties, and energy absorption.

In applying this formulation in calculating reflection and transmission coefficients, transfer ratios, synthetic seismograms, etc., some estimation must be made of the medium parameters. This usually means a frequency-independent loss and velocity which can be shown to violate causality (Futterman, 1962). However, since the frequency-dependence can be made weak over a finite frequency band, assuming a frequency-independent loss and phase velocity over the space-time dimensions considered here should not be critical.

(a) *Soils.* The effects of attenuation can be rather drastic in a highly dissipative material such as loosely compacted soils. The structure chosen (Table 1) is for the Richmond Field Station of the University of California, Berkeley and consists of mud deposited in San Francisco Bay. Borehole measurements of velocity and sample measurements of both velocity and density were available for this site. The Q structure represents a best guess for illustrative purposes (structure data from T. V. McEvilly, oral comm.). Figure 2 shows the vertical and horizontal displacement spectra for normally incident P and S waves, respectively. All input potentials were normalized to unity total displacement for incident $P(_nA_P = _nk_P^{-1})$ or $SV(_nA_S = _nk_S^{-1})$. The solid line is for an elastic stack while the broken line includes the effect of loss. The vertical motion is somewhat unstructured because the compressional wavelengths are greater than any of the layer thicknesses. The loss behaves as we might expect for purely homogeneous waves, mirroring the elastic behavior at a lower amplitude and becoming asymptotic to it toward low frequencies. Considering the shear spectra (Figure 2B) we begin to note some interesting effects. First, the elastic spectrum shows the characteristic peaks (shear wavelengths < layer thickness) which are

TABLE 1

PHYSICAL PARAMETERS FOR REPRESENTATIVE MODELS
CONSIDERED IN NUMERICAL CALCULATIONS

V_p(km/sec)	V_s(km/sec)	ρ(g/cc)	Q_p	Q_s	z(km)
Soil (Richmond)					
0.421	0.214	1.95	5	1	1.52×10^{-3}
0.641	0.299	1.95	10	2	1.53
1.007	0.299	1.95	10	3	1.52
1.296	0.305	2.00	20	4	1.43
1.464	0.305	2.00	20	5	2.14
1.525	0.317	2.05	20	5	1.83
0.488	0.305	1.97	20	5	2.13
1.739	0.427	2.08	50	10	3.05
1.647	0.397	2.00	50	10	3.75
1.739	0.427	2.05	50	10	1.52
1.678	0.323	1.92	20	5	3.05
1.952	0.372	1.97	50	10	2.44
1.793	0.329	1.92	20	5	4.27
2.034	0.488	2.19	100	20	3.66
1.983	0.900	2.30	∞	∞	∞
Crust (Berkeley)					
4.2	2.4	2.1	67	30	1.4×10^{0}
6.1	3.5	2.6	100	45	8.2
7.3	4.2	3.0	180	80	12.9
7.8	4.5	3.3	∞	∞	∞
Core-mantle Boundary					
13.63	7.30	5.60	∞	∞	∞
13.33	6.99	5.58	300	115	150
8.08	0	9.90	2500		∞

resonances associated with the total S-wave travel time (Bakun, 1971, Haskell, 1960). The total S-wave travel time of the stack is $T = 0.098$ sec and maxima and minima are expected at

$$f_{max} = \frac{n}{4T}, n = 1, 3, 5, \ldots; \qquad f_{min} = \frac{m}{2T}, m = 1, 2, 3, \ldots$$

$$= 2.6, 7.9, 12.7 \ldots \qquad\qquad = 5.1, 10.2, 20.3 \ldots$$

The peaks and troughs are not exact because the total stack travel-time effect is modulated by the layering. In the loss spectra we see that there is little information content at frequencies greater than about 14 Hz. The effect of attenuation is more drastic for shear waves due to the lower Q_s and the longer travel times. Also, it is important to note the slight shifting of the peaks in the case of loss. The velocities are the same in the elastic and attenuating layers and the shifting is due to the change in modulation as the loss affects the acoustic impedance.

In Figure 3 are shown the crustal transfer function ratio (w_0/u_0), the vertical spectra, and the horizontal spectra for an incident compressional wave at $i = 10$ for the same soil structure. It is interesting to note the considerable change in the ratio for the loss. Any inversion scheme not accounting for the loss would yield a different structure. Again the shear spectrum is the controlling mechanism but in this case the large discrepancy between

W. SILVA

the elastic and loss is largely due to the velocity anisotropy induced by the inhomogeneous waves (see equation 15).

(b) *The crust.* The crustal model (Table 1), excepting the Q structure, was taken from Bakun's best-fitting Berkeley crustal model (Bakun, 1970). The Q structure represents a
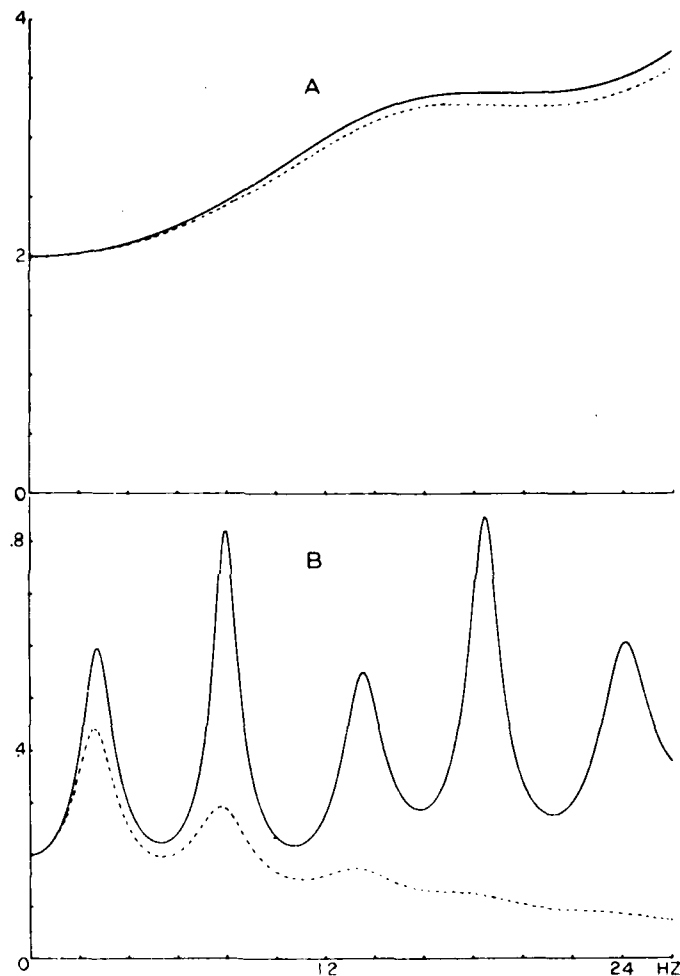

FIG. 2. Spectra of normalized surface displacements for a high-loss soil structure (Table 1). Solid lines are elastic layers, broken lines include loss. (A) Vertical displacement for incident P wave, (B) Horizontal displacement for incident S wave; both at normal incidence.

best guess for Q_S by the author based on some near-Berkeley crustal studies (Kurita, 1975, O'Neill and Healy, 1973) and the relation

$$Q_p = \tfrac{3}{4}Q_S(V_p/V_s)^2. \tag{27}$$

The transfer ratio for the crustal model for an incident compressional wave at $i = 25°$ is shown in Figure 4 along with the vertical and horizontal spectra. The transfer ratio for the elastic and loss agree well out to about 3 Hz which is high enough to resolve the structure.

The spectra of the vertical and horizontal surface displacements for the Berkeley crust have been synthesized and are shown in Figure 5, where (A) and (B) are the vertical elastic
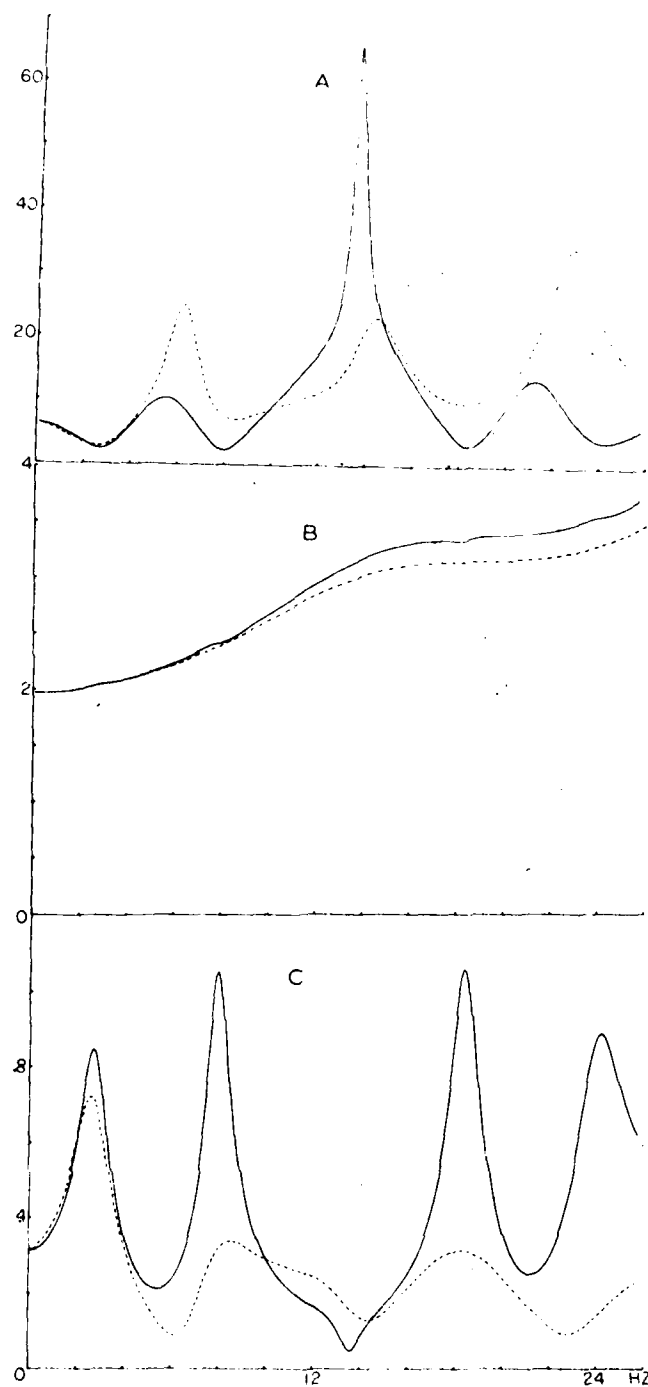
FIG. 3. Spectrum of normalized (A) crustal transfer function (w_0 u_0) (B) vertical surface displacement. (C) horizontal surface displacement for incident P wave at 10° for the Richmond structure (Table 1). Solid lines are elastic layers, broken lines include loss.
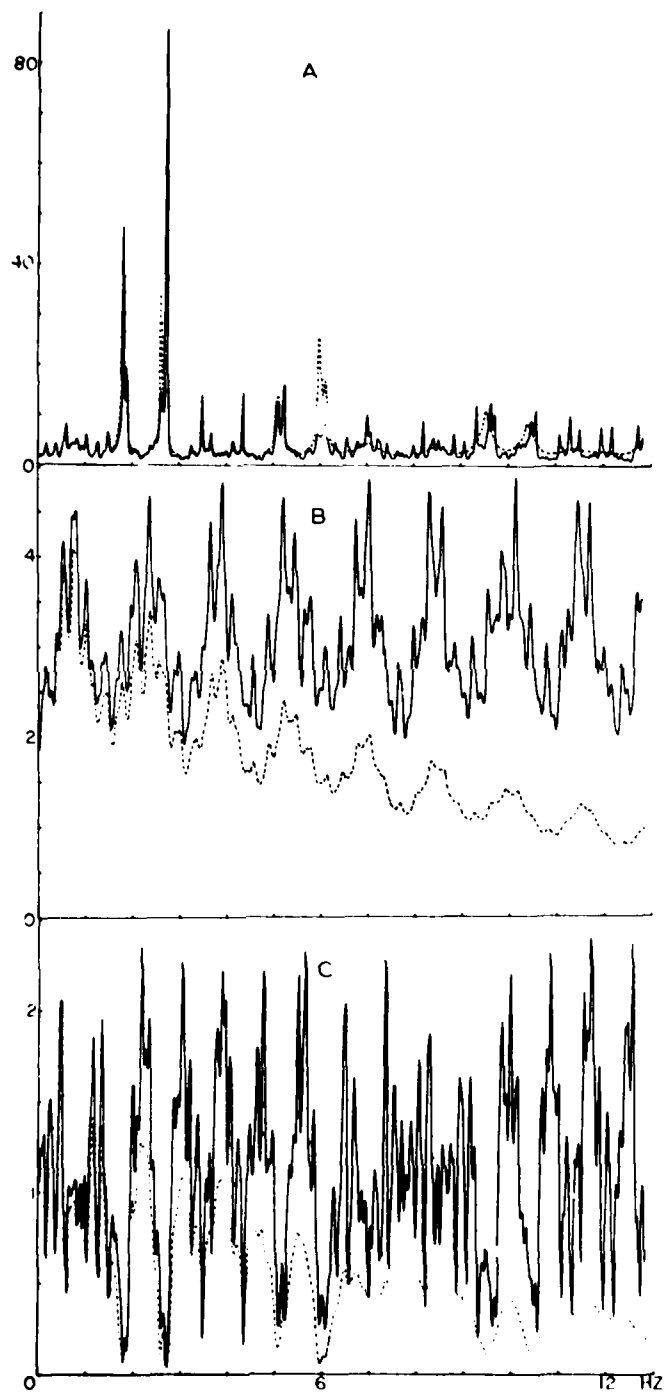
1548   W SILVA

FIG. 4. Spectra of normalized (A) crustal transfer function (w_0/u_0), (B) vertical surface displacement, (C) horizontal surface displacement for incident P wave at 25 for the Berkeley crust (Table 1). Solid lines are elastic layers, broken lines include loss.

and loss while (C) and (D) represent the horizontal. The effect of the loss shows a general smoothing of the record, a decrease of the higher-order reflections, and a reduction in amplitude (vertical peak to peak by 0.7, horizontal by 0.8).

(c) *Core-mantle boundary.* To demonstrate the effects of loss near the core-mantle boundary on PcP and PcS, the reflection spectrum for the core-mantle boundary structure of Table 1 was synthesized. The velocities are from Bolt (1972) and the boundary layer density was derived assuming the region to be a thermal boundary layer and to consist entirely of mantle material (Glyn Jones, personal comm.). The Q_P is from Kuster (1972) while Q_S is derived from equation (27) (zero loss in bulk). An incident P wave is considered with $i = 25$ and the synthesis is performed for a point 70 km from the boundary layer. Figures 6 and 7 show the synthesized potential coefficients ($_nB_p$ $_pA_p$, $_nB_{S'}$ $_nA_p$) for the same explosion source as the crustal seismograms. The first small pulse in Figures 6 and 7 represents reflected P and SV waves, respectively, from the abrupt transition between the lower mantle and the boundary layer. A more realistic gradient would largely eliminate this reflection. The figures then represent PcP and PcS sources to be convolved with suitable transfer functions and show the effect of attenuation on the reflected amplitudes (PcP zero-to-peak reduction 0.8, PcS 0.6). The effect on the wave forms seems to be small at this angle of incidence for such low Q values and indicates that a considerable amount of attenuation is possible in the boundary layer and still be unobservable.

APPENDIX

To consider a fluid layer ($\bar{\mu} = 0$) the matrix $D_m(Z_m)$ (equation 19) must be modified due to the overspecified boundary conditions at a solid-fluid interface. Using a development similar to Teng (1967) $D_m(Z_m)$ for a fluid layer becomes

$$
\begin{bmatrix}
0 & 0 & 0 & 1 \\
-k_{P_z}S_P & 0 & ik_{P_z}C_P & 0 \\
0 & 1 & 0 & 0 \\
-\rho\omega^2 C_P & 0 & -i\rho\omega^2 S_P & 0
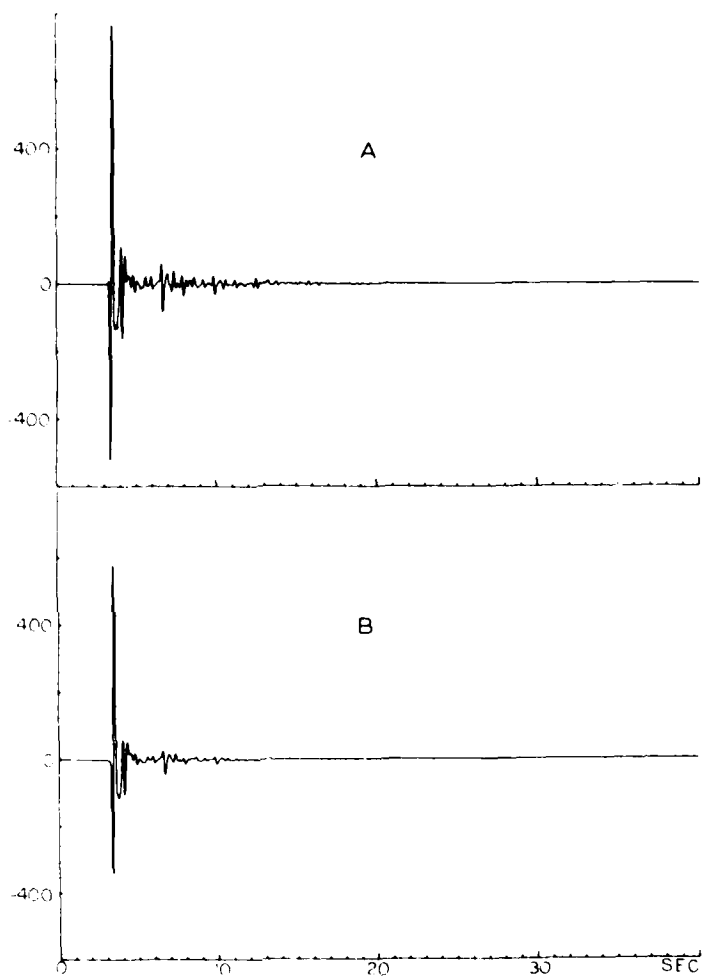\end{bmatrix}_m
$$

W. SILVA

FIG. 5, A AND B.

FIG. 5. Synthetic seismograms for the Berkeley crust. (A) and (B) are vertical motion (positive down) for the elastic and loss cases, respectively, which were synthesized from the spectra in Figure 4B. (C) and (D) are horizontal motion for the elastic and loss cases, respectively, which were synthesized from the spectra in Figure 4C. All were convolved with an explosion source function appropriate for BOXCAR (Helmberger and Harkrider, 1972), a Benioff short-period instrument, and a low-pass filter with a corner frequency at 5 Hz.
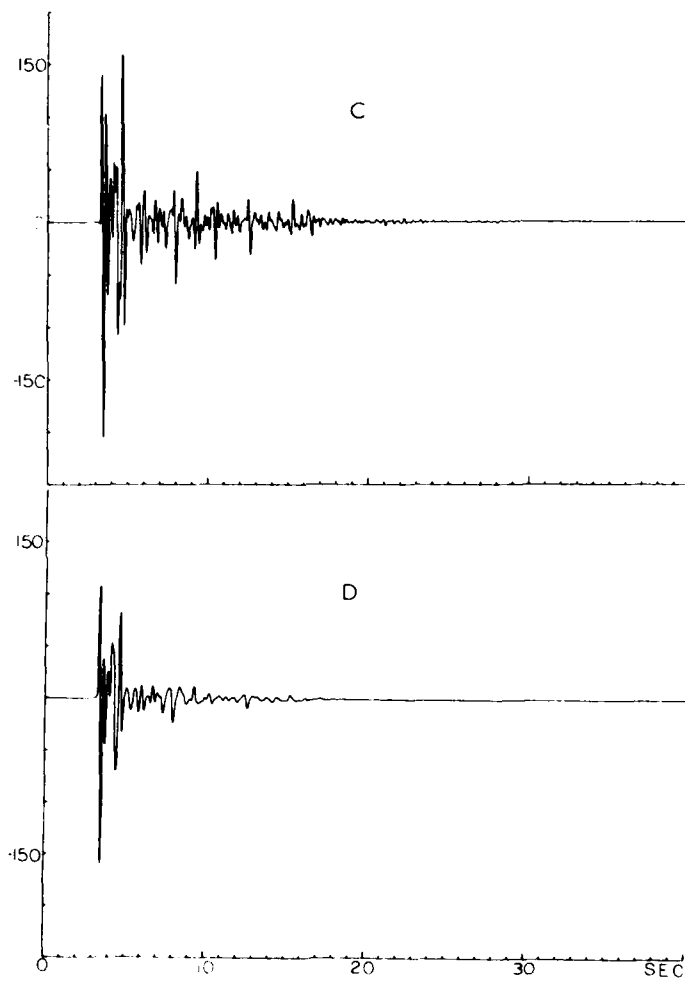
Fig. 5, C and D.

FIG. 6. Synthesized reflected P potential coefficient for incident P wave on core-mantle boundary structure of Table 1. The frequency interval was 0.01 Hz with 512 sample points. All spectra were filtered with a low-pass causal filter with corner frequency at 2.0 Hz. (A) elastic, (B) loss.
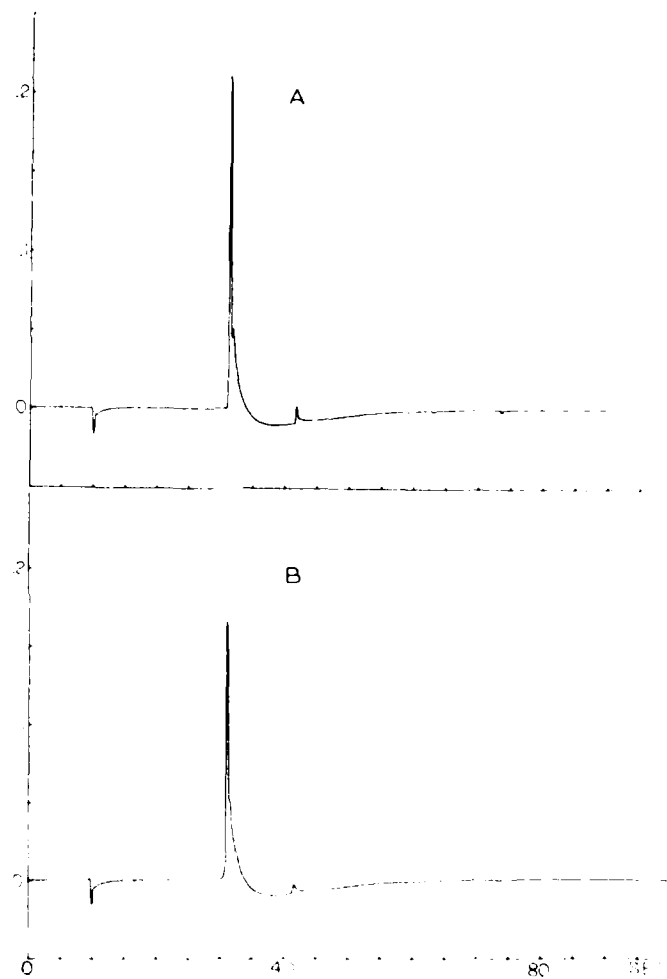
FIG. 7. Synthesized reflected S potential coefficient for incident P wave on core-mantle boundary structure of Table 1. The frequency interval was 0.01 Hz with 512 sample points. All spectra were filtered with a low-pass causal filter with corner frequency at 2.0 Hz. (A) elastic, (B) loss.
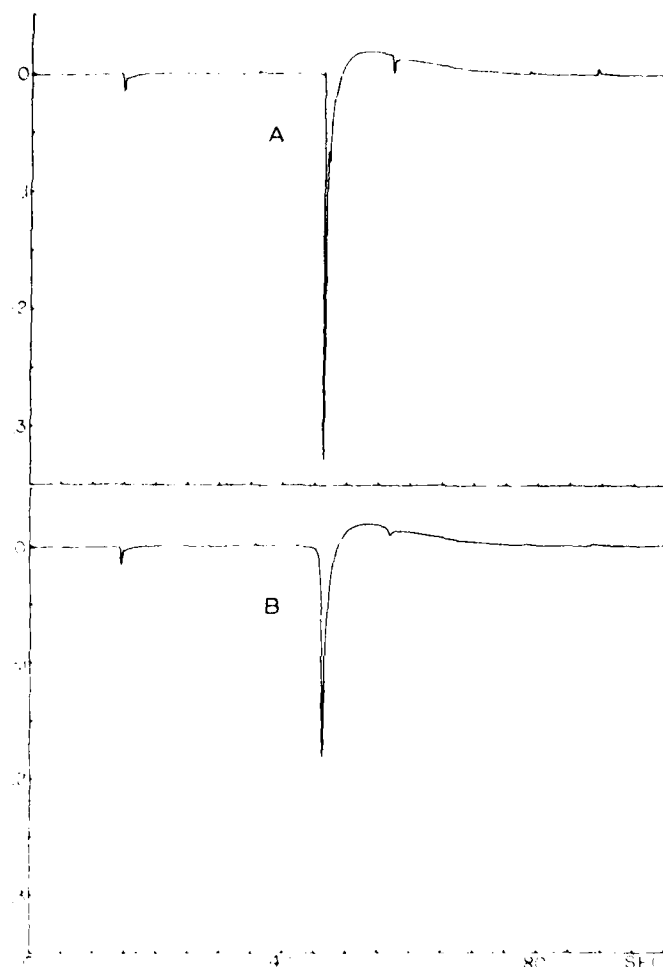
REFERENCES

Bakun, W. H. (1970) Body wave spectra and crustal structure: an application to the San Francisco Bay region. Ph.D. Thesis, University of California, Berkeley, 124 pp.
Bakun, W. H. (1971) Crustal model parameters from P-wave spectra. Bull. Seism. Soc. Am. 61, 913-935.
Bolt, B. A. (1972) The density distribution near the base of the mantle and near the earth's center. Phys. Earth Planet. Interiors 5, 301-311.
Borcherdt, R. D. (1971) Inhomogeneous body and surface plane waves in a generalized viscoelastic half-space. Ph.D. Thesis, University of California, Berkeley, 308 pp.

Borcherdt, R. D. (1973). Energy and plane waves in linear viscoelastic media. *J. Geophys. Res.* **78**, 2442 2453.

Buchen, P. W. (1971). Plane waves in linear viscoelastic media. *Geophys. J.* **23**, 531 542.

Cooper, H. F., Jr. (1967). Reflection and transmission of oblique plane waves at a plane interface between viscoelastic media. *J. Acoust. Soc. Am.* **42**, 1064 1069.

Futterman, W. I. (1962). Dispersive body waves. *J. Geophys. Res.* **67**, 5279 5291.

Grant, F. S. and G. West (1965). *Interpretation Theory in Applied Geophysics*, McGraw-Hill, New York.

Gurtin, M. E. and F. Sternberg (1962). On the linear theory of viscoelasticity, *Arch. Ration. Mech. Anal.* **11**, 291 356.

Haskell, N. A. (1953). Dispersion of surface waves in multilayered media. *Bull. Seism. Soc. Am.* **43**, 17 34.

Haskell, N. A. (1960). Crustal reflections of plane *SH* waves, *J. Geophys. Res.* **65**, 4147 4150.

Haskell, N. A. (1962). Crustal reflection of plane *P* and *SV* waves. *J. Geophys. Res.* **67**, 4751 4767.

Helmberger, D. V. and D. G. Harkrider (1972). Seismic source descriptions of underground explosions and a depth discriminate. *Geophys. J.* **31**, 45 66.

Knopoff, L. (1964). Q. *Rev. Geophys.* **2**, 625 660.

Kanai, K. (1950). The effect of solid viscosity of surface layer on the earthquake movements. *Bull. Earthquake Res. Inst., Tokyo Univ.* **28**, 31 35.

Kurita, T. (1975). Attenuation of shear waves along the San Andreas fault zone in central California, *Bull. Seism. Soc. Am.* **65**, 277 292.

Kuster, G. T. (1972). Seismic phase propagation in two-phase media and its application to the earth's interior, *Ph.D. Thesis*, Massachusetts Institute of Technology, June.

Lockett, F. J. (1962). The reflection and refraction of waves at an interface between viscoelastic media. *J. Mech. Phys. Solids* **10**, 53 64.

O'Neill, M. E. and J. H. Healy (1973). Determination of source parameters of small earthquakes from *P*-wave rise time. *Bull. Seism. Soc. Am.* **63**, 599 614.

Teng, Ta-Yiang (1967). Reflection and transmission from a plane-layered core-mantle boundary. *Bull. Seism. Soc. Am.* **3**, 477 499.

DEPARTMENT OF GEOLOGY AND GEOPHYSICS
UNIVERSITY OF CALIFORNIA
BERKELEY, CALIFORNIA 94720

II. APPLICATION

In this section the body wave formulation will be
applied to an earthquake (Briones Hills: 8 Jan. 1977,
$M = 4.3$, 37° $54.31'N$ 122° $10.97'W$, depth 9.5 km,
$\Delta = 13$ km) recorded at a vertical array. The array
consists of three 3-component accelerometers positioned
at depths of 120 feet (bedrock), 40 feet (bay mud), and
the surface (soil) located at the Richmond Field
Stations. The array is near the borehole referred to
in Secion I so the soil parameters listed in Table I
(Section I) can be used to calculate transfer functions.
The general problem of calculating the effect of local
geology on earthquake ground motion is critical in the
design of structures. Of particular concern is the
amplification factor associated with low velocity
surficial material. In order to test the suitability of
the body wave formulation in predicting the response
of the mud-soil structure, a comparison is made between
the observed surface acceleration records and the bedrock
accelerograms continued to the surface. Different
transfer functions (eq. 26, Section I), applied in the
frequency domain, encompassing different angles of
incidence will be considered. Also both elastic and
anelastic propagation will be compared to the observed
surface time histories. The entire accelerogram is
used in computing the spectra and no time window has
been applied. Twenty seconds of record is transformed

with 2048 points. The analysis will be restricted to horizontal components as the bedrock vertical instrument had a telemetry malfunction. Also, the actual orientation of the horizontal components have not yet been determined and will therefore be referred to simply as H1 and H2.

In Figure 1 are shown the bottom and surface H1 (horizontal) component acceleration records plotted to the same scale. The onset of the P-wave is clearly visible while the S arrival is somewhat emergent. Of particular interest is the long period component of the bottom S arrival compared to the corresponding part of the surface record. The surface trace appears to have more high frequency content. This observation is substantiated by the spectra shown at the end of the section. Compare the H1B and H1T spectrums. The peak in the H1T between 1 - 2 Hz is missing in the bottom spectra. Also the bottom record tapers off after the S-wave while the surface record continues with large amplitudes and points out the importance of high frequency surface waves in the duration of motion for near sources. The surface wave traces, either Love or Rayleigh waves, represents a laterally propagating disturbance and is not included in the theoretical model. A full treatment of the problem requires the inclusion of a non-plane wave source and is not considered here.

In order to simulate the layering effect, the
bottom trace (Figure 1, a) was continued to the surface
using the previously mentioned transfer function.
Figure 2 shows the computed surface motion assuming
Figure 1a as a normally incident S-wave. Figure 2a,
considers the soil elastic while Figure 2b includes the
loss (note different scales). In comparing the observed
surface motion with the computed (including loss)
several interesting features are observed. First,
the amplitudes are fairly close (not considering the
P-wave as it was continued as an S-wave) with the
calculated somewhat large. This indicates that the
Q structure is approximately correct. Also, the longer
period part of the S-wave is present on the continued
trace as we might expect since its wavelength is far
greater than the thickness of the soil section. In
addition, the large amplitudes following the S-wave
are not present on the computed seismograms. This
indicates that this part of the motion is propagating
in a horizontal direction. Figure 3 shows the same
input (assumed SV) continued with an incidence angle
of 10°. This trace demonstrated that converted waves
are unimportant in this case as it is virtually the
same as Figure 2.

Considering now Figure 4, we have the same analysis
for the other (H2) component. Again (a) and (b) are
the bedrock and surface records respectively. Again

the longer periods seem more dominant in the bedrock
component. Also, the surface waves are much more
dominant in this component, appear to arrive later,
and may be associated with Rayleigh waves. Comparing
the surface record (b) with the computed in Figure 5
we observe the amplitudes of the attenuation record
(b) are fairly close. The longer periods are continued
as dominant while the large amplitude and long period
wave train is absent. Figure 6 shows the continued
record for a transfer function with an incident SV
wave at 10° and is virtually the same as 0° in Figure 5.

In order to compare frequency domain data with
the model, spectral ratios (surface to bedrock) were
calculated for both components and are shown in Figure
7. The ratios shown have been smoothed with a 20
point averaging filter. Because of this smoothing,
coupled with the spectral contamination of a boxcar
window, the absolute magnitudes cannot be directly
compared with the theoretical transfer function.
However, the observed ratios (solid line in Figure 7),
except for the peak near 5 Hz, agree fairly well with
the theoretical transfer function (broken line in
Figure 7; also shown in Figure 2b, Section I (an
unfortunate error has the decimal on the wrong side
of the digit: i.e., $.4 \rightarrow 4.$)). The peak position
reflects the total stack travel time while the
amplitude decrease reflects the loss. The 5 Hz peak

may be due to the spectral contamination by the surface waves present in the surface records. Further analysis will require careful windowing to isolate the shear wave. The positions of the peaks are indicative of the travel time while the relative peak heights reflect the loss.

Following Figure 7 all nine acceleration records are shown along with their spectra.

III. CONCLUSION

In this section some success has been demonstrated in modeling the response of a soil structure. The method used an extension of the Haskell-Thompson matrix method presented in Section 1. In particular it was shown that a significant amount of attenuation was necessary in order to compare amplitudes. It was also shown that a large portion of significant motion was due to lateral propagation and therefore not present in the calculated response.

In addition the observed ratios (surface to bedrock) showed good agreement between components. Also, it was found that the observed ratios compared favorably with the calculated, both in peak position and in peak duminition with frequency.

5SEC.

1a

Fig. 1. Horizontal acceleration records for the Briones Hills event recorded at the Richmond Field Station vertical array: a) bedrock (120ft.), b) surface. H1 component.

2a

5SEC.

Fig. 2. Bedrock accelegram (H component; Fig. 1, a) propagated to the surface for normal incidence shear wave: a) elastic; b) including loss.

5SEC.

2b

Fig.3. Bedrock accelegram (H1 component; Fig. 1, a) propagated to the surface for 10°
incident SV wave: a) elastic, b) including loss.
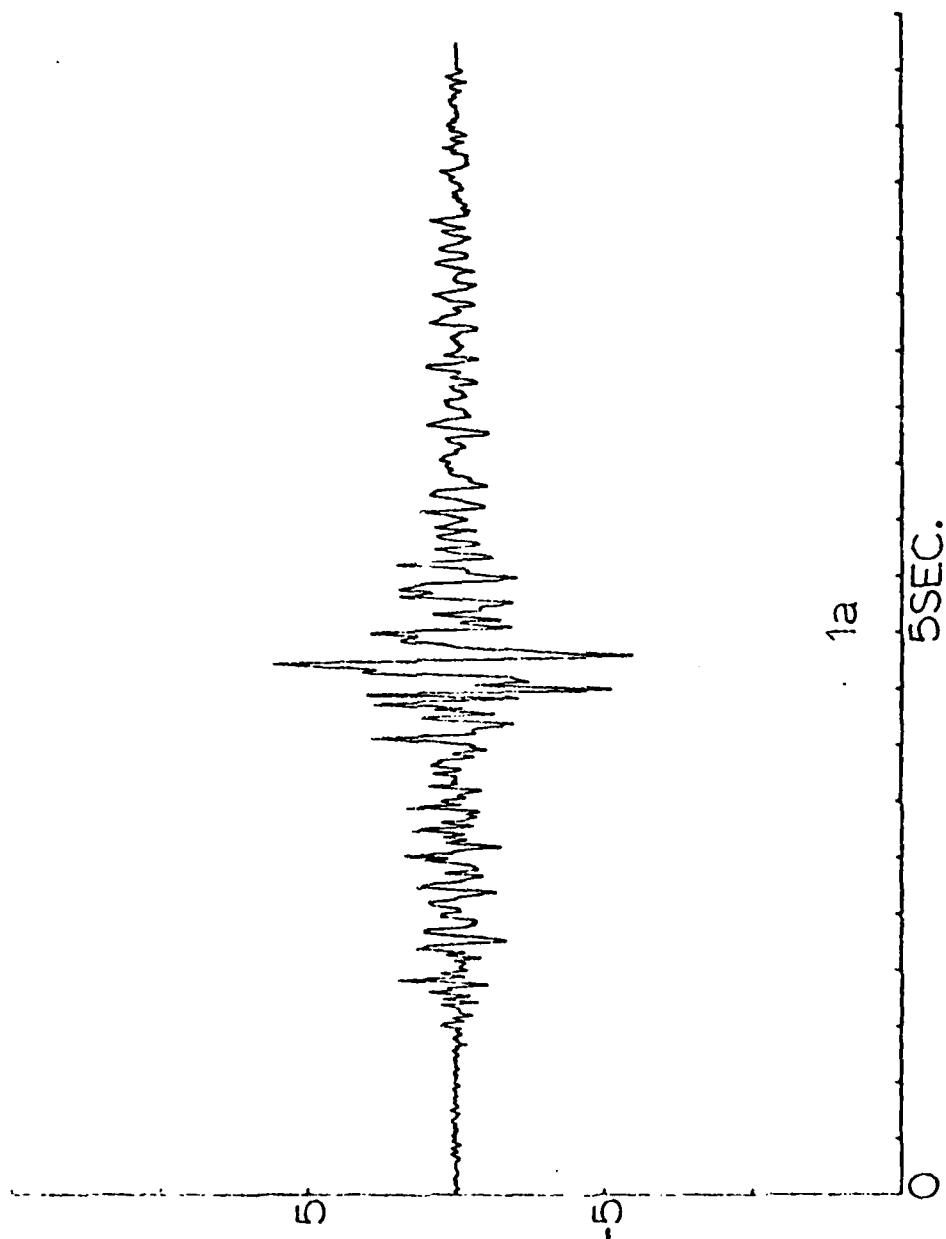
3b
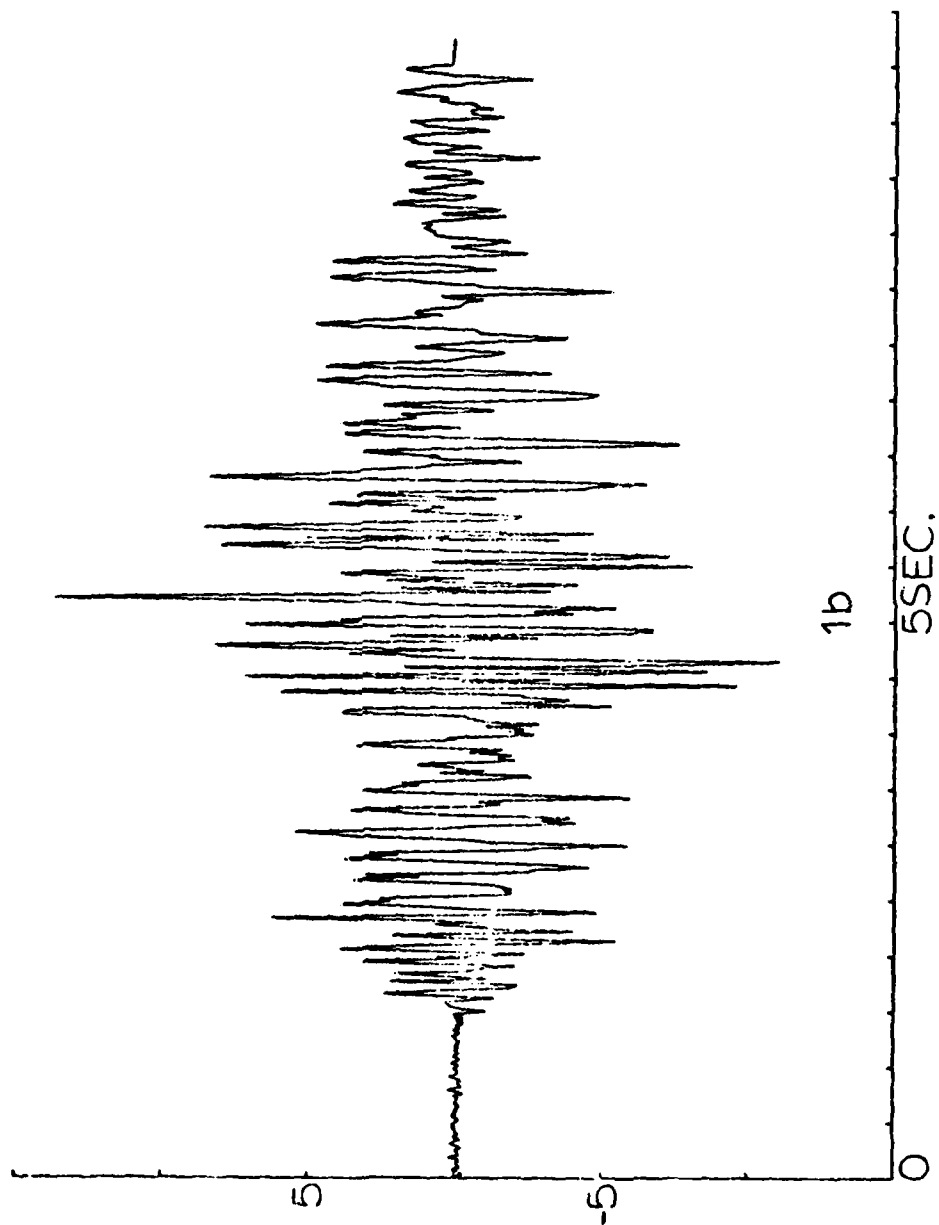
5SEC.

5 SEC.

4a

O

5

-5
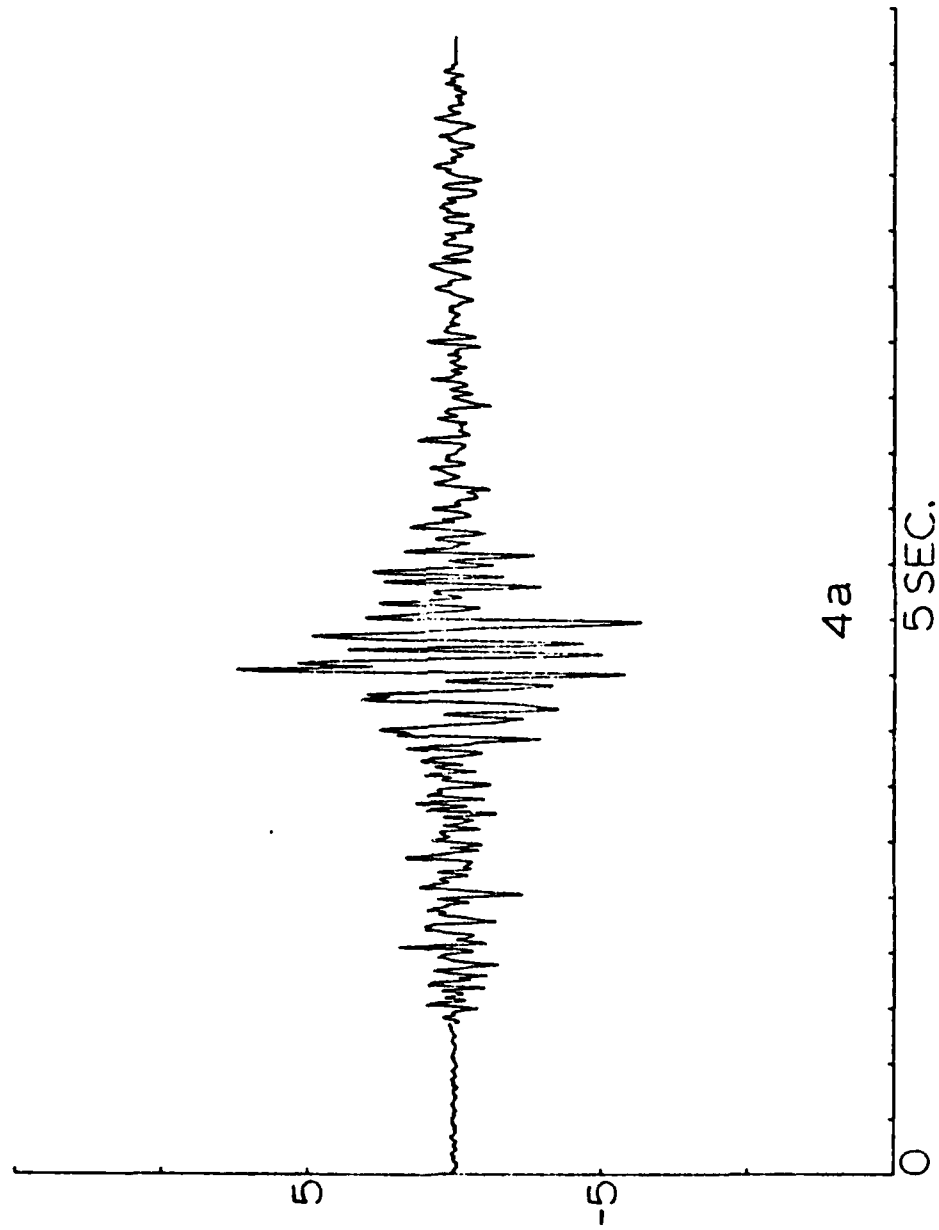
Fig. 4. Horizontal acceleration records for the Briones Hills event recorded at the Richmond Field Station vertical array; a) bedrock (120 ft.), b) surface. H2 component.
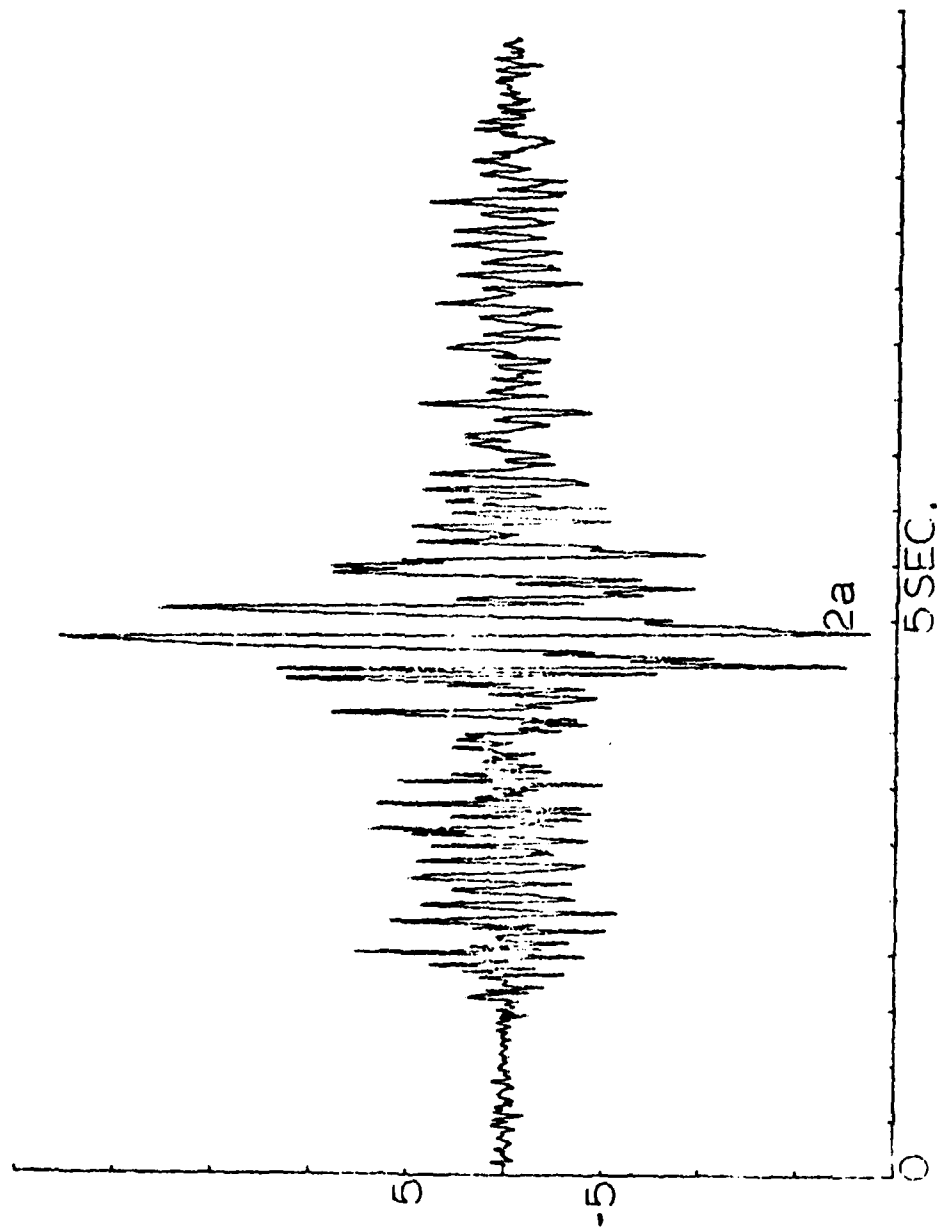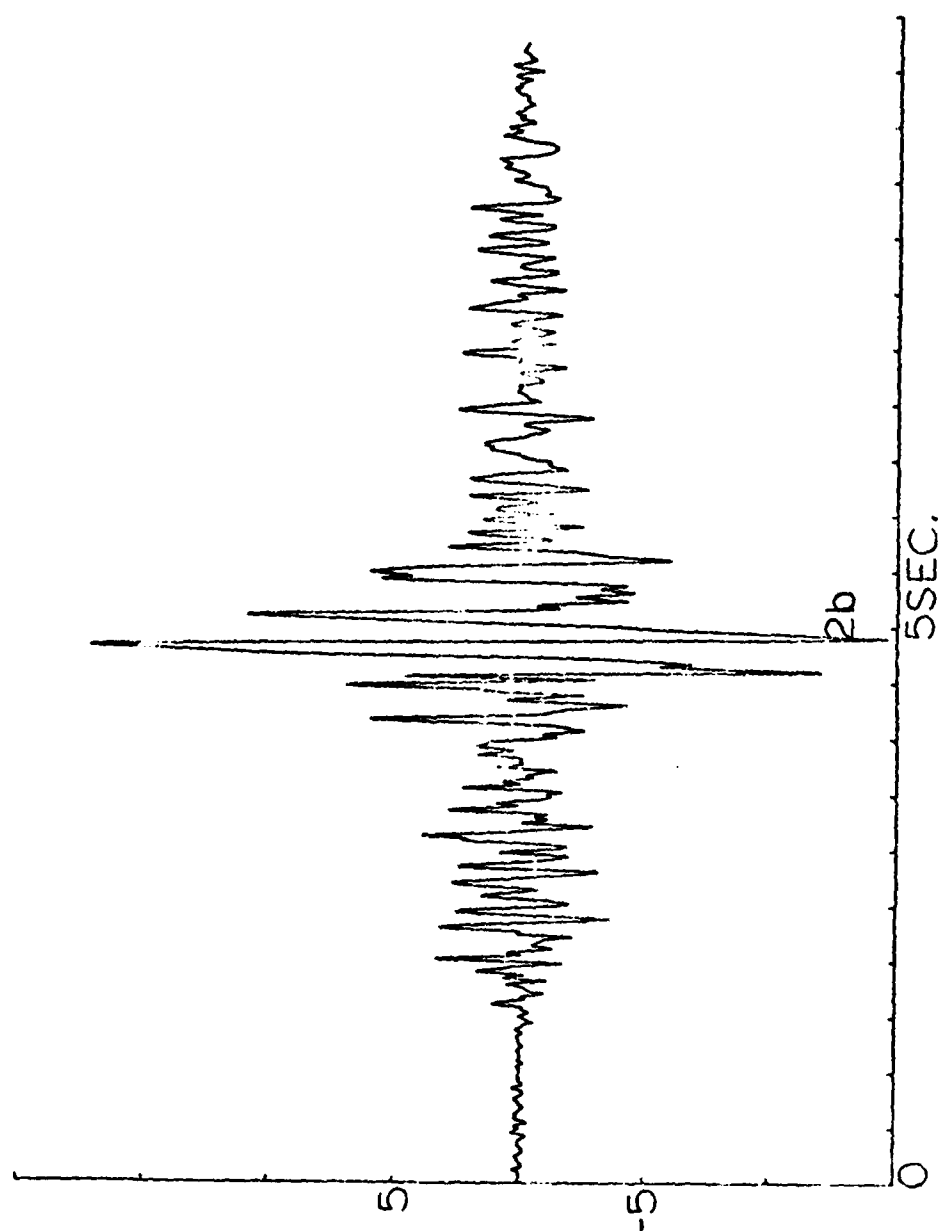
4b

5 SEC.

5a

5SEC.
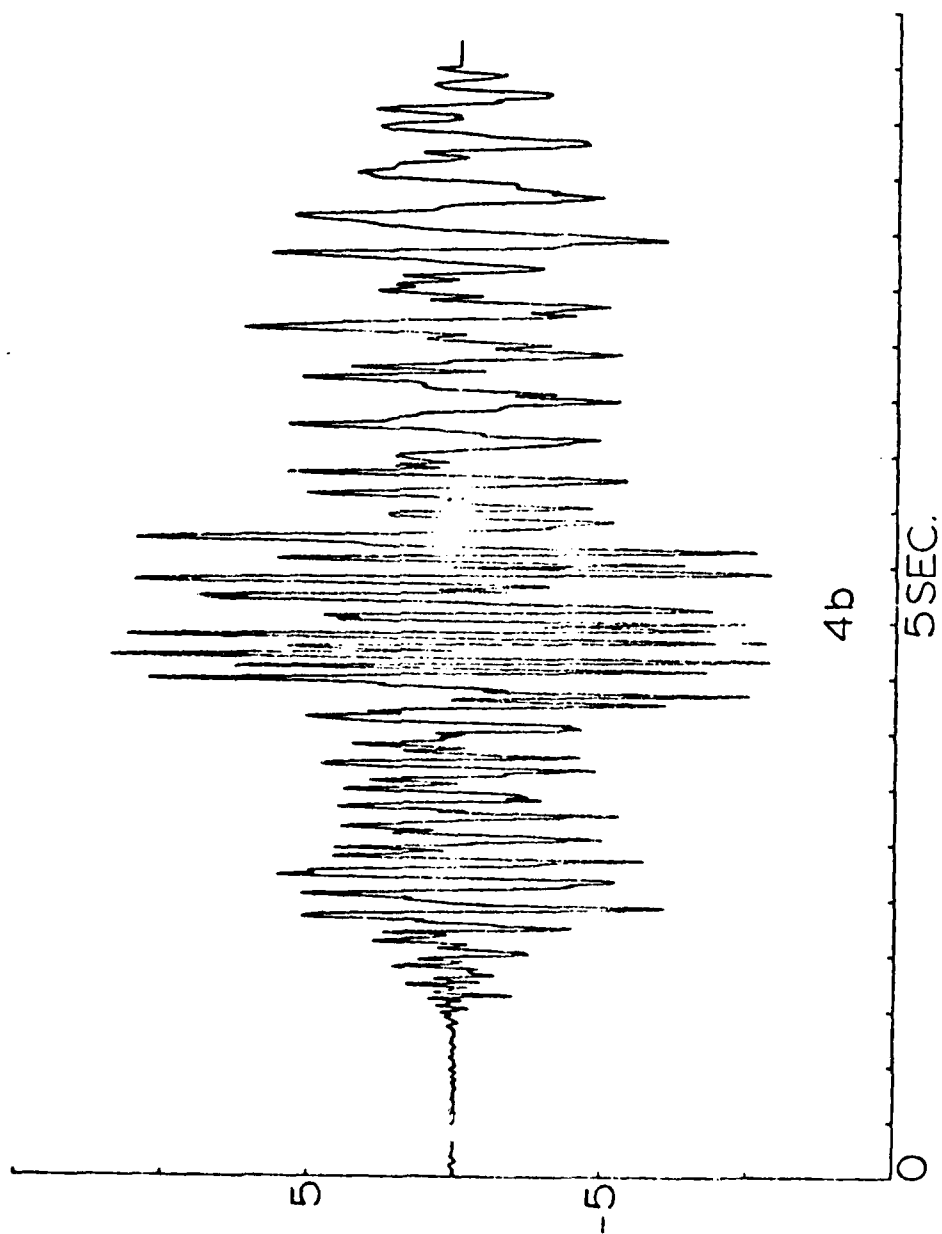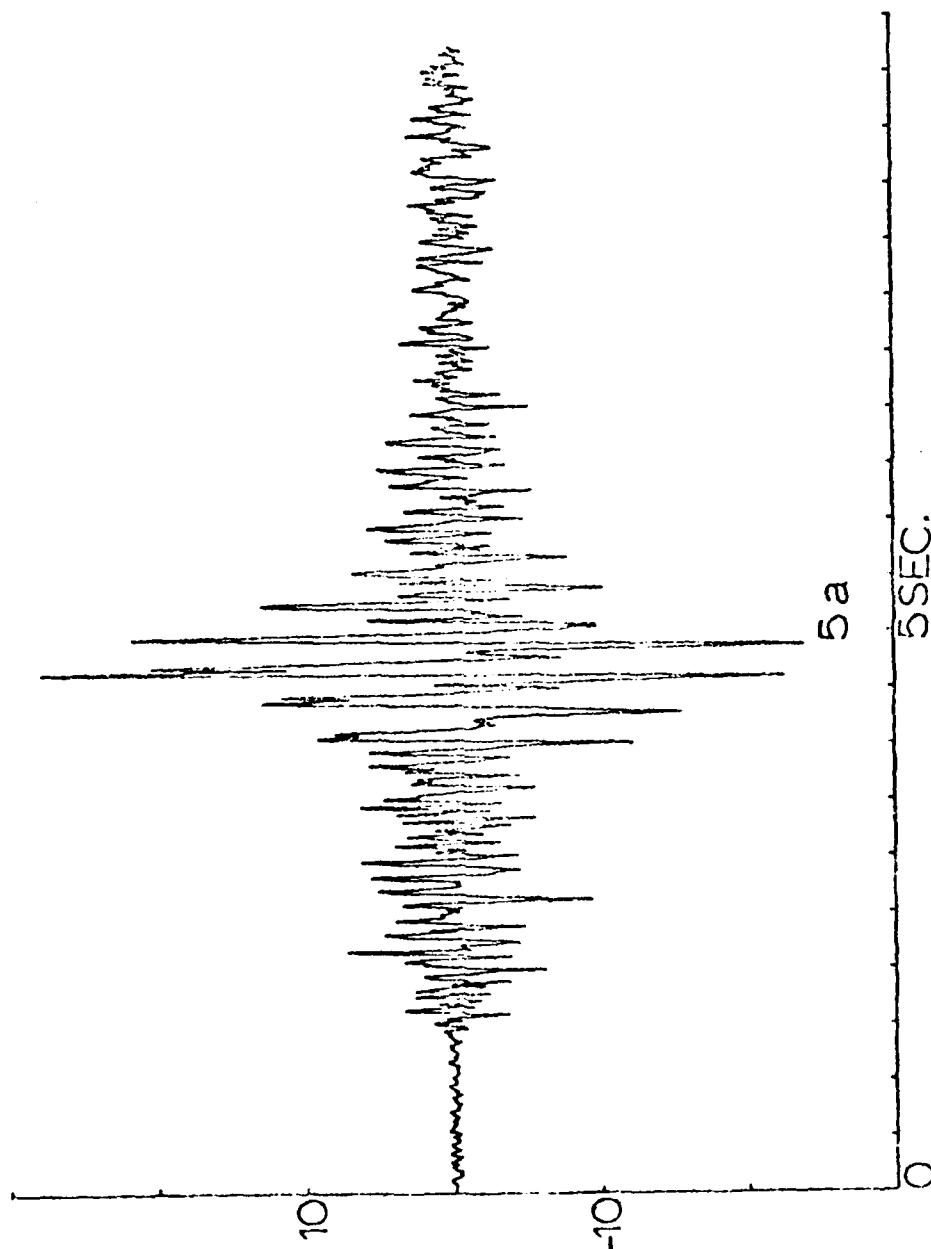
Fig. 5. Bedrock accelegram (H2 component; Fig. 1, a) propagated to the surface for normal incidence shear wave: a) elastic, b) including loss.

5b

5 SEC.

6a

5 SEC.
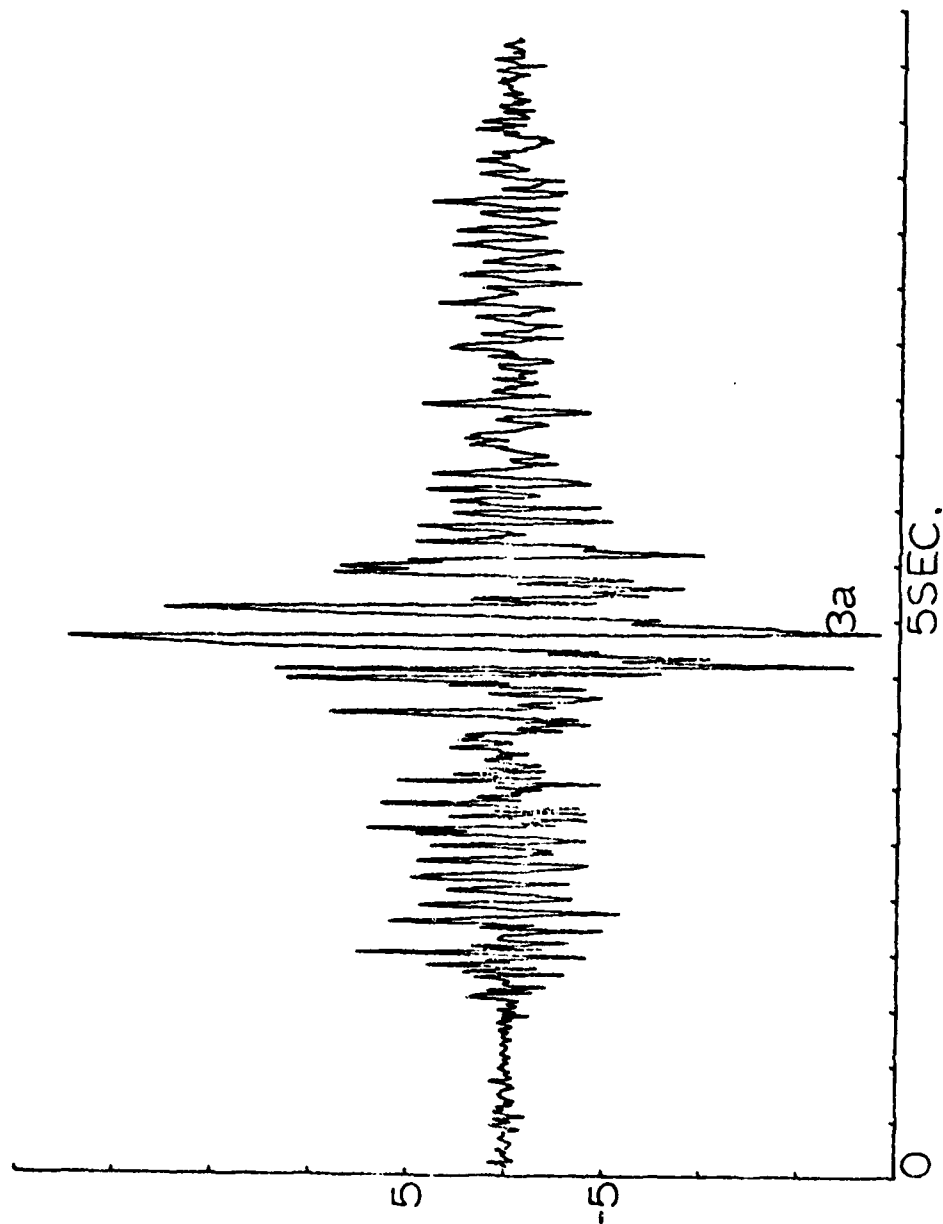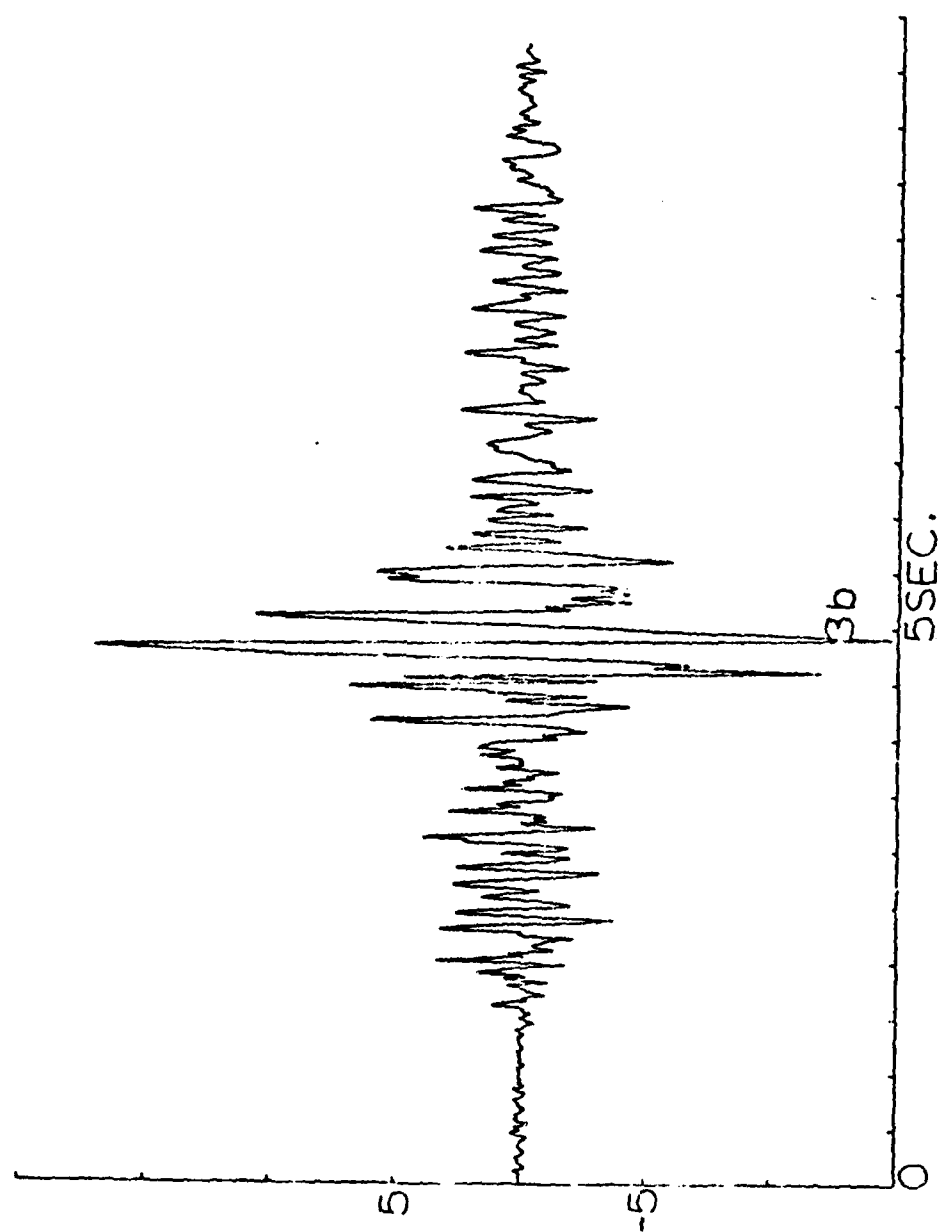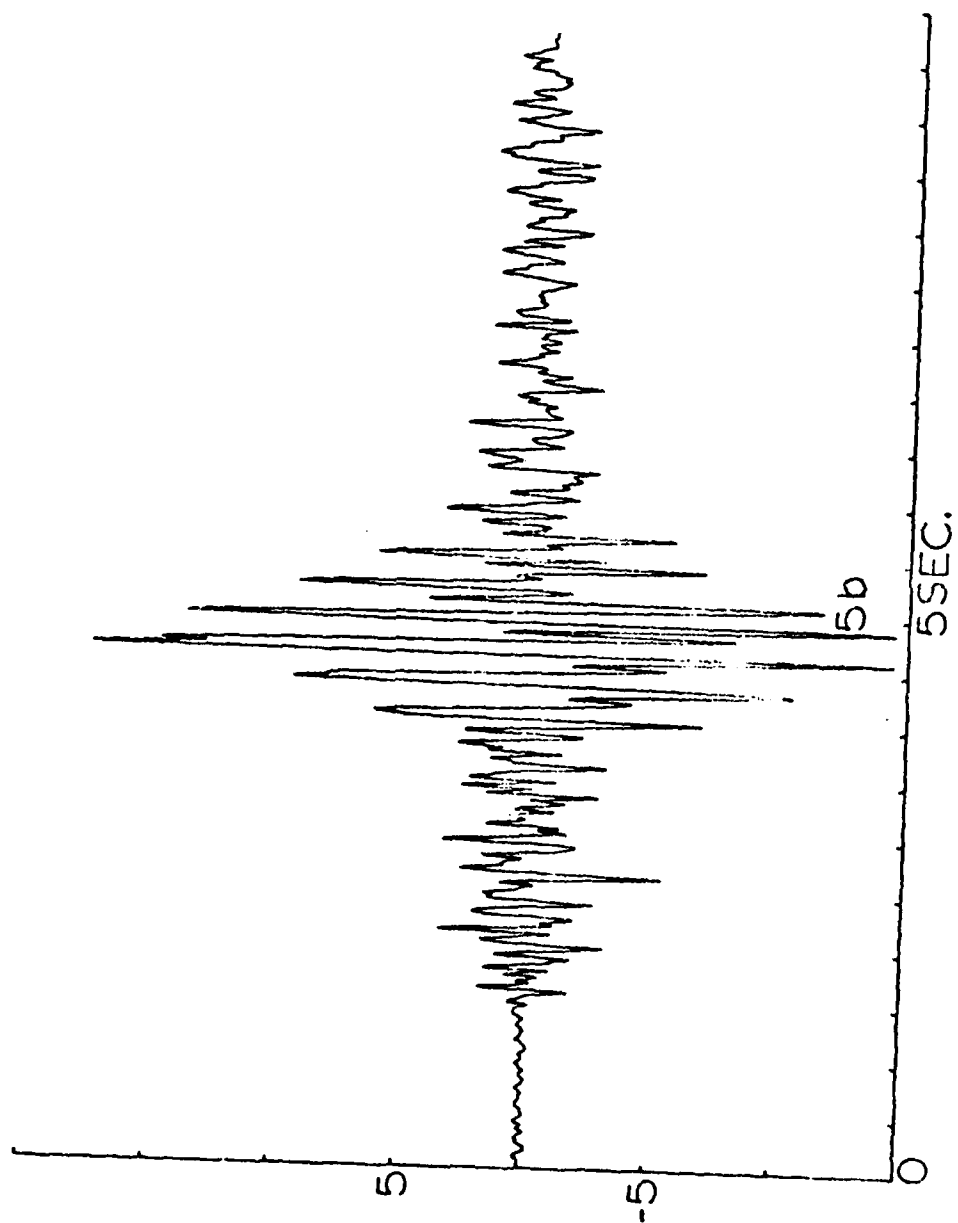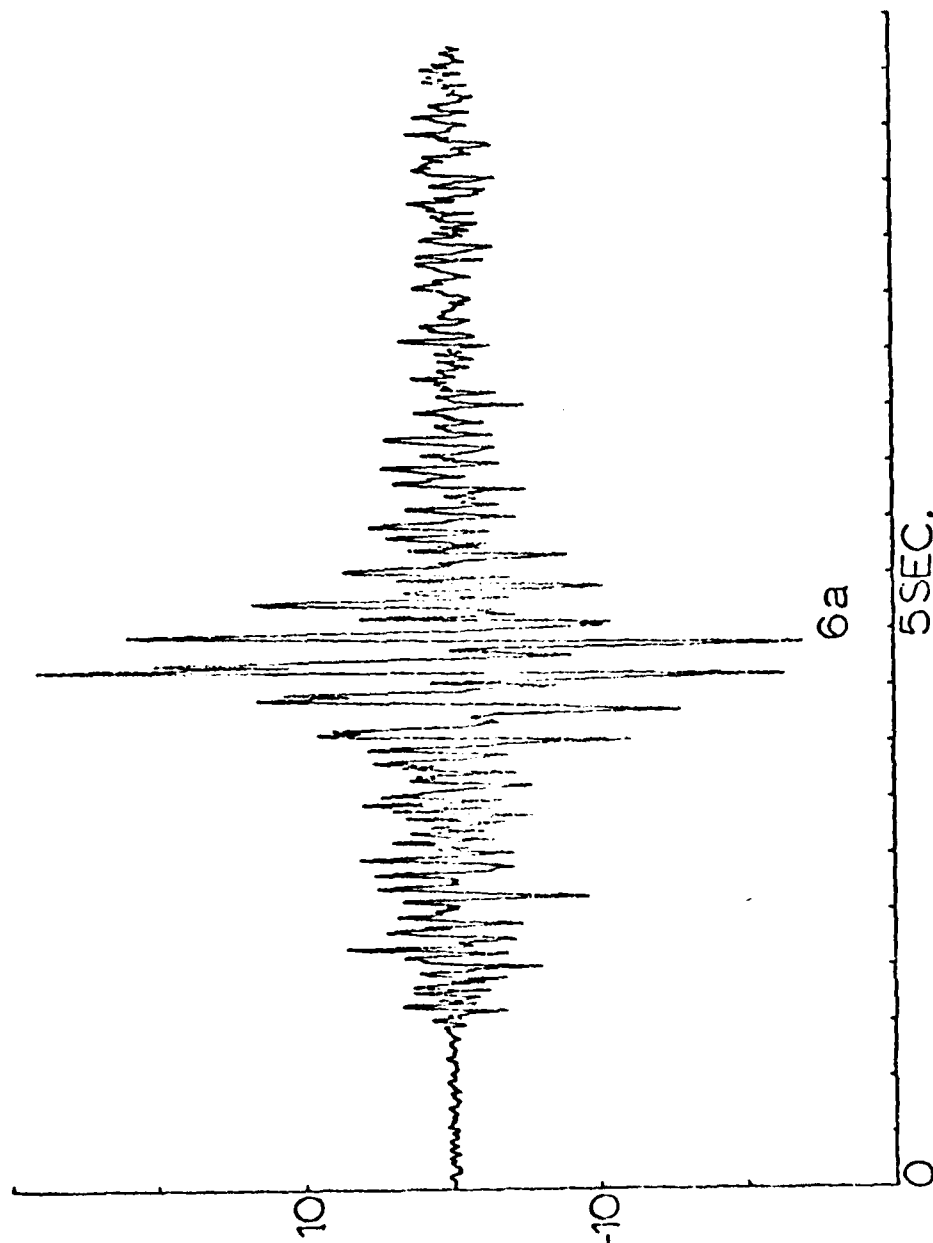
Fig. 6. Bedrock accelegram (H2 component; Fig.1, a) propagated to the sur-
face for 100 incident SV wave: a) elastic, b) including loss.
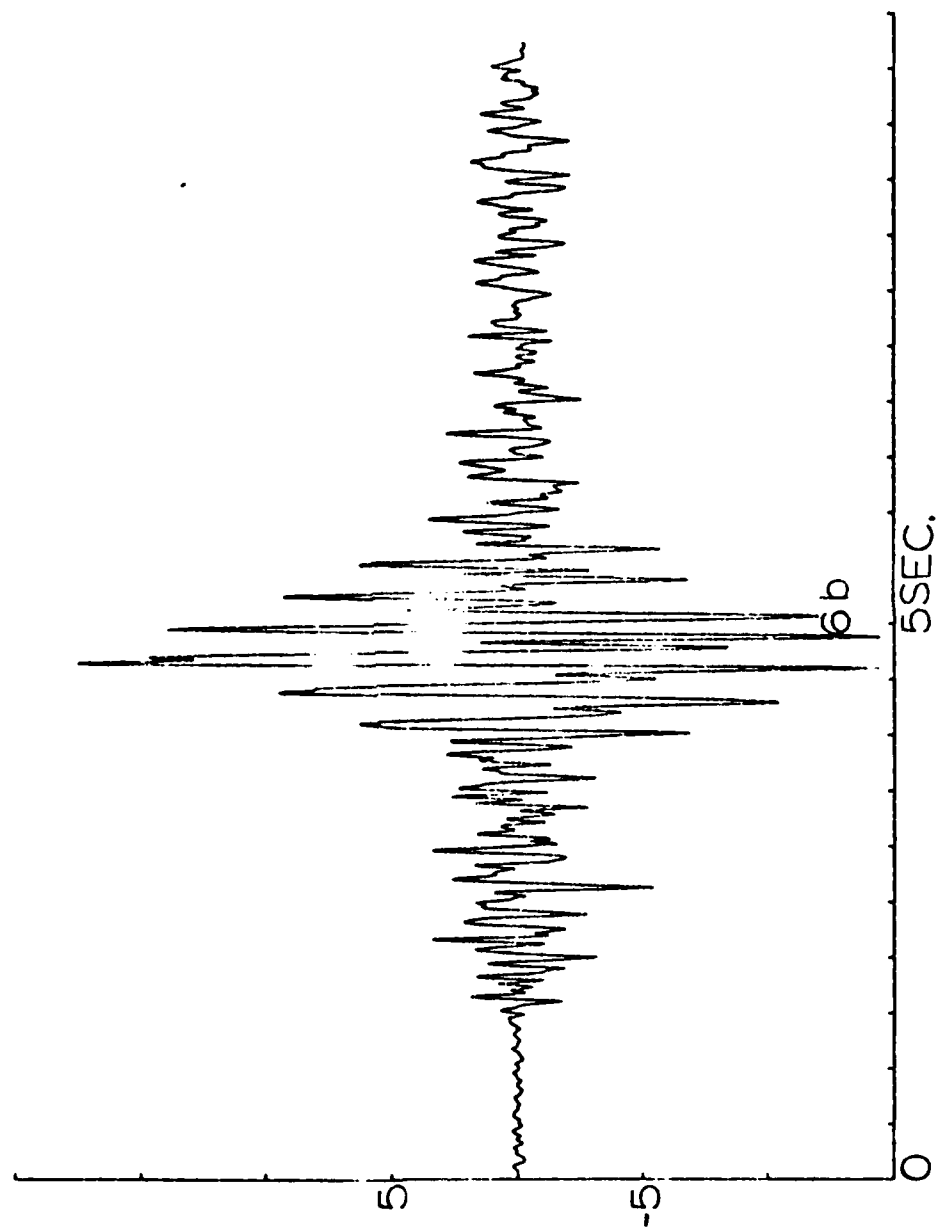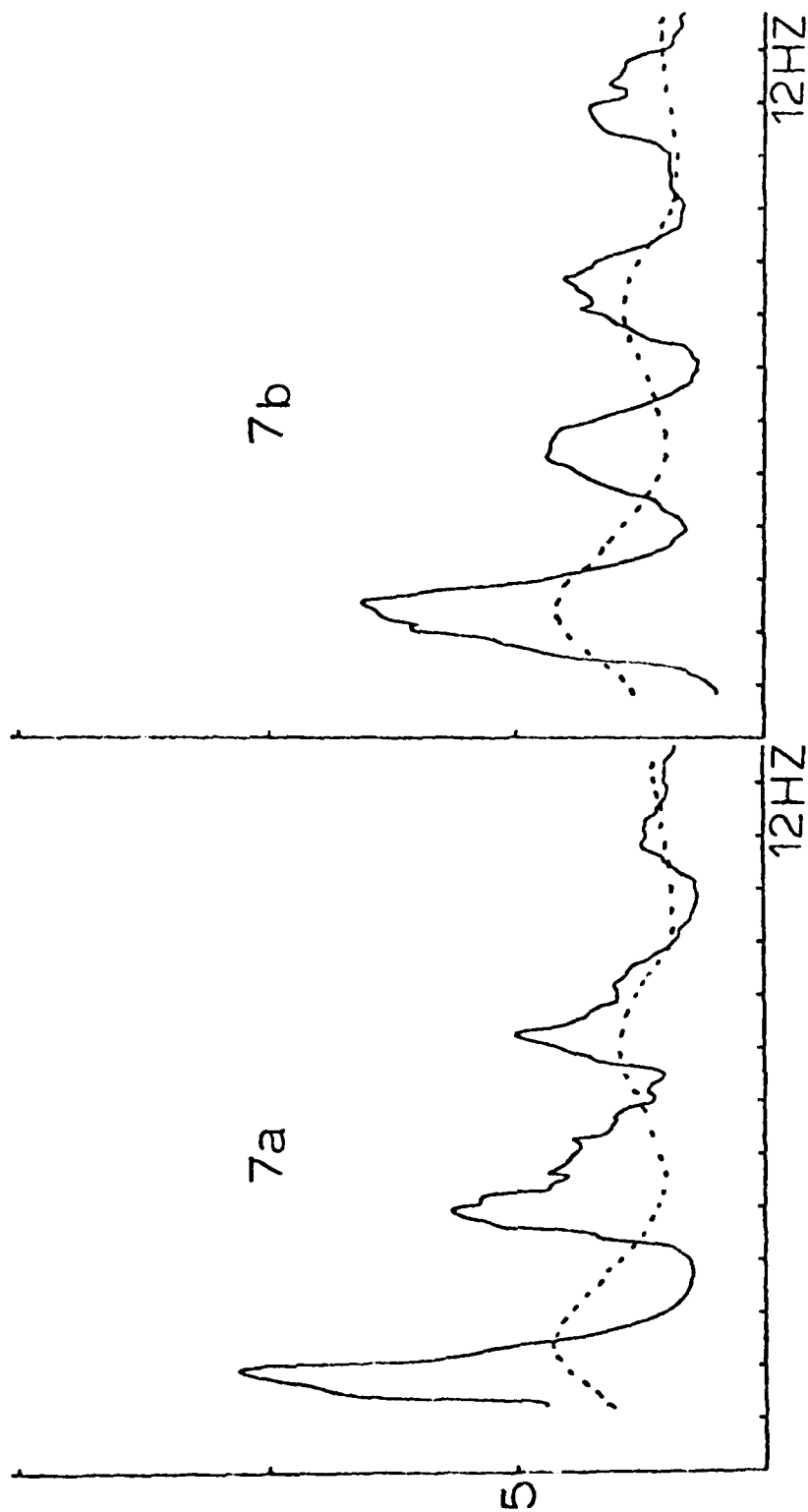
Fig. 7. Observed spectral ratios (surface to bottom): a) H1 component, b) H2 component. Ratios are smoothed with a 20 point moving average. Broken line is the theoretical ratio shown in Fig. 2, B in Section I.

The following nine figures represent the
acceleration records and their spectra (dashed line
is noise spectra windowed prior to signal) as recorded
by the Richmond Fiel Station vertical array for the
Briones Hills event. Components are labeled. The
poor bedrock (ZB) record was the result of telementry
difficulty which has subsequently been repaired.

10

ZB

1500

5   SEC.

.1   1   10   HZ.

H1B

10

600

.1   1   5   SEC.
                          10   HZ.

H2B

H1M

H2M

10

800

5   SEC.

1   1   10   HZ.

H1T

10

1000

5   SEC.

.1   1   10   HZ.

H2T

10

1000

5   SEC.

.1   1   10   HZ.
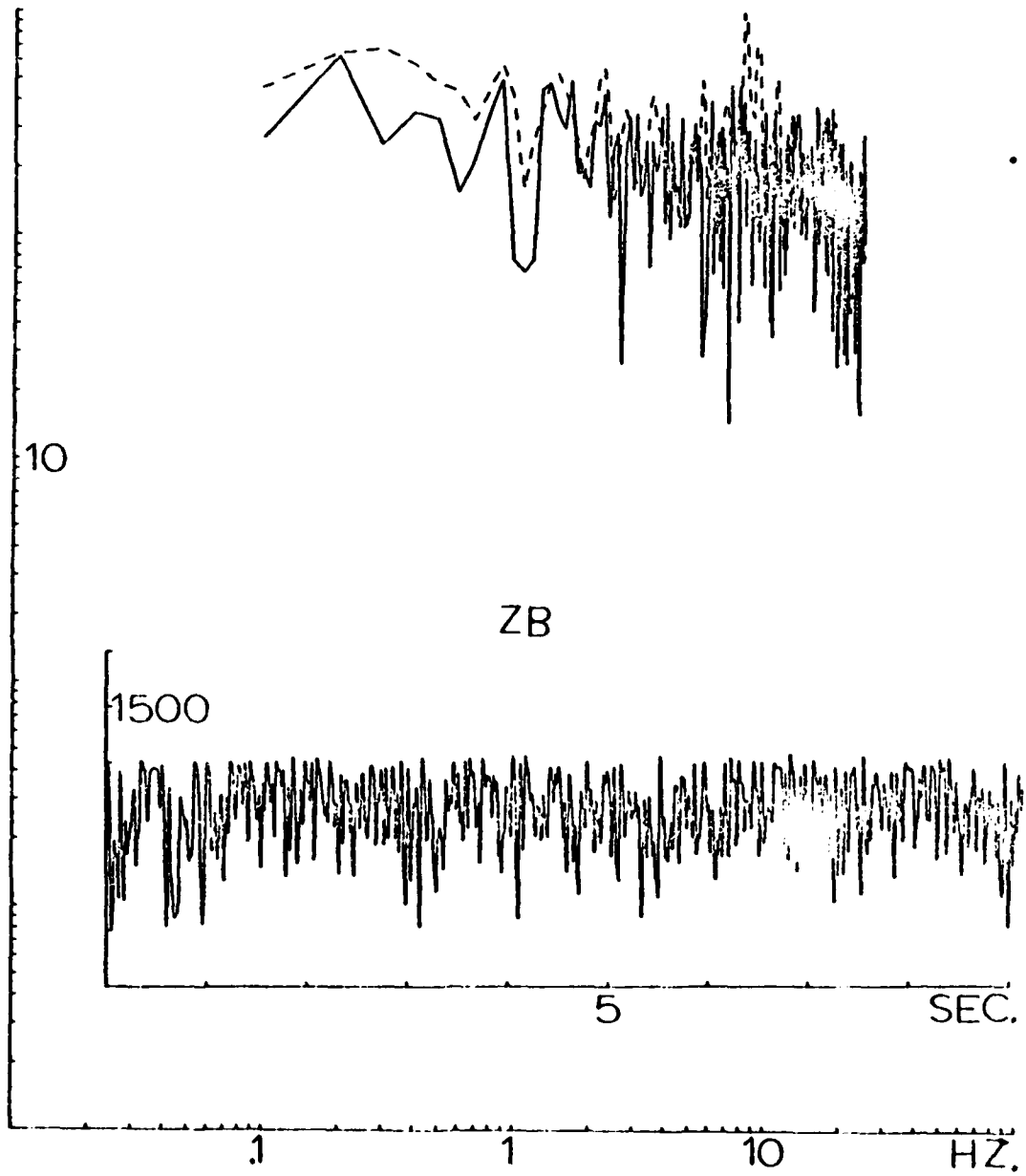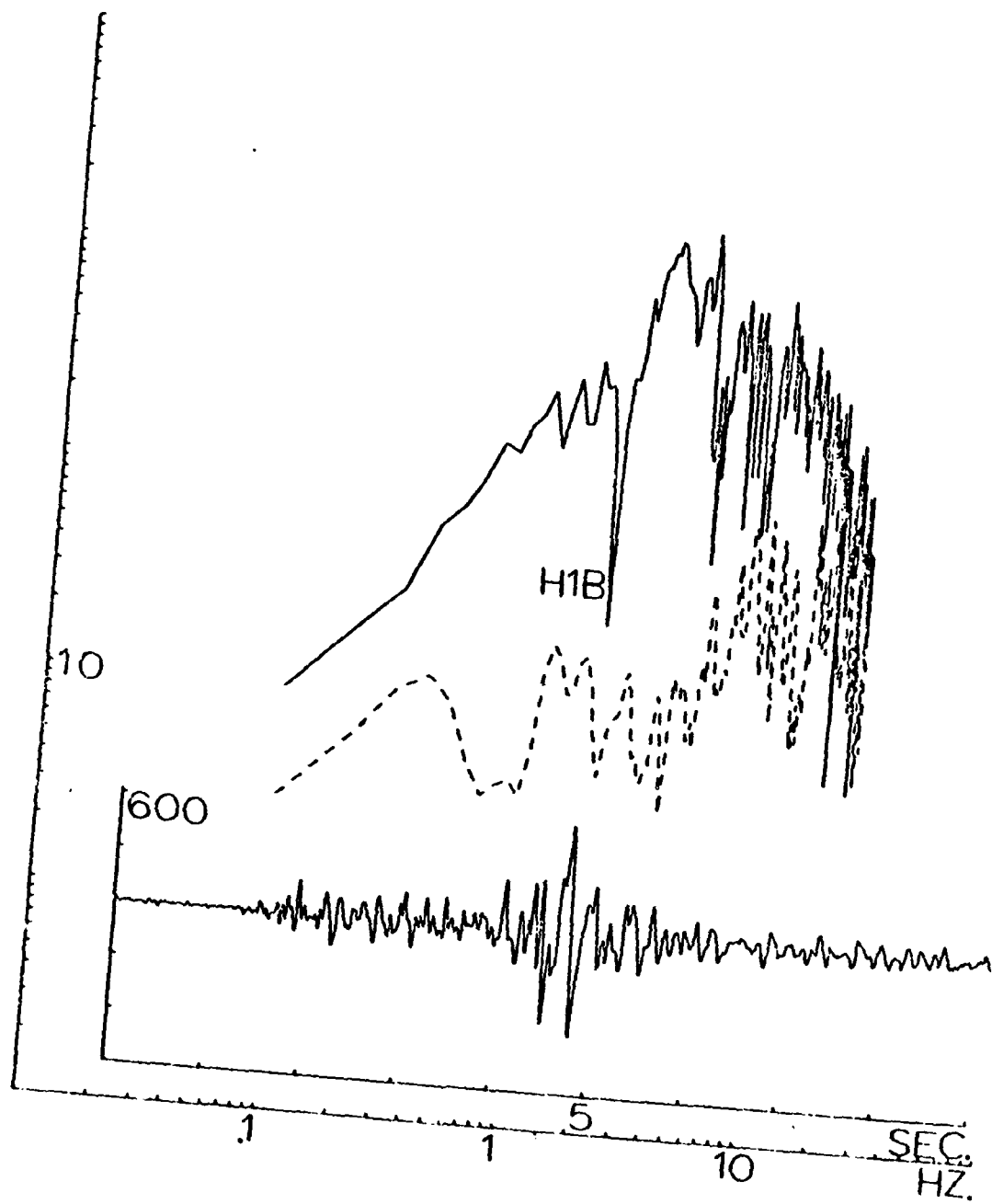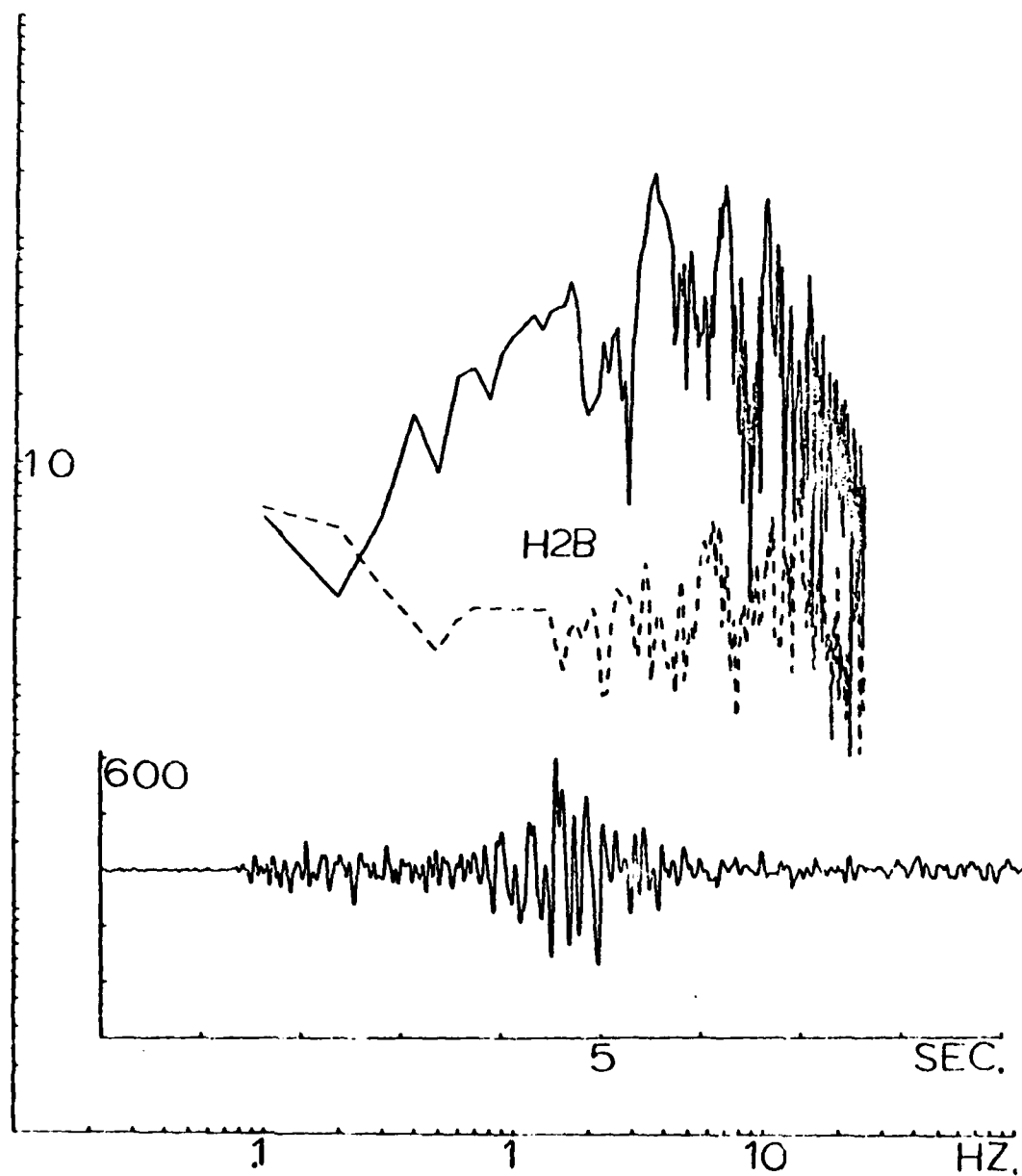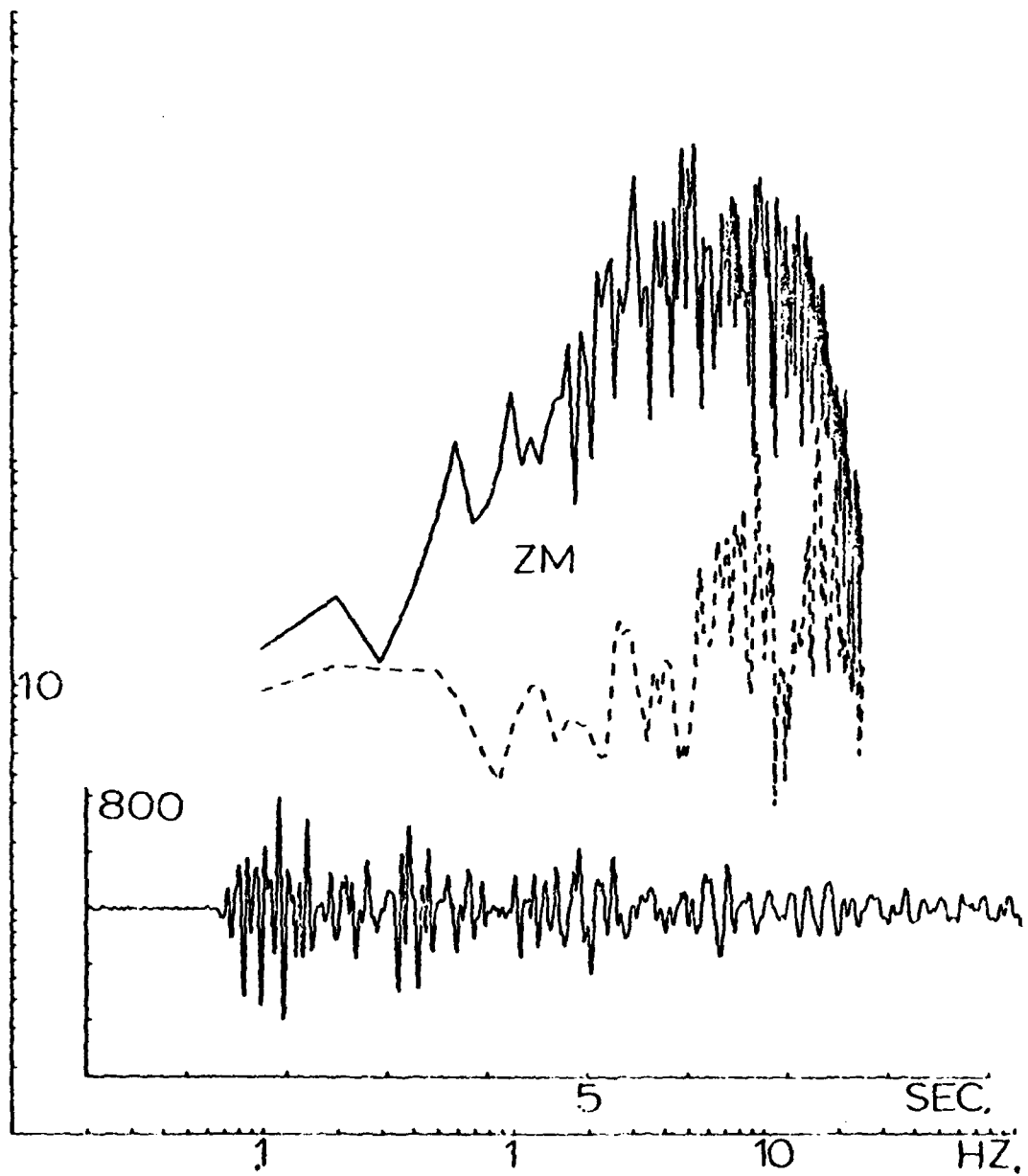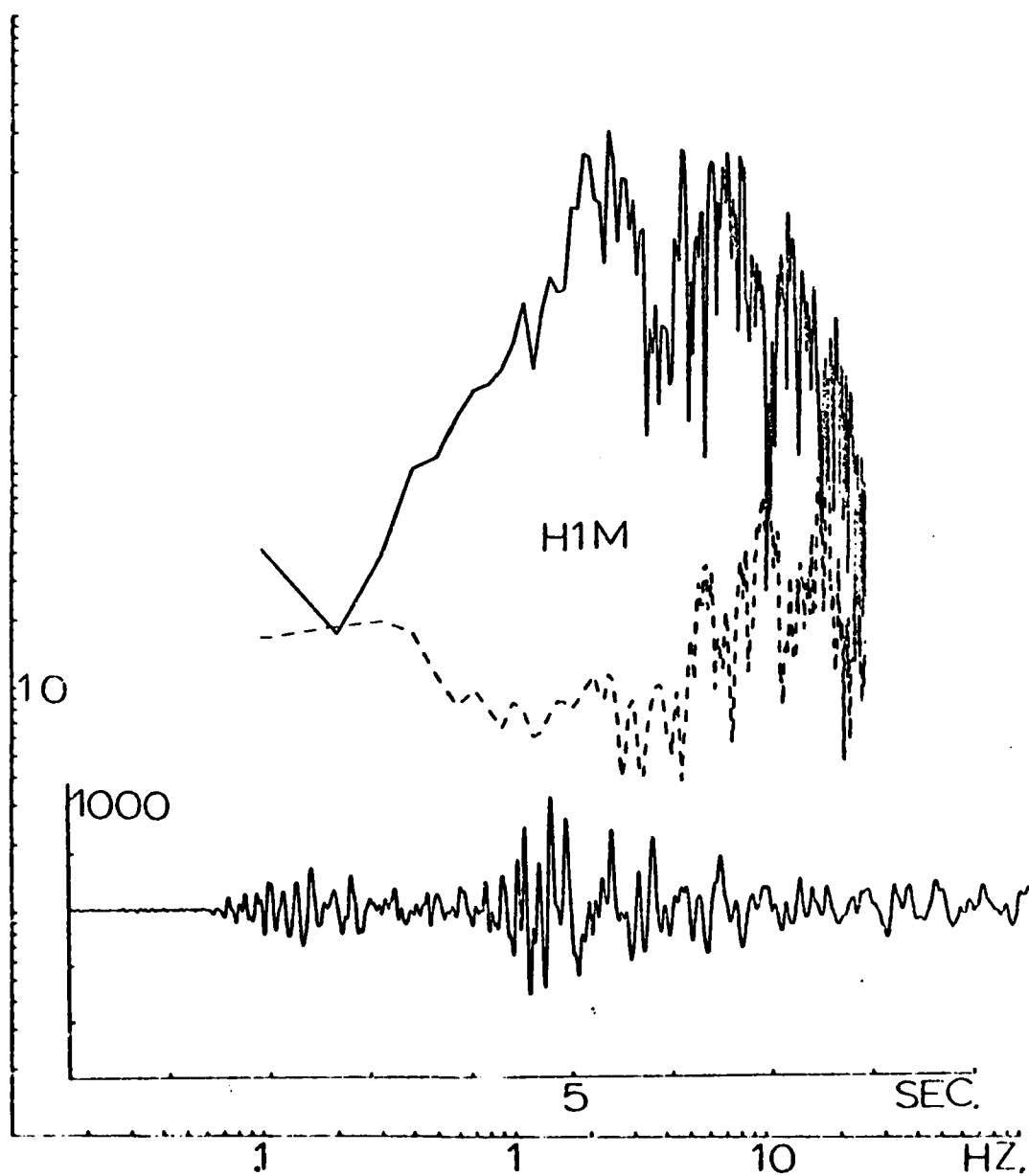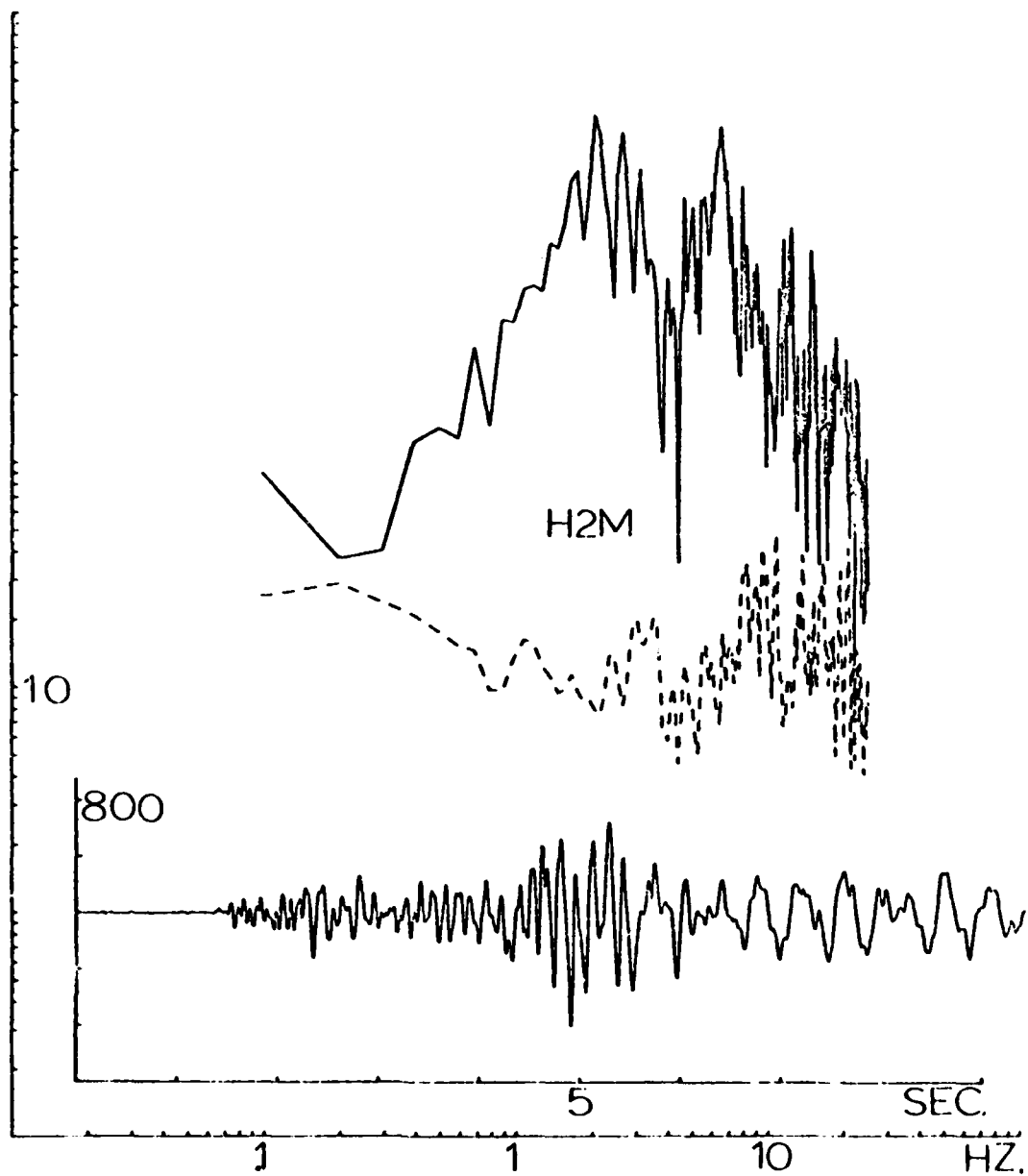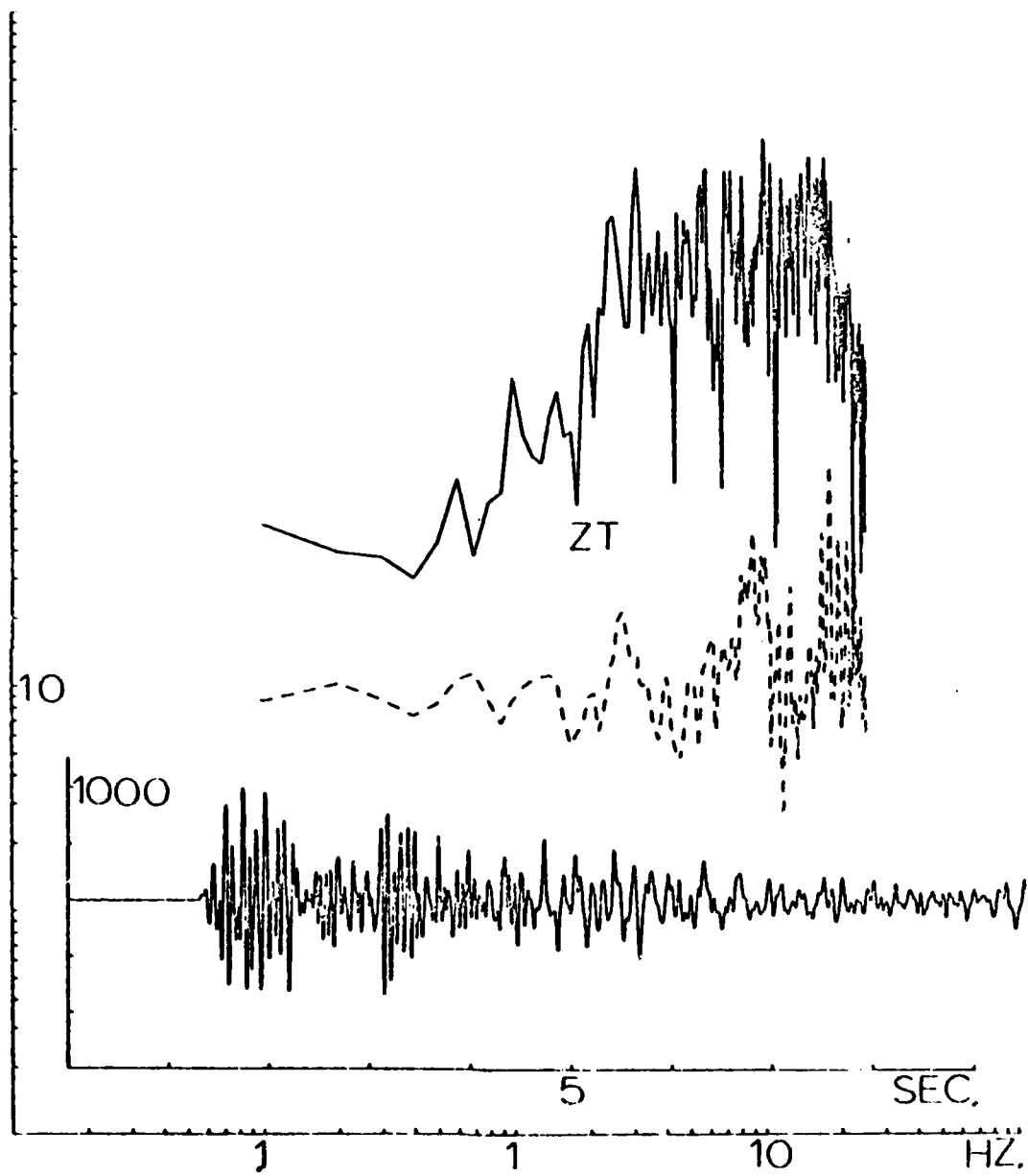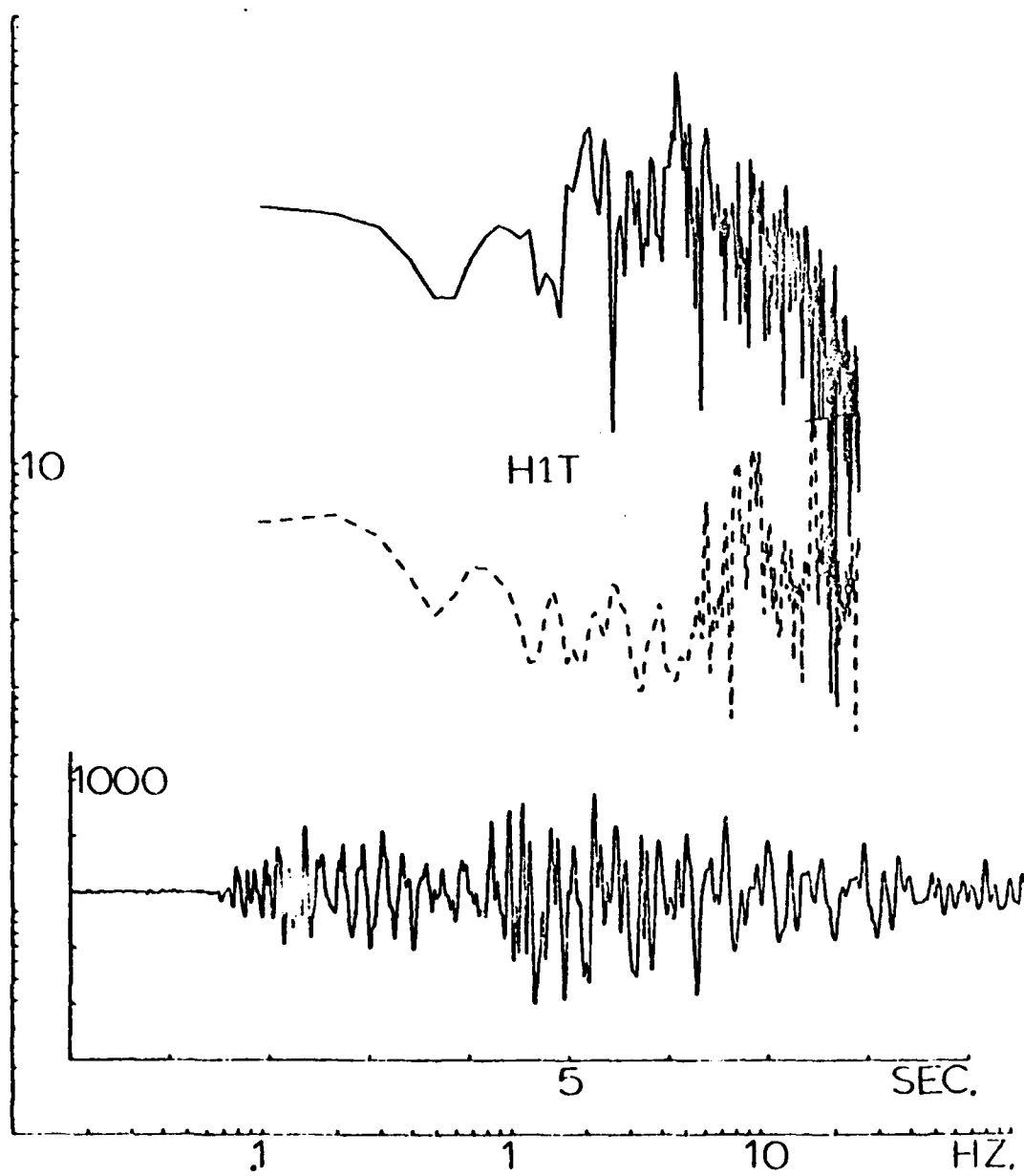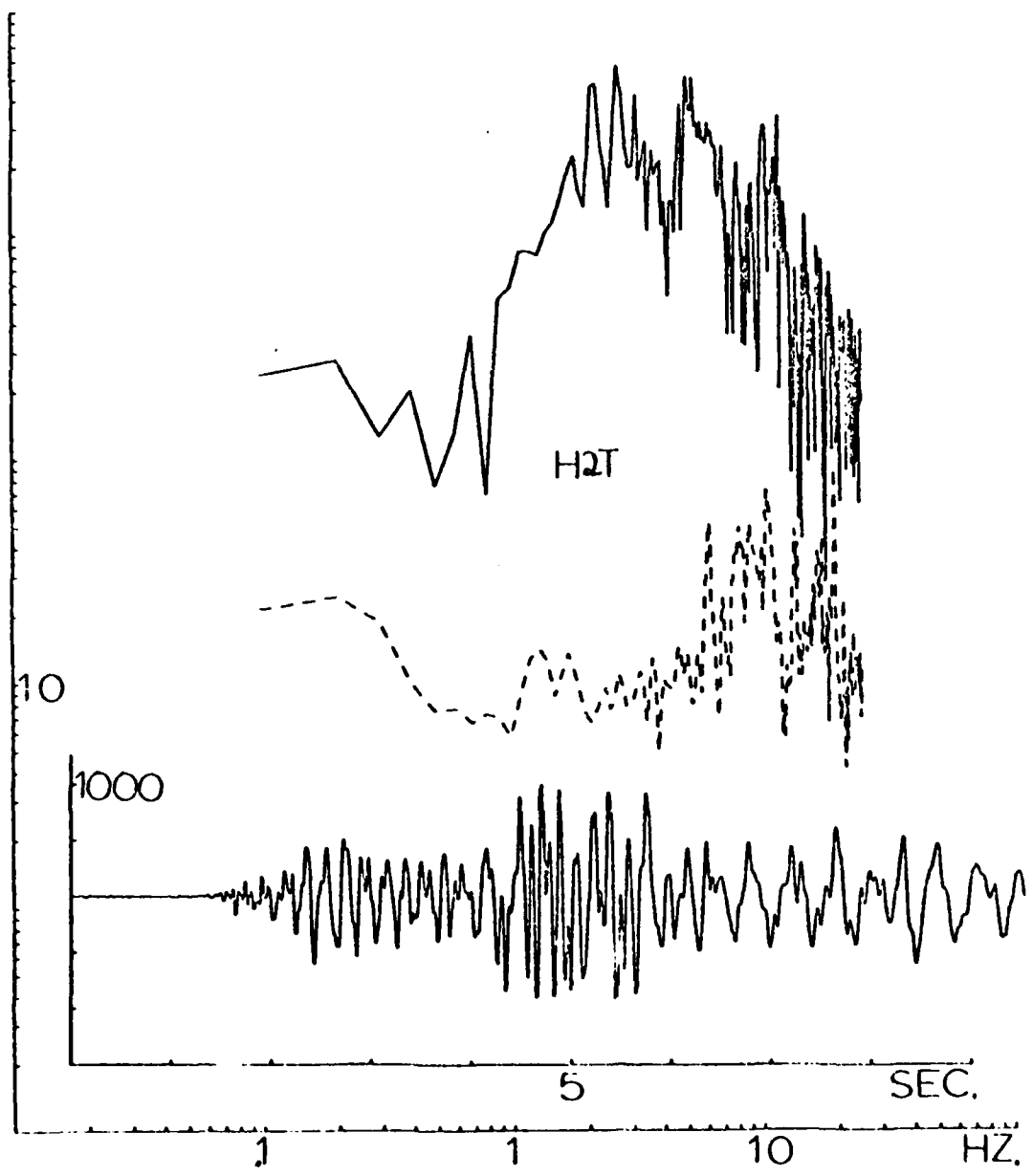
CHAPTER 2

SURFACE WAVES

I. FORMULATION

The development presented in Chapter 1 which incorporates attenuation in an exact manner into a Haskell-Thompson formulation is extended here to surface waves. The extension follows quite naturally for the period equation as the horizontal wave number now becomes complex in order to accommodate the surface wave quality factor. This now requires the determination of complex roots of the complex determanental equation. The details are outlined in Appendices 1 and 3.

II. FORWARD PROBLEM

In this section the surface wave formulation (Love and Rayleigh waves) will be applied to a soil structure and a crust and upper mantle structure. It is thought that this will demonstrate in which parts of the earth and over which period ranges anelastic attenuation may be significant.

A. Soils

A typical soil structure is that of San Francisco Bay mud and is shown in Table 1 of Chapter 1. Velocity and density values were measured from samples taken

from a borehole located at the Richmond Field Station
while Q values represent a best guess (Chapter 1,
Section I).

1. Love Waves

Figure 1 shows the dispersion and attenuation
parameters for Love waves over the soil structure.
The phase velocities C (E, elastic; L, including loss)
are very similar (no causality corrections applied)
and shows the anelastic phase velocity can actually
be greater than the elastic. The group velocity U_E
is the elastic because the Q structure (≈ 10) is too
low to apply the variational method of Appendix 2
meaningfully.

The Q_L curve is the phase quality factor and
has a frequency dependence similar to the elastic
group velocity curve. It is most essential, since the
group quality factor is the physically meaningful
parameter, to develop some reliable means of obtaining
the attenuating group velocity for highly attenuating
media.

2. Rayleigh Waves

In Figure 2 are shown the dispersion and attenu-
ation parameters for Rayleigh waves over the same soil
structure. In this plot we note some interesting
features. The two phase velocities, elastic and loss,
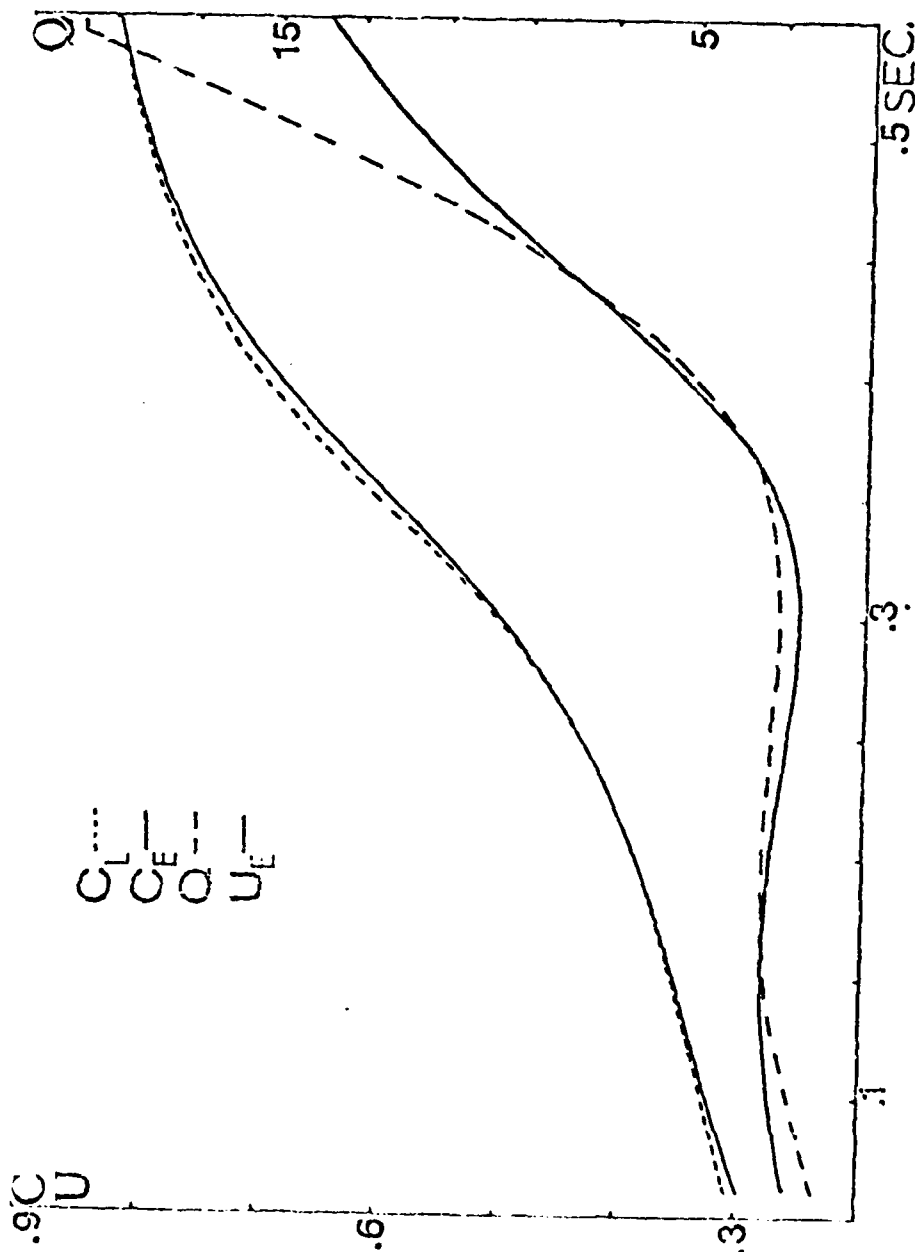
Fig. 1. Plot of phase velocity C (E, elastic; L, including loss), phase quality factory Q_L, and elastic group velocity U_E for Love waves in the Richmond soil structure (Chapter 1, Section 1, Table 1). (C, U in km/sec)
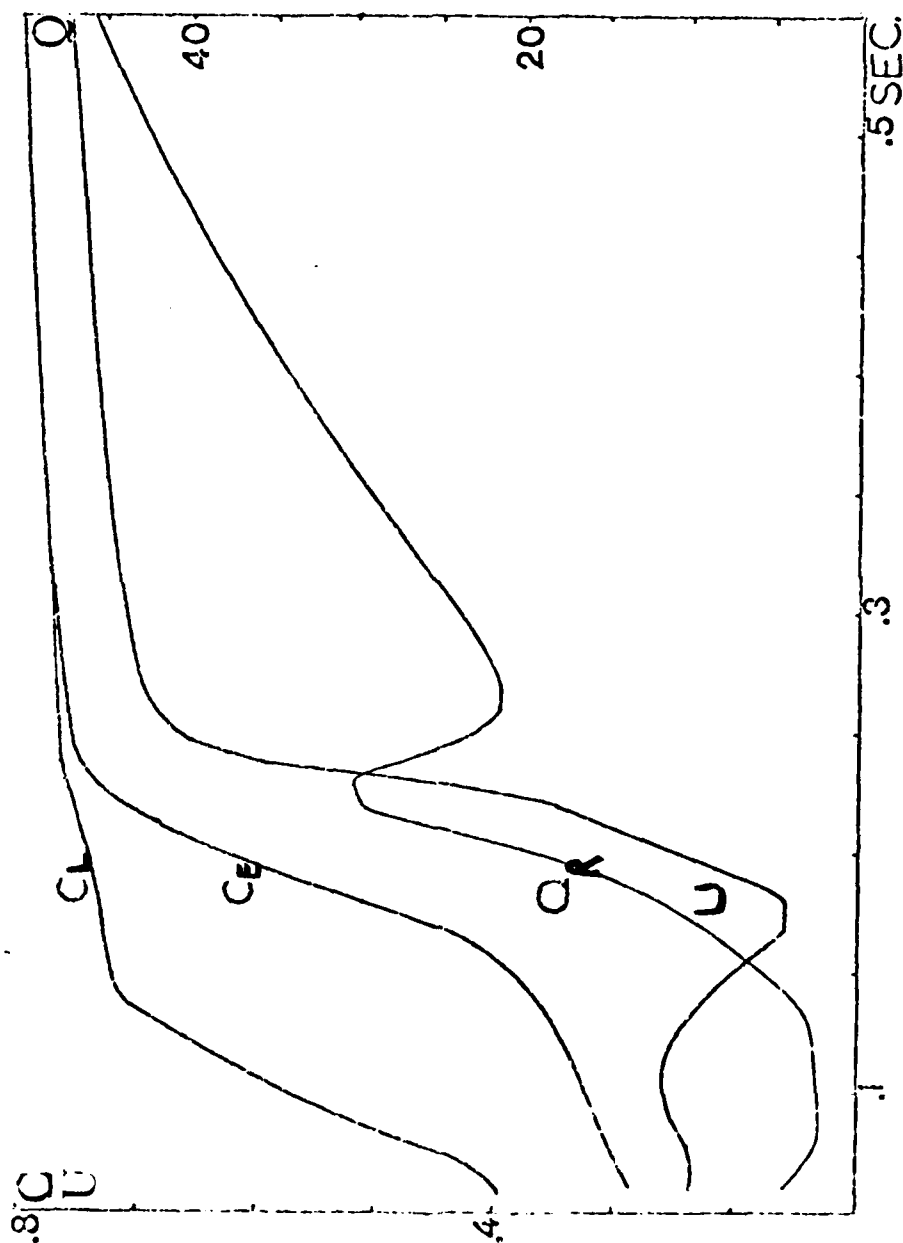
Fig. 2. Plot of phase velocity C'(E, elastic; L, including loss), phase quality factor Q_E, and elastic group velocity U_E for Rayleigh waves in the Richmond soil structure (Chapter 1, Section 1, Table 1). (C, U in km/sec)

are asymptotic at the longer periods but diverge significantly toward the shorter periods. The attenuating phase velocity (C_L) is significantly greater than the elastic at the shorter periods and actually very nearly corresponds to the first overtone elastic phase velocity for periods less than about 0.15 seconds (near the Airy phase). Meanwhile, the first overtone attenuating phase velocity corresponds nearly to the elastic fundamental phase velocity over this range. This suggests that a mode has been skipped in the calculation procedure but this does not appear to be the case because the Q_R associated with the two modes are considerably different and both appear to be continuous (a much finer sample interval was used in this range to check continuity). This presents the interesting possibility that two modes may possess the same phase velocity at some period but degeneracy is avoided through distinct attenuation factors. This may be the result of the rather large layer attenuation significantly perturbing the mode shapes. Further work along these lines is needed. These results also demonstrate the need for a means of accurately calculating the group velocity (or some more meaningful physical parameter) in highly attenuating media.

In Figure 3 is shown the phase of the surface displacement ratio U_o/W_o for the elastic and loss
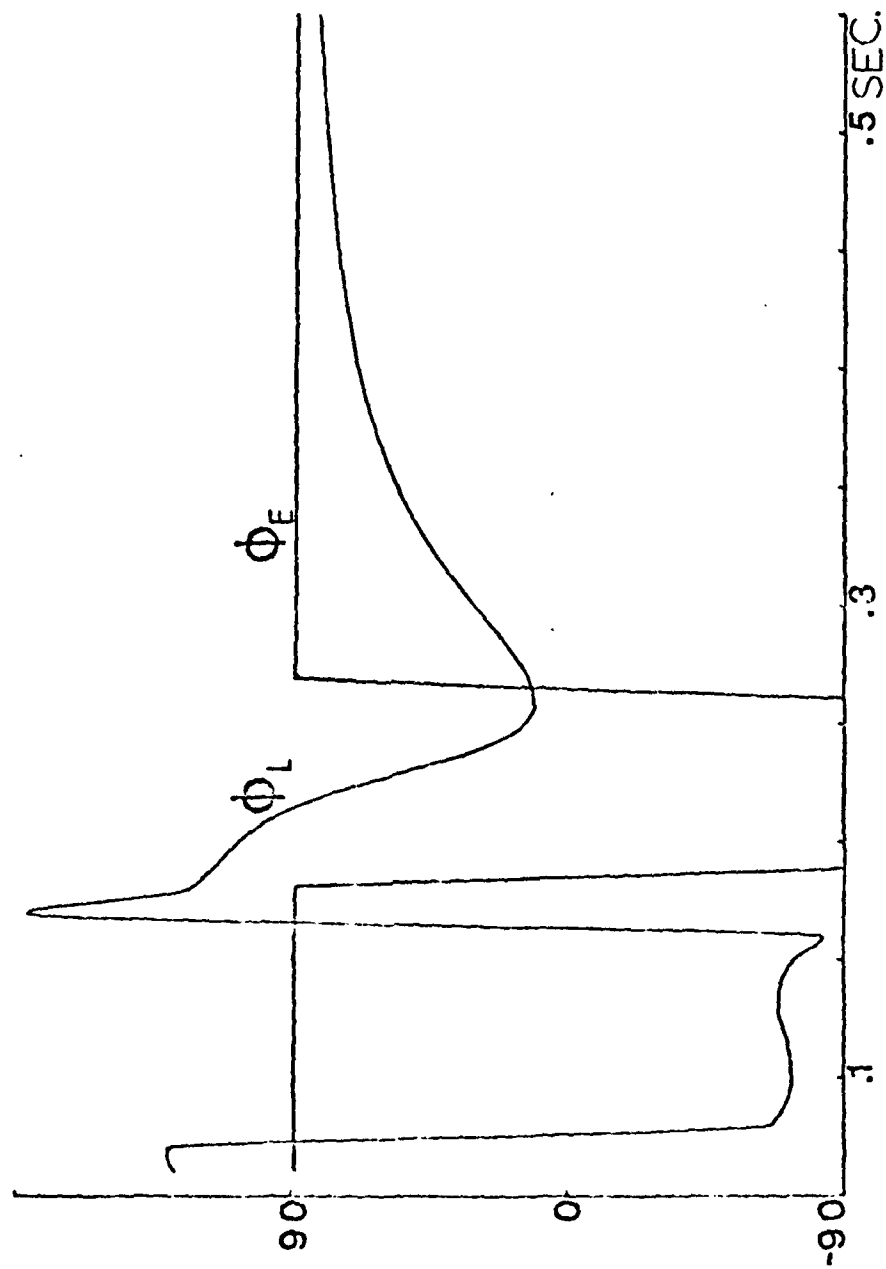
Fig. 3. Phase of the surface displacement ratio Uo/Wo (L, loss; E, elastic) for Rayleigh waves in the soil structure.
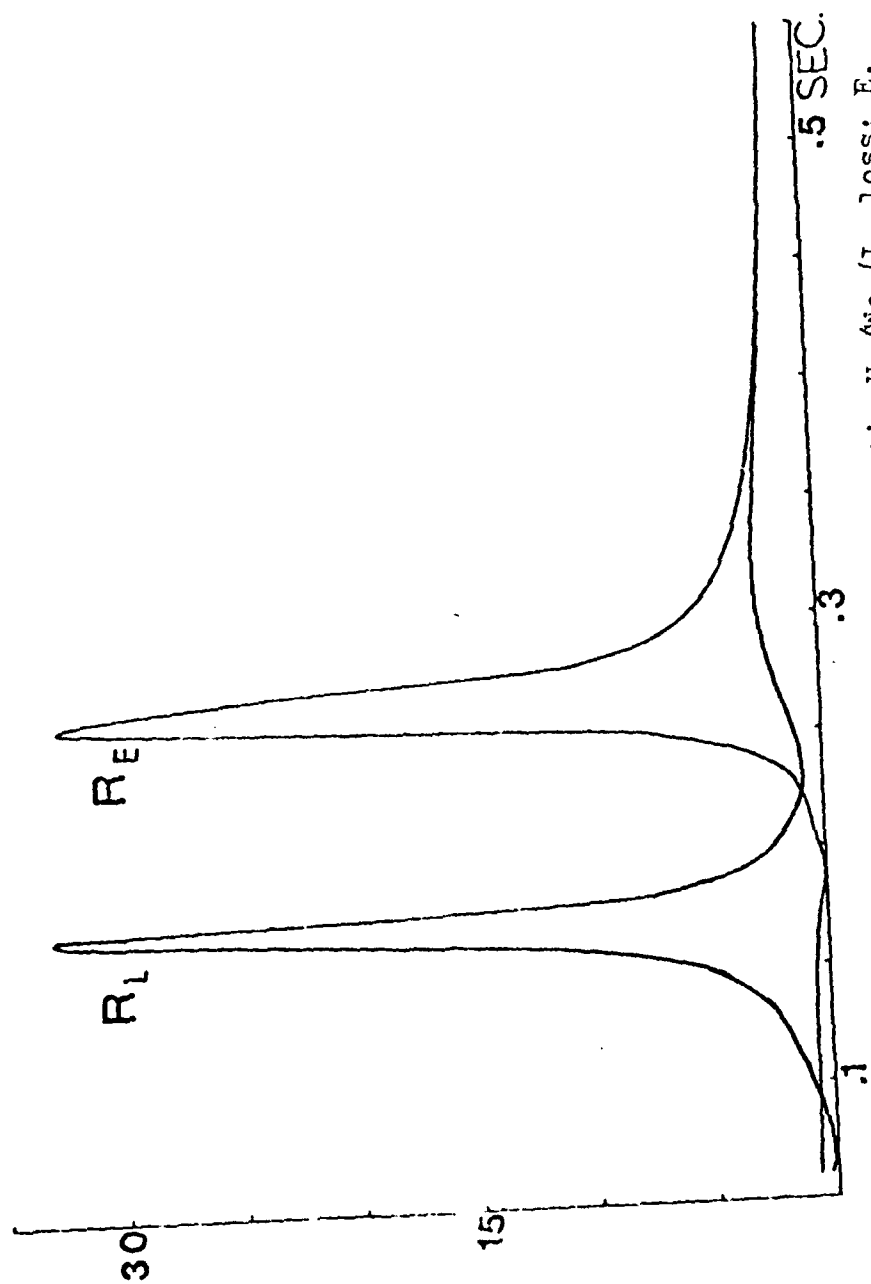
Fig. 4. Modulus of the surface displacement ratio Uo/Wo (L, loss; E, elastic) for Rayleigh waves in the soil structure.

cases. The two curves are significantly different
from each other, particularly in the region near the
Airy phase. The two moduli are shown in Figure 4.
It is interesting that the magnitude remains nearly
the same at the peak while the loss shifts it to
shorter periods (towards the Airy phase). Clearly
there are significant differences between the surface
waves for elastic and highly dissipative media, and a
complete understanding of these differences will
require more work.

B. Upper Mantle

The upper mantle elastic structure which is
investigated in this section is basically that shown in
Knopoff and Chang (1977) for a typical oceanic structure
and is listed in Table 1. An oceanic model was used
because it is appropriate for the data to be considered
in the next section, which was collected for great
circle paths that were over 70% oceanic.

The attenuation structures were chosen to be
broadly consistent with popular models yet tailored
to give a chosen starting fit for the inverse problem
considered in the next section. They are therefore
different for the two data sets considered (see
Section III).

1. Love Waves

Figure 5 shows the dispersion and attenuation
parameters for Love waves over the upper mantle struc-
ture. Again Q_L is the phase quality factor and Q_U the
group quality factor. Both the phase velocity C and
group velocity U include attenuation and are within
0.01% of the corresponding elastic results. Group
velocity is calculated as outlined in Appendix 2.
No dispersion corrections are applied (Kanamori and
Anderson, 1977) since the effect is too small to be
noticable. The SH earth stretching transformation
was applied according to the method of Schwab and
Knopoff (1972).

2. Rayleigh Waves

Figure 6 shows the same parameters for Rayleigh
waves. Again dispersion corrections are not applied.
The P-SV earth stretching transformation was applied
according to the method of Schwab and Knopoff (1972).

III. INVERSE PROBLEM

In order to apply the inversion kernels presented in
Appendix ʃ on observational data, an initial attempt
was made at inverting 400-25 sec. fundamental mode
Love and Rayleigh wave data. The data consist of phase
velocity and phase quality factors for great circle
paths through Berkeley recorded on a broadband system.

The main objective of this exercise is not to derive
a realistic upper mantle structure, but rather to
investigate the possible difficulties present in using
the exact kernels with conventionally extracted amplitude
data.

A. Data Analysis

For the Berkeley data the following procedure was
used. The record tapes are filtered to remove alias
frequencies and then digitized. Seismograms are then
group velocity windowed between 4.50 and 4.30 km/sec
for Love waves and between 4.00 and 3.45 km/sec for
Rayleigh waves. The mean is removed before spectra
are taken. Phase velocity is then determined using
the smoothed (Appendix 5) phase difference for two
great circle paths (Toksöz and Ben-Menahem, 1963).
The amplitude spectra is smoothed with a seven point
moving average and then, if necessary, further smoothed
by eye. The phase quality factors (defined by $\exp(- \frac{\omega x}{2 c Q})$;
C is the phase velocity) are determined using the single
station method (Kanamori, 1970).

The other data set was taken from Anderson et al.
(1965) with both the Love and Rayleigh wave data
augmented at the short and long periods. For Love waves
the long period data (T=400,360) are from Press et al.
(1961) the short period data (T=39.55, 36.38, 24.92)
are from two sources; the velocity data are synthetic

from Case 122 of Sykes et al. (1962) and the attenuation
data are that of Tsai and Aki (1969). The Rayleigh wave
long period data (T=400.00, 370.37) are from Ben-
Menahem and Toksöz (1962). The short period data
(T=39.29, 33.12, 24.63) are also from two sources:
the velocities are synthetic from model 8099 of Dorman
et al. (1960) while the attenuation data are from
Tsai and Aki (1969). The conversion to phase quality
factors (Q_L, Q_R) has been made according to the
equation $\frac{U}{C}\ Q_U = Q_{L,R}$ U group velocity
                                       C phase velocity.

B. Inversion Algorithm

The inversion method is simply a damped Gauss-
Newton algorithm using the fundamental decomposition
theorem (Lancsoz, 1961), as in Appendix 1 with synthetic
data, to obtain the singular values and the inverse
of the Jacobian. An overdetermined system is used
since it is assumed that the Q starting model, although
hopefully close enough for local convergence, probably
is in considerable error. The resolution matrix
(Jackson, 1972) is used along with the condition number
to guide in structure reduction and in parameter
constraint. Standard errors of the parameter adjust-
ments are calculated using the goodness of fit as an
estimate of the data variance. In order to avoid fixing
parameters at the wrong value, only those parameters
whose corrections failed to stabilize were held constant.

This allows the other parameters to adjust themselves somewhat more freely without compensating for the fixed erroneous value. This, of course, results in somewhat unreasonable values of the less well determined parameters. However, the standard errors are usually large thus keeping the parameters within acceptable bounds.

During the course of many trial and error inversions, it was found that a critical factor is the choice of layering. This makes a very good case for either of two alternatives: 1) the use of the above procedure with thickness derivatives to aid in the choice of layering; 2) the underdetermined system coupled with a suitable resolution and or stabilization method. In favor of the underdetermined system the point should be made that perhaps the same layering may not be optimum for both a velocity and attenuation inversion. Adjustments for this could easily be made in the underdetermined system simply by using different resolving kernels (Knopoff and Jackson, 1972). This must, of course, be weighed against the heavy dependence upon starting models implicit in the underdetermined system.

C. Love Waves

Figure 7 shows the spectra (a, unsmoothed and noise; b, smoothed) of the G pulses 3 through 6 for the Tang Shan event (7/27/76, $\Delta = 88^{\circ}$, M=7.5). For

the Q_L data (Figure 9) the harmonic mean of the two ratios 6/4 and 5/3 was used. The phase data (Figure 9) were taken from the 6/4 ratio only as it seemed the best behaved. The phase difference ($\Delta\phi$) of the observed and smoothed is shown in Figure 8.

In Table 1 is shown the starting model used in the inversions (Anderson et al. augmented data has a different Q starting model and is listed in appropriate tables). The model (elastic parameters) is a typical oceanic structure (Knopoff and Chang, 1977) slightly modified to aid the Love wave convergence since it is a poorer resolvent than Rayleigh waves. The Q_S structure was designed from trial and error to give the closest starting fit while being as generally consistent as possible with other results. The notable exception being the lack of a low Q layer coinciding with the low velocity layer. Any attempt to start a low Q layer there resulted in either divergence or a definite increase and slow convergence. It simply seems to be incompatible with this data. The crustal Q was fixed at 500 while the half space Q was fixed at 200. The crustal and half space velocities were also fixed due to the limited bandwidth. Allowing the half space parameters to vary did not significantly affect the layer above but resulted in less reasonable half space parameters (particularly velocities).

In Table 2 are shown the inversion results using the Berkeley data. The most significant result, which appears to be general, is the incompatibility between the velocity and amplitude data with respect to the velocity. That is, inclusion of the derivative $\dfrac{\partial Q_{L,R}}{\partial V_s}$ generally results in an unstable system. The $Q_{L,R}$ residuals are reduced at the expense of the C residuals and the system becomes unstable after several iterations (thirty-one is the maximum number of iterations in all cases). A look at sections (B) and (D) of Table 2 reveals the unfortunate dilemma. Section (B) shows the results without the derivative $\dfrac{\partial Q_L}{\partial V_s}$. The velocity structure is reasonable with the sum square residuals reduced by a factor of ten while the Q structure shows a high Q lid with a broad low Q zone below the low velocity layer and the sum square residuals reduced by 1/3. The large discrepancy between the residual reduction in the velocity and in the attenuation might be an indication that the amplitude data is also not representative of the Q structure. Section (D) shows the results including the derivative $\dfrac{\partial Q_L}{\partial V_s}$ which became unstable after the ninth iteration. Note the phase velocity residuals have not been reduced while the Q residuals are reduced by another 1/3 over section (B). A look at the standard errors of the velocities (ΔV_s) for both cases shows generally smaller values when the derivative $\dfrac{\partial Q_L}{\partial V_s}$ is included in spite of the

much larger residuals. This indicates more information

(orthogonal to $\frac{\partial c}{\partial V_s}$) as discussed in Appendix 1;

however, a look at the two velocity structures shows

that this information is not compatible. In section

(C) is shown the same conditions as in (B) without the

dispersion correction applied. The result is a more

pronounced low velocity layer (Hart et al., 1976) with

generally lower velocities throughout. The Q structure

is also somewhat different, as expected, but still

generally indicates a broad low Q zone below the low

velocity layer. Figure 10 shows the corrected data

along with the phase velocity and phase quality factor

for the derived model of section (B).

In Table 3 are shown the inversion results with

the augmented Anderson et al. Love wave data. Here

only two cases are shown: (B) without the derivative

$\frac{\partial Q_L}{\partial V_s}$ and; (C) including the derivative with dispersion

corrections applied in both cases. The starting model

(A) has a different Q_S structure which was based on

the Q_L data (data listed in Table 6). The general

pattern is very similar to the Berkeley data. Neither

the velocity nor the Q_S structure are significantly

different; however, this Q_S structure is generally

lower with a much more attenuating lid. Again, there

is no low Q zone corresponding to the low velocity

layer but rather a very broad low Q zone below the

layer. Also, a look at section (C) which includes

the derivative $\dfrac{\partial Q_L}{\partial V_s}$ reveals a similar pattern to the
Berkeley data. The Q_L residuals were reduced at the
expense of the increased C residuals, a different
velocity structure, and an unstable system after six
iterations. This indicates that the augmented Anderson
et al. (1965) Q_L data is also inconsistent with respect
to velocity. Also, the poor Q_L residuals in section (B)
indicate that the Q_L data may not be consistent with
respect to a Q_s structure. The data and fit are shown
in Figure 11.

D. Rayleigh Waves

Figure 12 shows the spectra (a, unsmoothed and
noise; b, smoothed) for R_1 and R_3 for the Indonesian
event (8/19/77, Δ=118°, M=8.0). Due to noise and system
problems only R_1 and R_3 were used for Q_R while R_2 and
R_4 were used for the phase data. Figure 13 shows the
phase difference $\Delta\phi$ and the smoothed fit.

Table 4 shows the results for the Berkeley data.
The starting model (A) is the same as in the Love wave
case using the Berkeley data. The starting Q_p structure
is simply 2.25 Q_s and is an inversion parameter set
(Appendix 2). The V_p structure is varied by maintaining
a fixed starting Poisson's ratio. The density remains
fixed. For the Rayleigh wave inversions it was found
necessary to vary the half space parameters to allow
the layer above to converge to a reasonable velocity.

Twenty-four was the maximum number of iterations
used in all Rayleigh wave inversions.

In section (B) of Table 4 are shown the results
without the derivative $\frac{\partial Q_R}{\partial V_S}$. The residuals have been
reduced nicely; one order for Q_R and two orders for C.
However, both the Q_S and V_S structures show oscillations
which are probably due to non-optimum layering. Since
the layering was guided by the Love wave resolution
matrix only (because they have poorer resolution than
Rayleigh waves (Appendix 1)) and since the resolution
matrix is made up of partial derivatives which have
different shapes for the wave types, a different layering
is probably required for the case of Rayleigh waves.
This also makes another argument for the use of an
underdetermined system. Figure 14 shows the data and
the model fit.

In section (C) of Table 4 are shown the results
including the derivative $\frac{\partial Q_R}{\partial V_S}$. Again, the results are
very similar to the Love wave inversions. The system
becomes unstable, the C residuals are not significantly
reduced, and the solution becomes more oscillatory in
the velocity. This indicates that the Q_R and C are
competing for different velocity structures. Again,
since the Q_R residual in section (B) has not been
reduced as significantly as the C residual, it may
indicate that the Q_R data is not representative of the
attenuation in the earth.

Turning now to the augmented Anderson et al. (1965)
data, the results are shown in Table 5. Section (A)
shows the starting model which is identical to the Love
wave case for the same data. As in the previous case
the solution is oscillatory though stable when the
derivative $\frac{\partial Q_R}{\partial V_s}$ is not included (section (B)) and
unstable with respect to velocity when the derivative
is included (section (C)). No further conclusions should
be drawn from the Rayleigh wave analysis, especially
with regard to parameter values.

IV.   CONCLUSION

Concerning the forward calculations, some inter-
esting features were noted for Rayleigh waves in high
loss material. It appears that, near the Airy phase,
the loss can significantly perturb mode shapes such
that the phase velocity can become multi-valued.
Degeneracy is avoided through distinct attenuation
factors for each mode. These observations are pre-
liminary and clearly more work needs to be done. Also,
a reliable means of determining group velocity for such
high loss material must be developed.

In the inverse problem investigations, probably
the most salient result is the incompatibility of the
Q data with the C data with respect to the velocity
structure. The incompatibility is expressed through

the derivative $\frac{\partial Q_{L,R}}{\partial V_s}$, its inclusion rendering the system unstable in velocity and adversely affecting the C residuals. The fact that the $Q_{L,R}$ residuals are much larger than the C residuals when the derivative $\frac{\partial Q_{L,R}}{\partial V_s}$ is neglected also indicates that conventionally extracted surface wave Q data probably are in considerable error. The error is probably due to multi-path propagation and affects the spectral modulus to a greater degree than the phase (Pilant and Knopoff, 1964). A method of accurate amplitude determination which seems hopeful is that of phase-matched filters (Herrin and Goforth, 1977) and future work will be undertaken along these lines.

Another result which emerges from the inversion investigations is the possible inadequacy of the overdetermined system. It appears that it would be most difficult to derive a layering that is simultaneously optimum for velocity and attenuation with both Love and Rayleigh waves. To optimize the Love and Rayleigh layering, a simultaneous inversion seems appropriate, but this does not resolve the velocity and attenuation layering problem. Some investigations are needed into the development of a suitable underdetermined formulation with its heavy dependence on starting models.

Another approach, if a model rather than local averages is desired, might be the use of a suitable

non-linear algorithm such as the Marquardt-Levenberg
(Marquardt, 1963). Perhaps this algorithm would
tolerate a larger condition number (more layers) thereby
reducing the layering incompatibility.

CHAPTER 3

SUMMARY

Lately, albeit belatedly (Jeffreys, 1965), it
has become apparent that the earth can no longer be
treated as an elastic body. An essential point of this
work has been to establish that it is equally insuf-
ficient to treat it as a perturbation on an elastic
body.

An exact plane layer propagator matrix which
includes attenuation was presented. Application of
the formulation to continue an incident elastic wave
through a realistic soil structure to the earth's
surface, demonstrated the importance of energy
absorption in predicting ground motion. The minor
importance of converted waves was demonstrated and
it was further shown that lateral propagation, not
included in the formulation, can affect the duration
of motion. In addition to time domain analysis,
spectral ratios (surface to bedrock) show fair agree-
ment with model calculations.

In applying the matrix formulation to surface
wave eigenvalue and surface displacement calculations,
several results were discussed. It appears that
attenuation perturbs Rayleigh waves significantly more
than Love waves in a high loss structure. In par-
ticular, different mode phase velocities may cross

near the Airy phase. Degeneracy is avoided, however,
through distinct quality factors.

Surface wave inversions for both velocity and
attenuation structures using an overdetermined system
revealed an incompatibility with respect to the
velocity structure between phase and attenuation data.
In particular inclusion of the derivative $\dfrac{\partial Q_{L,R}}{\partial V_s}$
with real data greatly degraded the velocity solution
compared to inversions using only the derivative
$\dfrac{\partial C}{\partial V_s}$.. Poor attenuation solutions compared with
velocity solutions further indicates the inadequacy
of presently used attenuation data. Clearly a reliable
formulation is needed in order to extract meaningful
amplitude data from surface wave observations.

Of particular concern in dealing with an over-
determined system which also bears on the quality of
attenuation solutions, is the choice of layering.
This appears to be critical at least for the velocity
structure. The same layering may not be optimum for
both Love and Rayleigh waves in addition to both
velocity and attenuation structures.

The general conclusion of this thesis is that
amplitude information is most essential in furthering
our understanding of both the velocity and attenuation
structures of the earth. It has also been demonstrated
that realistic calculations with earth materials require

simultaneous consideration of both velocity and attenuation.

TABLE 1

Starting model for both Love and Rayleigh wave
inversions. The model is based on a typical oceanic
structure (Knopoff and Chang, 1977). The low velocity
layer thickness was increased 20 km at the expense of
the layer below to aid convergence in the Love wave
inversions (Berkeley data).

V_p(km/sec)	V_s(km/sec)	(cgs)	Q_p	Q_s	thickness (km)
2.10	1.00	2.10	1200	500	1.0
6.41	3.70	3.07	1200	500	5.0
8.10	4.65	3.40	4500	2000	70.0
7.60	4.15	3.40	425	200	130.0
8.80	4.75	3.65	275	125	240.0
9.80	5.30	3.98	225	100	200.0
11.15	6.20	4.43	225	100	400.0
11.78	6.48	4.63	350	150	240.0
12.02	7.20	4.71	450	200	∞

Fluid layer included in Rayleigh calculation

1.50	0.00	1.00	1200		4.0

TABLE 2

Results of Love wave inversions with Berkeley data: A) starting model; B) inversion without the derivative $\frac{\partial Q_L}{\partial V_s}$ with dispersion correction applied; C) inversion without both the derivative $\frac{\partial Q_L}{\partial V_s}$ and dispersion correction; D) inversion including both the derivative $\frac{\partial Q_L}{\partial V_s}$ and dispersion correction. (ΔQ_s, ΔV_s = standard error; SSRQ, C = sum square residual $Q_{R,L}$, $C_{R,L}$; (I), (F) = initial, final; NI = number of iterations).

	Layer	Q_s	ΔQ_s	V_s	ΔV_s		SSRQ	SSRC	NI
	1	500		1.00					
	2	500		3.70					
	3	2000		4.65					
	4	200		4.15					
A	5	125		4.75					
	6	100		5.30					
	7	100		6.20					
	8	150		6.48					
	9	200		7.20					
	1	500		1.00					
	2	500		3.70					
	3	2289	20050	4.47	0.02				
	4	165	129	4.32	0.03	(I)	6.0	7.0×10^{-4}	31
B	5	144	100	4.62	0.02	(F)	2.0	4.0×10^{-5}	
	6	84	142	5.37	0.08				
	7	80	159	6.77	0.10				
	8	126	85	7.02	0.07				
	9	200		7.20					
	1	500		1.00					
	2	500		3.70					
	3	2090	47413	4.47	0.06				
	4	196	368	4.29	0.06				
C	5	124	46	4.55	0.02	(I)	6.0	2.0×10^{-3}	31
	6	102	156	5.36	0.07	(F)	2.0	5.0×10^{-5}	
	7	87	167	6.57	0.10				
	8	144	82	6.80	0.06				
	9	200		7.20					

TABLE 2 (continued)

	Layer	Q_s	ΔQ_s	V_s	ΔV_s		SSRQ	SSRC	NI
	1	500		1.00					
	2	500		3.70					
	3	194	5854	4.42	0.00				
	4	198	127	4.44	0.00	(I)	6.0	7.0×10^{-4}	9
D	5	122	51	4.46	0.01	(F)	1.0	7.0×10^{-4}	
	6	97	56	5.70	0.08				
	7	99	22	6.23	0.10				
	8	151	13	6.52	0.08				
	9	200		7.20					

TABLE 3

Results of Love wave inversions with augmented
Anderson et al. (1965) data: A) starting model
(different Q_s structure only); B) inversion without
the derivative $\frac{\partial Q_L}{\partial V_s}$; C) inversion including the
derivative $\frac{\partial Q_L}{\partial V_s}$. Dispersion corrections applied in
all cases.

	Layer	Q_s	ΔQ_s	V_s	ΔV_s		SSRQ	SSRC	NI
A	1	500		1.00					
	2	500		3.70					
	3	500		4.65					
	4	100		4.15					
	5	100		4.75					
	6	100		5.30					
	7	100		6.20					
	8	100		6.48					
	9	200		7.20					
B	1	500		1.00					
	2	500		3.70					
	3	423	3470	4.99	0.06				
	4	126	77	4.18	0.01				
	5	88	124	4.43	0.04	(I)	14	3.0×10^{-3}	31
	6	108	393	5.66	0.11	(F)	12	4.0×10^{-4}	
	7	88	429	6.18	0.19				
	8	129	203	6.33	0.10				
	9	200		7.20					
C	1	500		1.00					
	2	500		3.70					
	3	505	871	4.66	0.02				
	4	102	113	4.37	0.00				
	5	101	132	4.56	0.03	(I)	14	3.0×10^{-3}	6
	6	104	76	5.51	0.14	(F)	7	2.0×10^{-3}	
	7	104	40	5.94	0.13				
	8	156	21	6.21	0.14				
	9	200	94	7.20					

TABLE 4

Results of Rayleigh wave inversions with Berkeley data: A) starting model; B) inversion without the derivative $\frac{\partial Q_R}{\partial V_s}$; C) inversion including the derivative $\frac{\partial Q_R}{\partial V_s}$. Dispersion corrections applied in all cases.

	Layer	Q_s	ΔQ_s	Q_p	ΔQ_p	V_s	ΔV_s	V_p		SSRQ	SSRC	NI
A	1	500		1200		0.00		1.52				
	2	500		1200		1.00		2.10				
	3	500		1200		3.70		6.41				
	4	2000		4500		4.65		8.10				
	5	200		425		4.15		7.60				
	6	125		275		4.75		8.80				
	7	100		225		5.30		9.80				
	8	100		225		6.20		11.15				
	9	150		350		6.48		11.78				
	10	200		450		7.20		12.82				
B	1	500		1328	18956	0.00		1.52				
	2	500		1329	152452	1.00		2.10				
	3	500		1304	40199	3.70		6.41				
	4	366	104	4604	314	4.21	0.01	7.33				
	5	172	6	394	79	4.08	0.01	7.49	(I)	4.0	7.0×10^{-2}	
	6	69	5	322	35	4.99	0.02	9.24	(F)	.4	5.0×10^{-4}	24
	7	595	436	197	24	4.66	0.05	8.62				
	8	224	37	66	3	6.73	0.06	12.00				
	9	27	10	229	1	7.32	0.08	13.31				
	10	67	1	447	0	7.35	0.00	13.09				
C	1	500		1098	5225	0.00		1.52				
	2	500		1095	38155	1.00		2.10				
	3	500		1161	7962	3.70		6.41				
	4	745	217	4409	324	4.39	0.06	7.64				
	5	126	8	538	62	3.80	0.03	6.96	(I)	4.0	7.0×10^{-2}	24
	6	77	13	322	22	5.73	0.07	10.62	(F)	.6	2.0×10^{-2}	
	7	230	194	229	31	4.47	0.13	8.26				
	8	176	23	217	4	6.36	0.24	11.44				
	9	70	18	341	14	7.60	0.33	13.82				
	10	194	1	449	0	8.28	0.10	14.74				

TABLE 5

Results of Rayleigh wave inversions with augmented Anderson et al. (1965) data: A) starting model (same as Love wave in Table 4); B) inversion without the derivative $\frac{\partial Q_R}{\partial V_s}$; C) inversion including the derivative $\frac{\partial Q_R}{\partial V_s}$. Dispersion corrections applied in all cases.

	Layer	Q_s	ΔQ_s	Q_p	ΔQ_p	V_s	ΔV_s	V_p		SSRQ	SSRC	NI
A	1	500		1200		0.00		1.52				
	2	500		1200		1.00		2.10				
	3	500		1200		3.70		6.41				
	4	500		1200		4.65		8.10				
	5	100		225		4.15		7.60				
	6	100		225		4.75		8.80				
	7	100		225		5.30		9.80				
	8	100		225		6.20		11.15				
	9	150		350		6.48		11.78				
	10	200		450		7.20		12.82				
B	1	500		1348	39573	0.00		1.52				
	2	500		1341	144248	1.00		2.10				
	3	500		982	67967	3.70		6.41				
	4	2017	4426	1040	7909	4.27	0.03	7.71				
	5	91	24	363	1082	4.66	0.03	8.53	(I)	8.0	2.0×10^{-2}	24
	6	213	131	309	612	4.28	0.04	7.94	(F)	2.0	2.0×10^{-3}	
	7	118	112	274	190	6.35	0.39	11.73				
	8	503	2106	141	221	5.48	0.31	9.86				
	9	103	79	242	118	7.63	1.47	13.88				
	10	67	60	431	3	8.33	0.14	14.83				
C	1	500	.	1175	94	0.00		1.52				
	2	500		1138	663	1.00		2.10				
	3	500		1122	254	3.70		6.41				
	4	165	14	1339	14	4.23	0.09	7.36				
	5	84	6	296	9	4.74	0.01	8.69	(I)	8.0	2.0×10^{-2}	24
	6	196	15	366	3	4.14	0.06	7.66	(F)	.1	3.0×10^{-2}	
	7	149	11	364	3	6.28	0.23	11.62				
	8	325	3	68	1	5.75	0.16	10.33				
	9	112	6	211	1	5.78	0.36	10.51				
	10	68	0	441	0	8.15	0.02	14.52				

TABLE 6

Data used in inversions: A) Berkeley data;
B) augmented Anderson et al. (1966) data.

	Love				Rayleigh		

A)

T	Q_L	C	C_{cor}	T	Q_R	C	C_{cor}
409.6	88	5.609	5.695	384.0	96	5.895	5.976
341.3	99	5.349	5.417	341.3	108	5.504	5.569
292.6	111	5.177	5.234	307.2	116	5.229	5.285
256.0	120	5.055	5.105	279.3	124	5.026	5.075
227.6	128	4.964	5.008	256.0	129	4.869	4.914
204.8	135	4.894	4.934	236.3	131	4.746	4.788
186.2	141	4.838	4.875	219.4	131	4.646	4.686
170.7	145	4.792	4.827	204.8	130	4.563	4.602
157.5	150	4.755	4.787	192.0	128	4.493	4.531
146.3	156	4.723	4.753	180.7	124	4.433	4.472
136.5	161	4.696	4.725	170.7	120	4.382	4.420
128.0	166	4.674	4.701	161.7	117	4.336	4.374
120.5	169	4.654	4.679	153.6	114	4.296	4.334
113.8	174	4.637	4.662	146.3	112	4.259	4.297
107.8	177	4.622	4.646	139.6	111	4.225	4.263
102.4	181	4.609	4.632	133.6	110	4.194	4.231
97.5	185	4.598	4.619	128.0	110	4.165	4.202
93.1	189	4.588	4.609	122.9	111	4.138	4.174
89.0	192	4.579	4.599	118.2	113	4.112	4.146
85.3	196	4.572	4.592	113.8	116	4.088	4.120
81.9	198	4.565	4.584	109.7	120	4.064	4.095
78.8	201	4.559	4.577	105.9	124	4.042	4.071
75.8	203	4.553	4.571	102.4	130	4.020	4.048
73.1	206	4.548	4.565	99.1	136	3.999	4.025
70.6	208	4.543	4.560	96.0	143	3.979	4.004
68.3	209	4.538	4.555	93.1	149	3.961	3.983
66.1	211	4.534	4.549	90.4	156	3.942	3.964
64.0	213	4.529	4.545	87.8	164	3.925	3.945
62.1	216	4.525	4.540	85.3	172	3.909	3.928
60.2	217	4.520	4.535	83.0	180	3.894	3.912

TABLE 6 (continued)

T	Q_L	C	C $_{cor}$	T	Q_R	C	C $_{cor}$
58.5	222	4.516	4.530	80.8	187	3.880	3.987
56.9	227	4.511	4.525	78.7	193	3.867	3.883
55.4	233	4.507	4.521	76.8	200	3.855	3.871
53.9	237	4.503	4.516	71.4	220	3.827	3.841
52.5	244	4.499	4.511	68.3	234	3.814	3.827
51.2	250	4.495	4.507	65.4	243	3.806	3.818
49.9	259	4.491	4.503	62.7	253	3.802	3.813
48.8	271	4.488	4.499	59.1	266	3.801	3.811
47.6	281	4.485	4.495	56.9	270	3.803	3.813
46.6	294	4.482	4.492	53.9	280	3.808	3.817
45.5	311	4.497	4.489	51.2	282	3.812	3.821
44.5	329	4.478	4.486	48.8	275	3.814	3.823
43.6	350	4.476	4.484	46.5	280	3.812	3.820
42.7	367	4.475	4.482	44.5	283	3.806	3.815
41.8	375	4.474	4.481	42.7	288	3.799	3.807
40.9	380	4.473	4.480	40.4	279	3.789	3.797
40.2	386	4.472	4.479	36.1	320	3.782	3.788
34.7	466	4.465	4.470	29.3	321	3.823	3.788
30.1	497	4.452	4.457	25.2	369	3.737	3.737
26.6	547	4.455	4.459				

B)

T	Q_L	C	C $_{cor}$	T	Q_R	C	C $_{cor}$
400.0	112	5.500	5.565	400.0	138	5.985	6.042
360.0	110	5.380	5.443	370.4	147	5.760	5.811
333.3	113	5.307	5.366	333.3	189	5.548	5.581
312.5	114	5.243	5.300	312.5	170	5.383	5.422
294.1	115	5.185	5.240	294.1	156	5.251	5.292
277.8	113	5.134	5.189	277.8	157	5.132	5.171
263.2	112	5.088	5.142	263.2	149	5.012	5.052
250.0	113	5.046	5.098	250.2	142	4.917	4.958
238.1	114	5.008	5.059	238.1	144	4.824	4.863
227.3	116	4.972	5.021	227.3	138	4.754	4.793
217.4	115	4.940	4.988	217.4	140	4.674	4.712
208.3	115	4.911	4.959	208.3	136	4.616	4.654
200.0	116	4.885	4.931	200.0	137	4.569	4.606
192.3	117	4.861	4.906	192.3	134	4.517	4.554
185.2	117	4.840	4.885	185.2	136	4.469	4.504
178.6	118	4.821	4.865	178.6	137	4.436	4.470
172.4	118	4.805	4.848	172.4	138	4.407	4.441
166.7	119	4.790	4.332	166.7	138	4.374	4.407
161.3	116	4.776	4.819	161.3	140	4.348	4.380
156.2	117	4.761	4.303	156.2	141	4.319	4.350

TABLE 6 (continued)

T	Q_L	C	C	T	Q_R	C	C
151.5	116	4.748	4.789	151.5	142	4.299	4.329
125.0	101	4.690	4.734	125.0	132	4.250	4.281
113.6	102	4.673	4.715	113.6	140	4.196	4.224
104.2	106	4.662	4.701	104.2	145	4.173	4.199
96.2	113	4.652	4.688	96.2	139	4.167	4.193
89.3	120	4.650	4.683	89.3	135	4.159	4.185
83.3	122	4.627	4.658	83.3	129	4.167	4.194
78.1	118	4.613	4.644	78.1	128	4.169	4.195
73.5	106	4.603	4.637	73.5	128	4.160	4.185
69.4	100	4.595	4.630	69.4	127	4.170	4.195
65.8	95	4.588	4.624	65.8	125	4.163	4.188
62.5	95	4.577	4.612	62.5	121	4.159	4.184
59.5	95	4.558	4.592	59.5	117	4.155	4.180
56.8	96	4.539	4.572	56.8	115	4.150	4.175
54.3	98	4.522	4.554	54.3	116	4.145	4.169
52.1	101	4.519	4.549	51.2	118	4.141	4.164
50.0	105	4.498	4.526	50.0	122	4.136	4.158
39.6	164	4.490	4.506	39.3	151	3.985	4.000
36.4	246	4.480	4.490	33.1	170	3.988	4.000
24.9	492	4.460	4.464	24.6	166	3.980	3.990
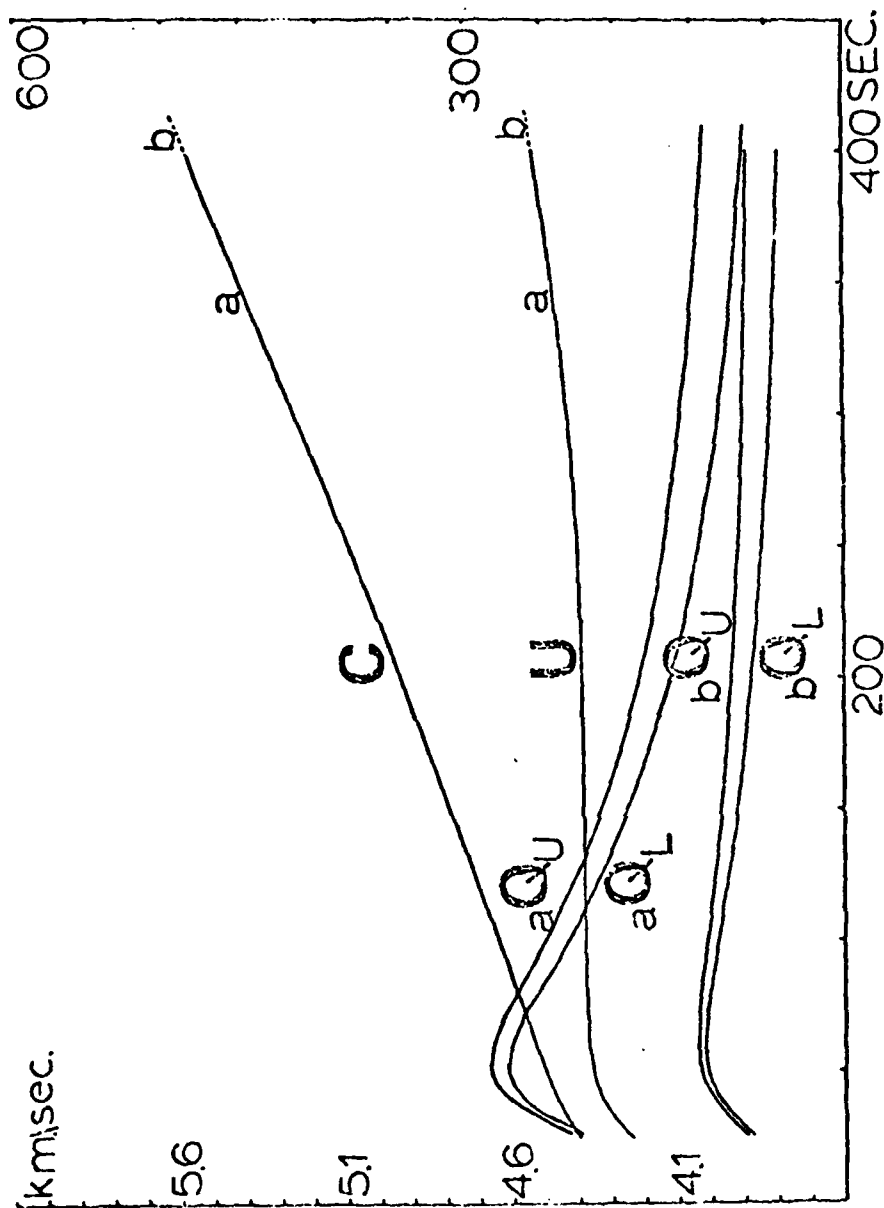
Fig. 5. Plot of phase velocity C, phase velocity factor Q_L, group quality factor Q_U, and group velocity U for Love waves in a typical oceanic upper mantle; a) Berkeley data structure in Table 1; b) Anderson et al. (1966) data structure in Tables 1 and 3.
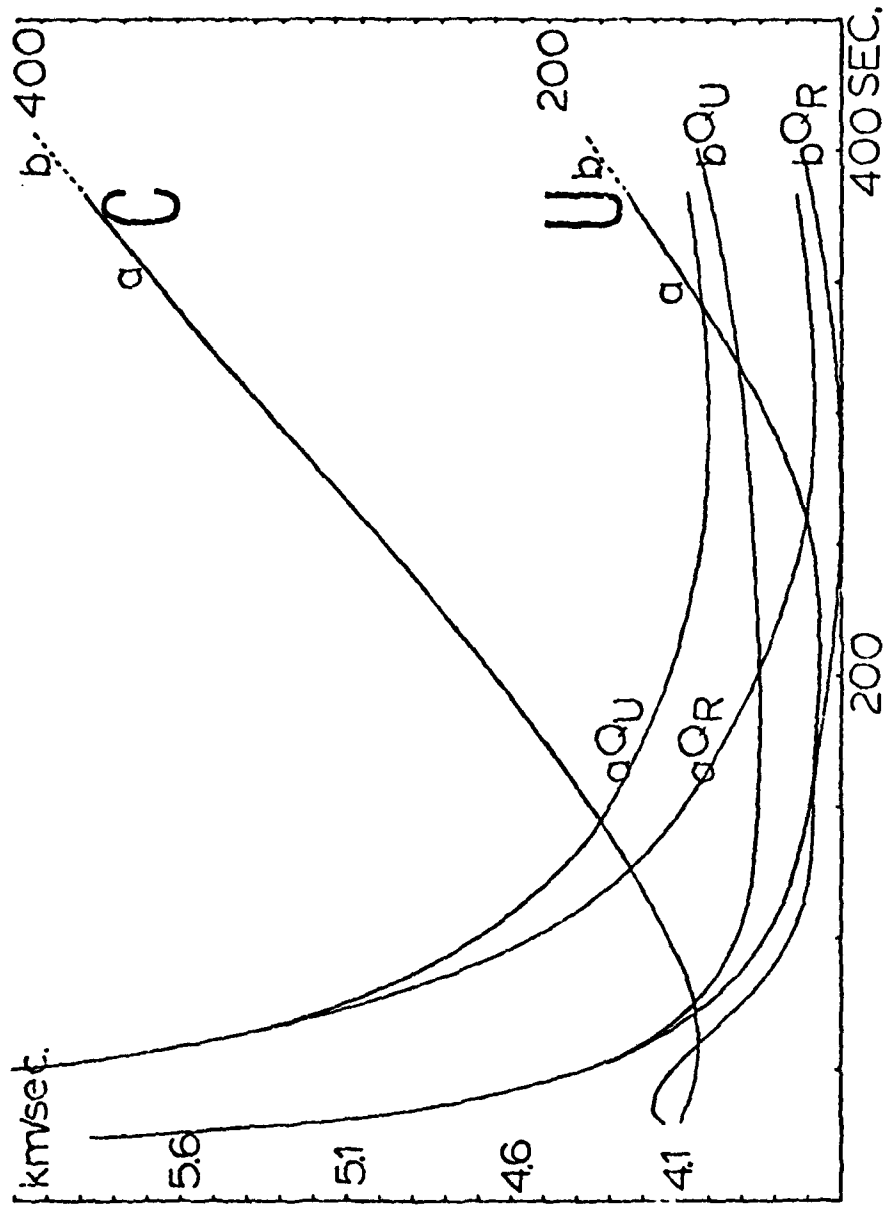
Fig. 6. Plot of phase velocity C, phase quality factor Q_L, group quality factor Q_U and group velocity U for Rayleigh waves in a typical oceanic upper mantle: a) Berkeley data structure in Table 1; b) Anderson et al. (1966) data structure in Tables 1 and 5.
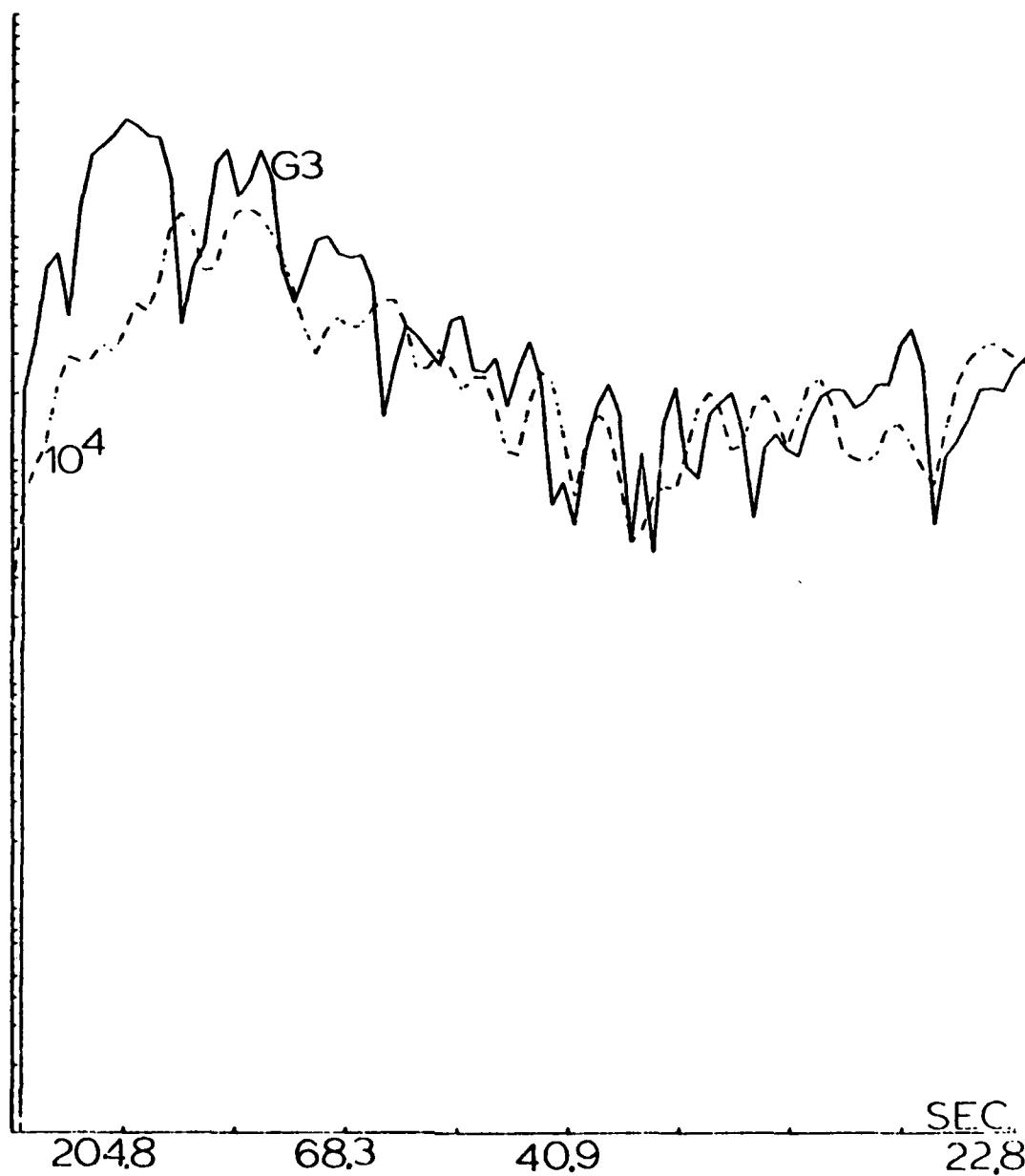
Fig. 7 a.   Plots of the G pulse spectrums.   Dashed curve
is a noise sample windowed leading the pulse.

G4

10^4

204.8   68.3   40.9   SEC.
22.8

G5

10^4

204.8   68.3   40.9   SEC. 22.8
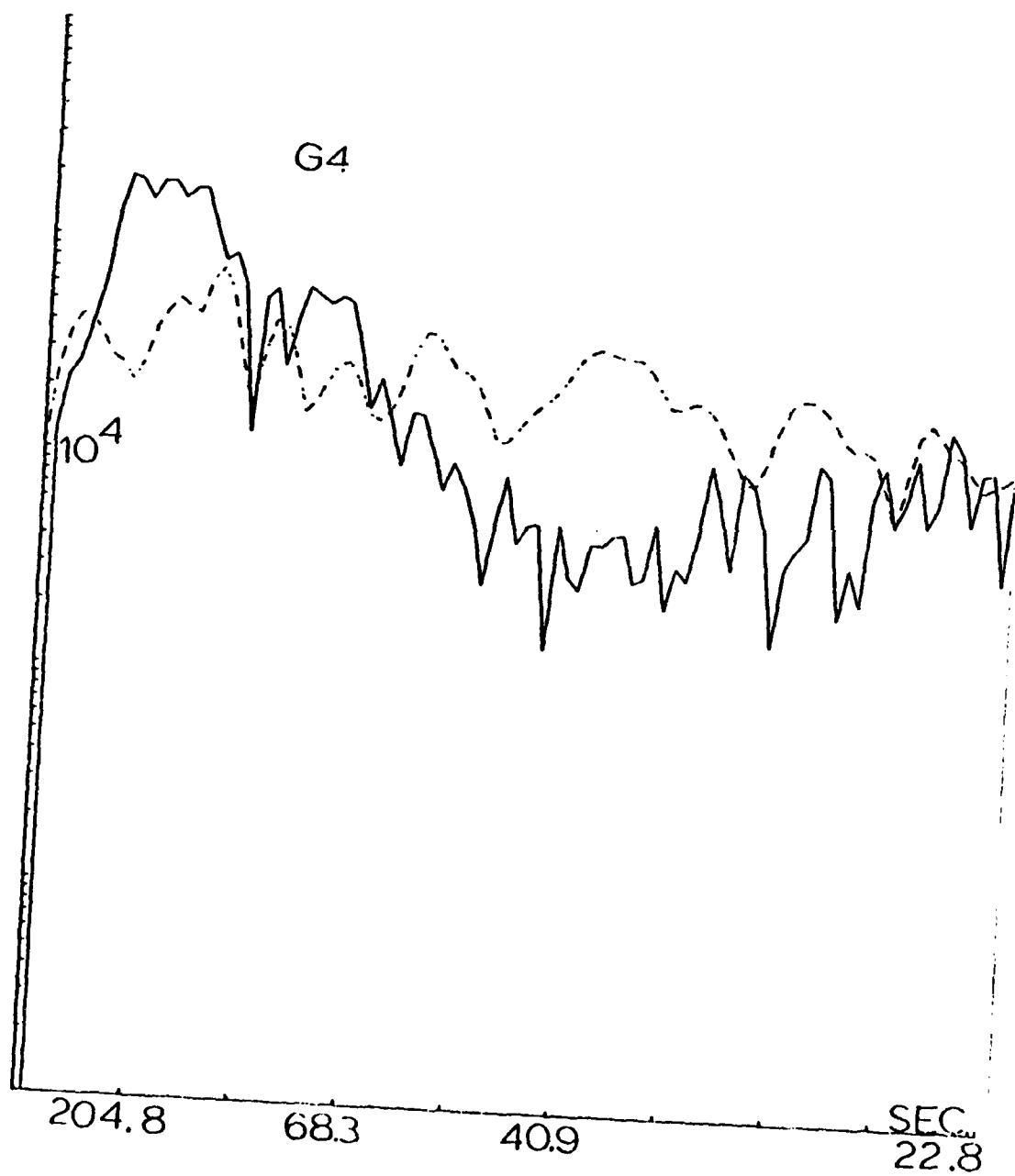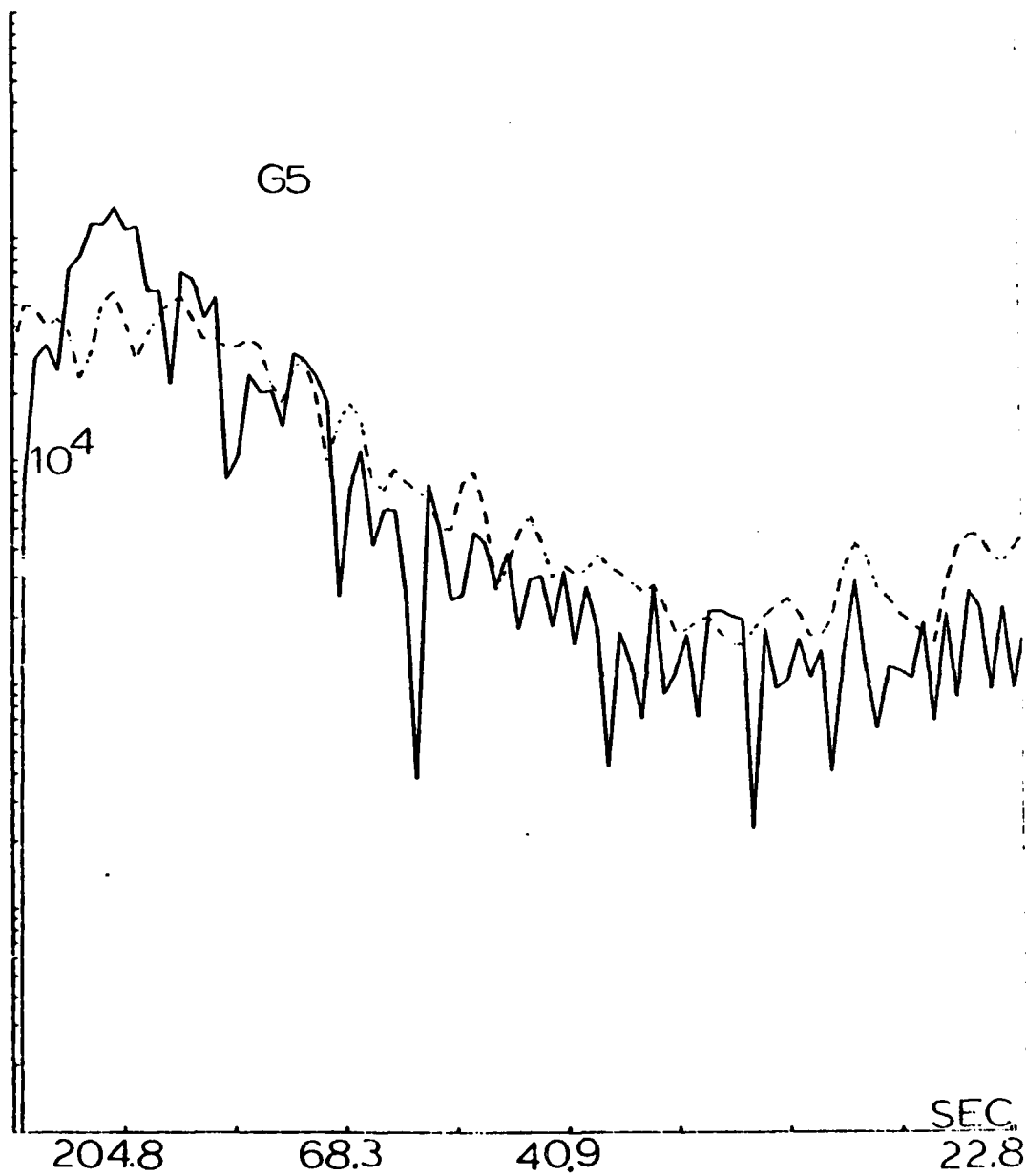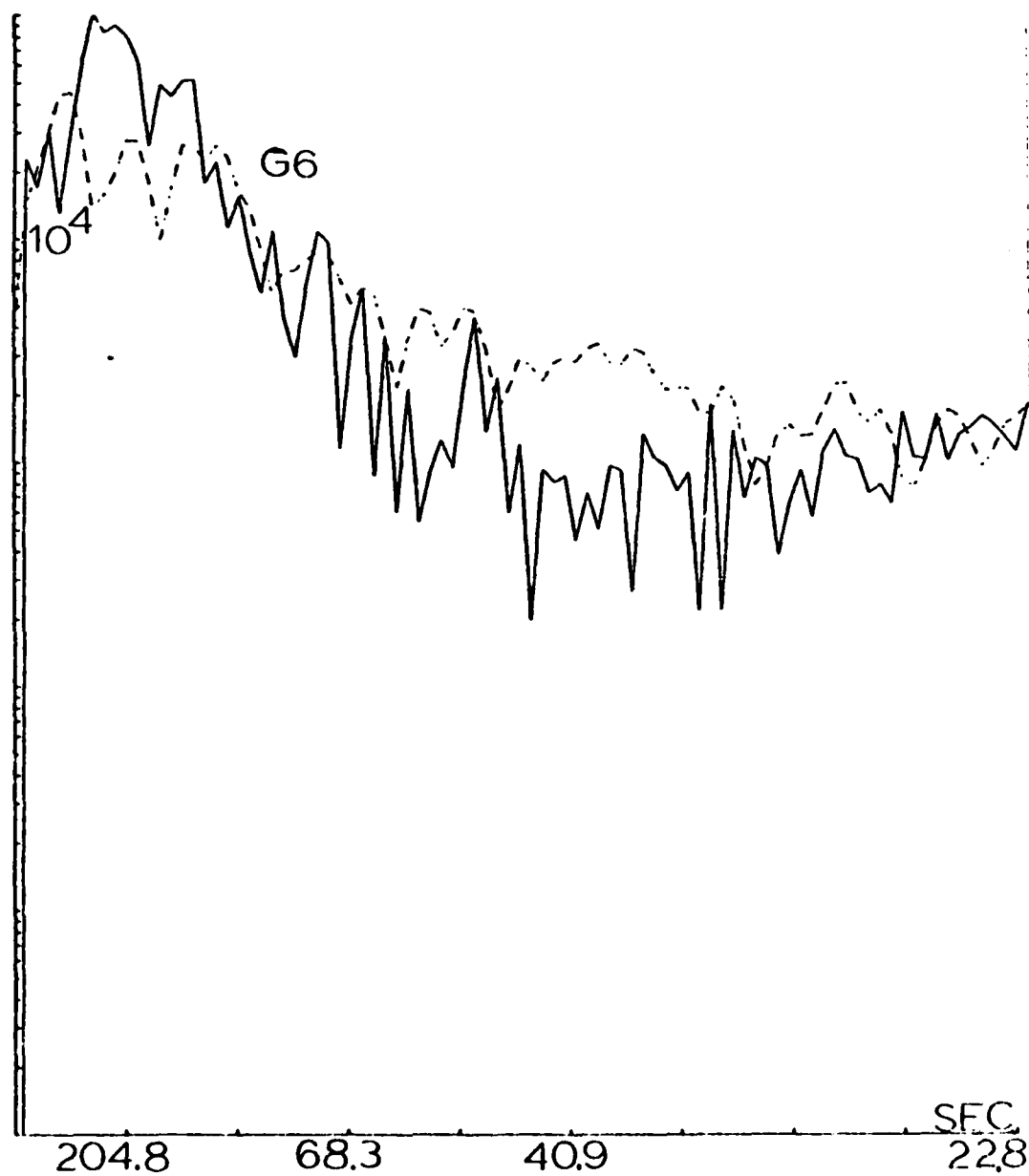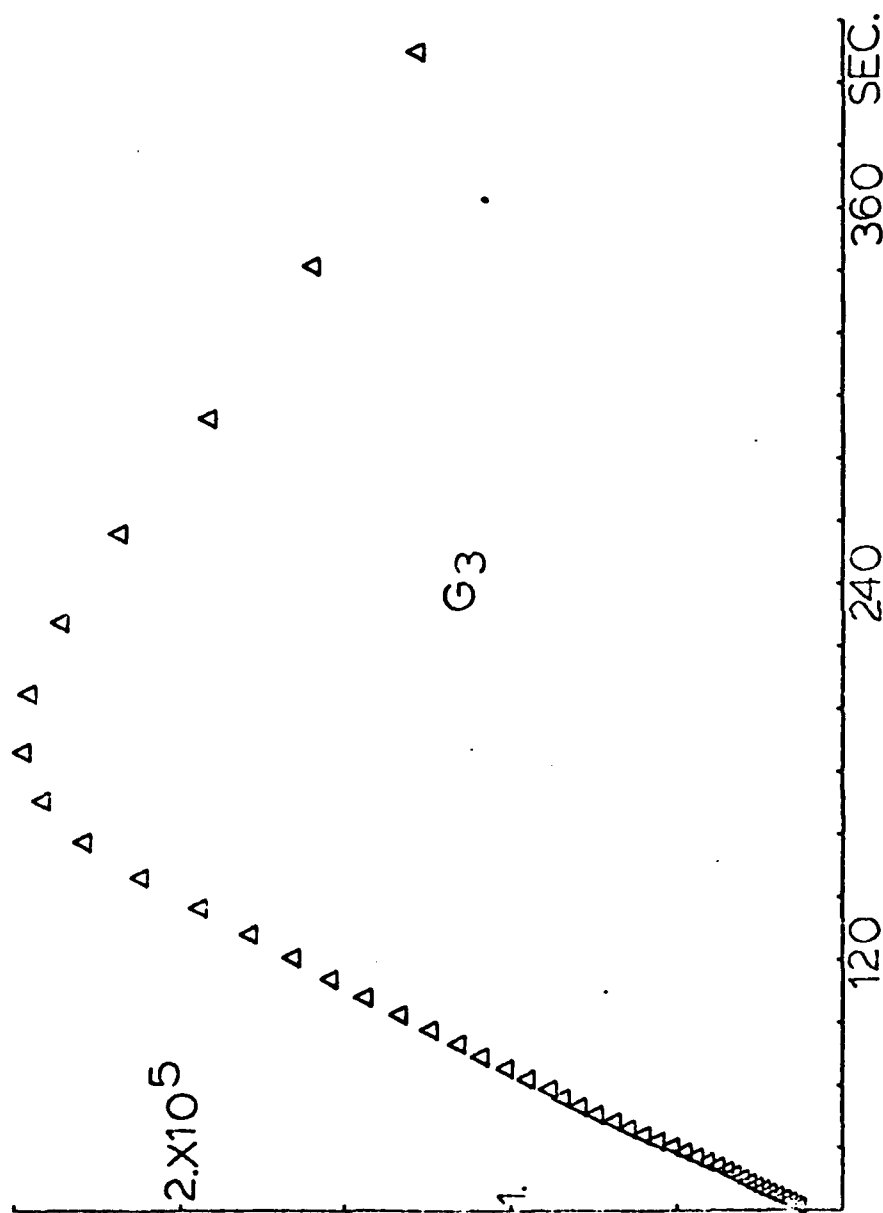
Fig. 7 b. Plots of the smoothed G pulse spectrums. Data shown to 40 sec. only as three shorter period data were later added.

G4

$6.\times10^4$

3.

G5

120   240   360   SEC.

$8.\times 10^4$

4.

G_6

120   240   360   SEC.
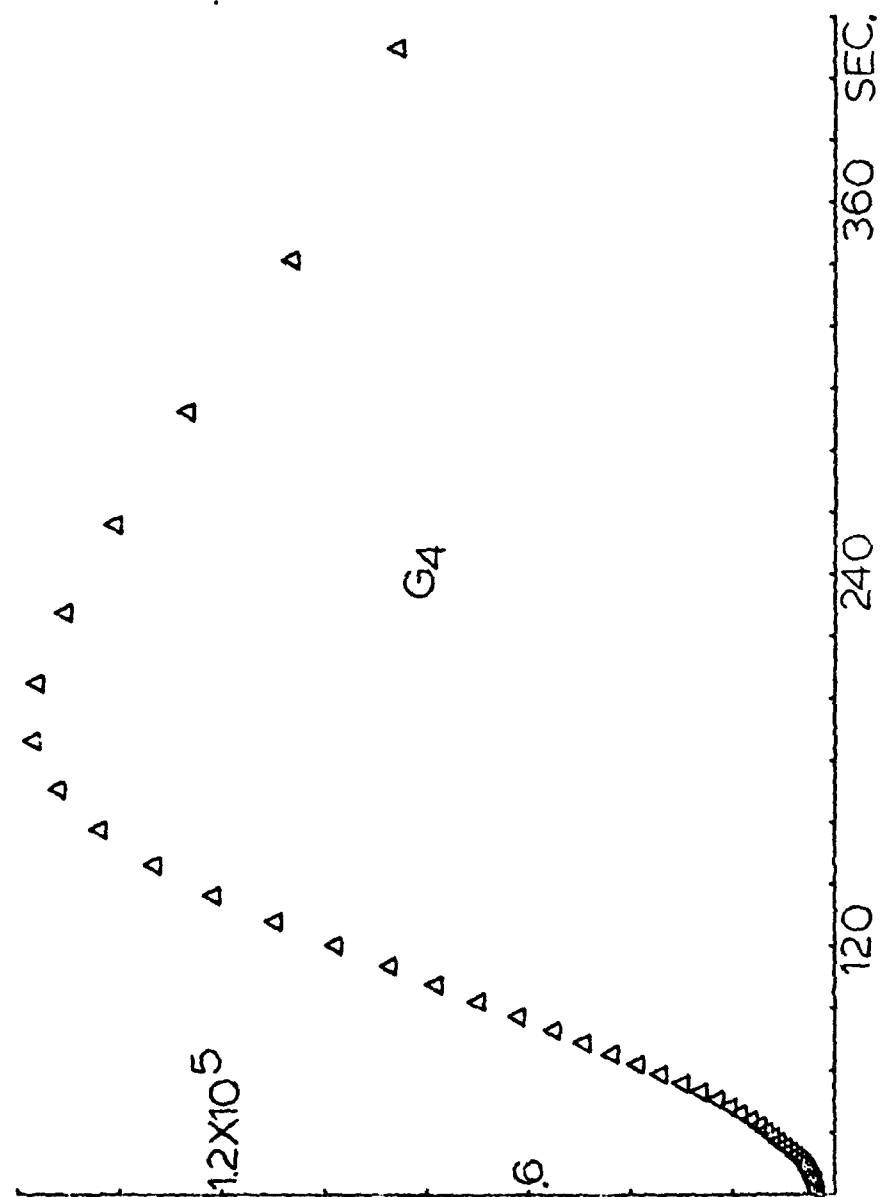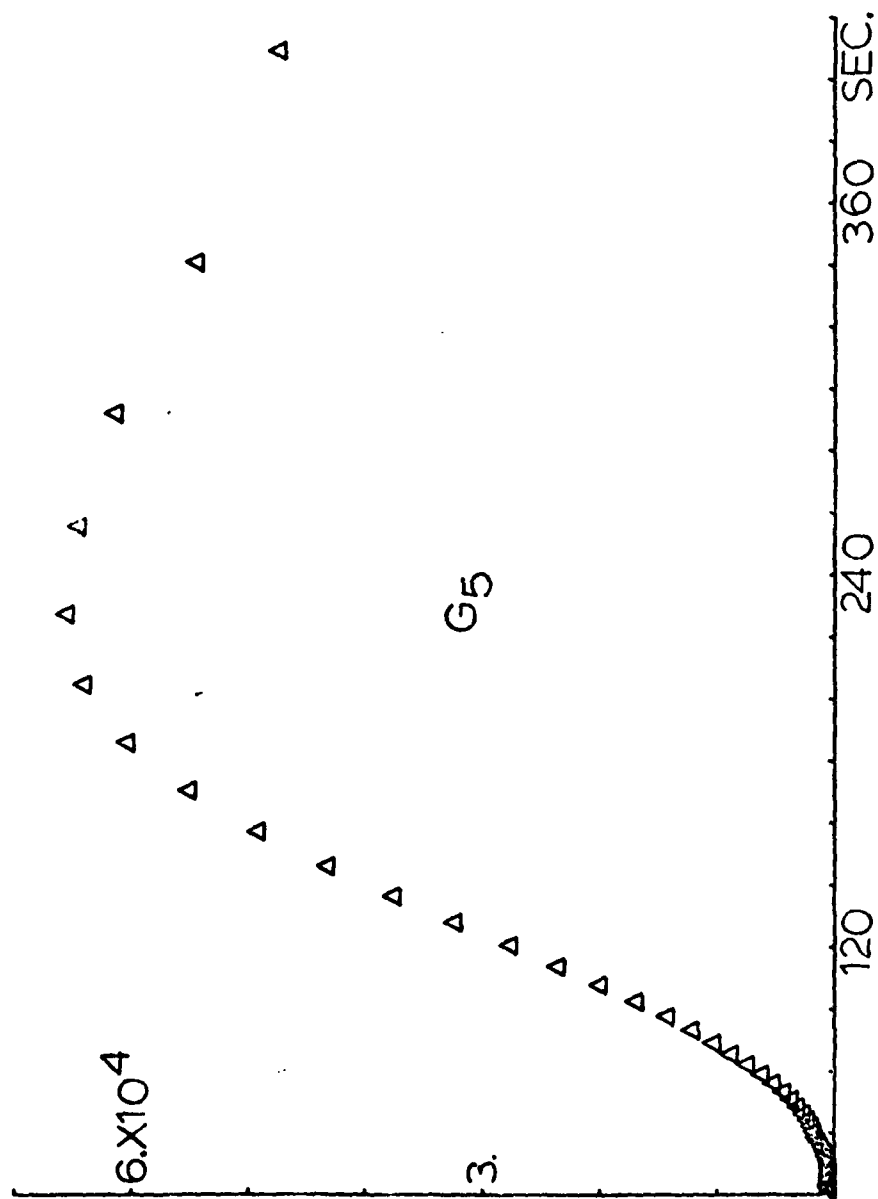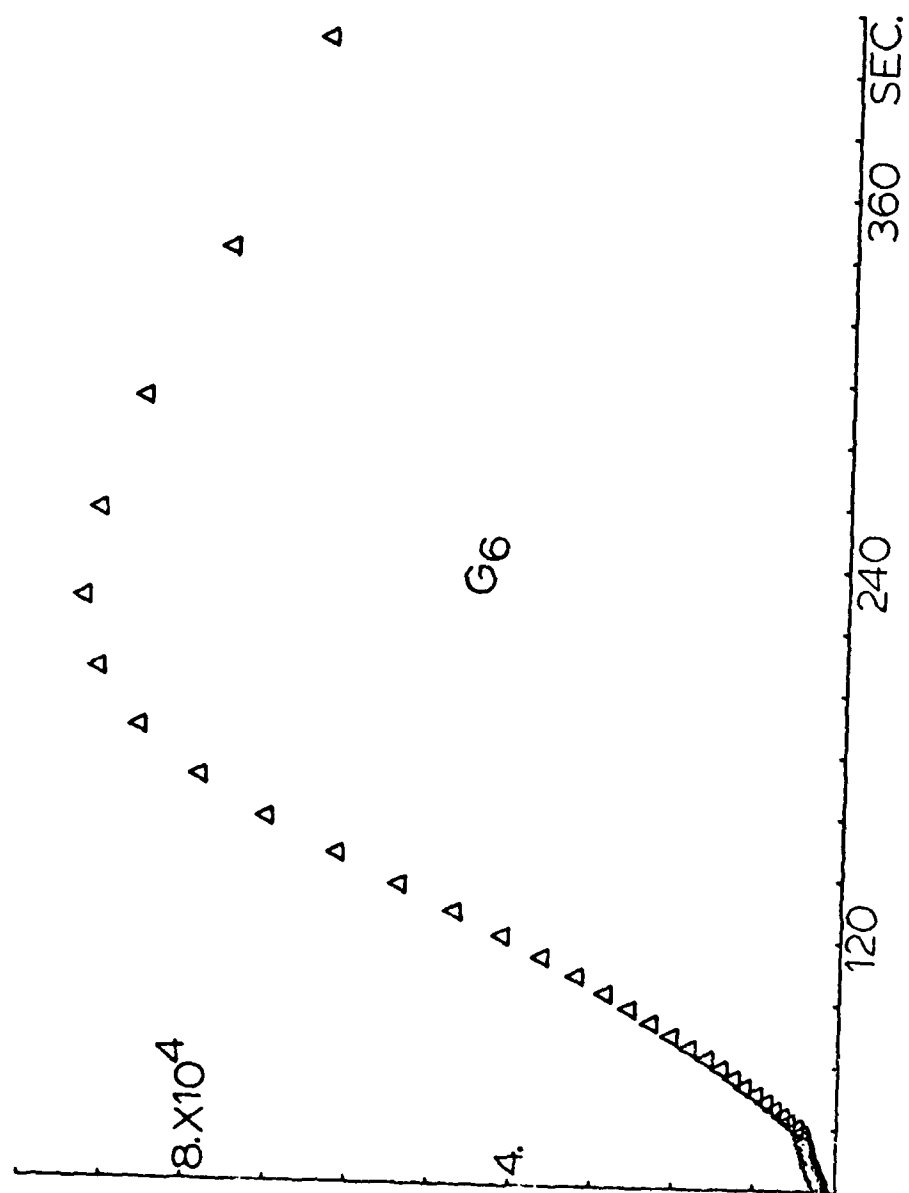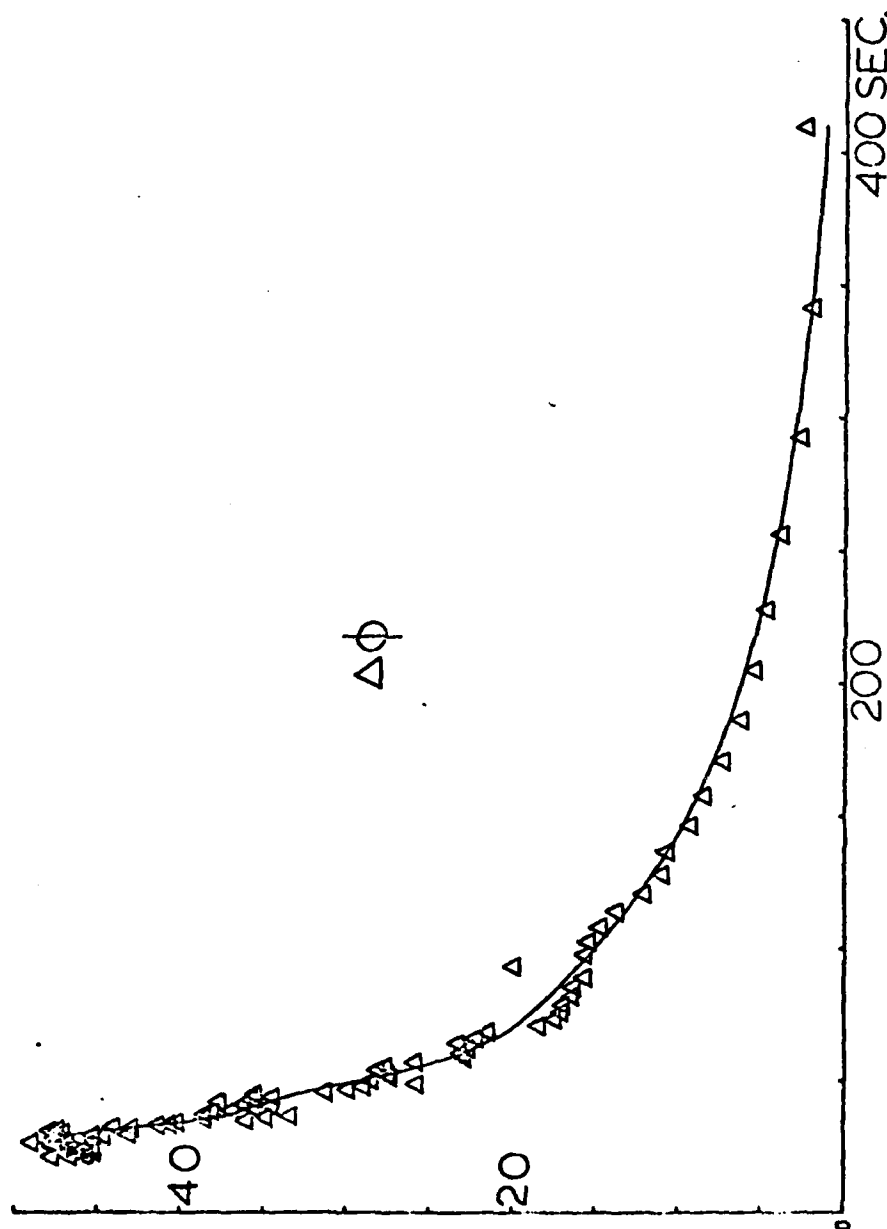
Fig. 8. Plot of phase difference ($\Delta \phi$) between the Love pulses G_6 and G_4. Triangles are data while curve is smoothed (Appendix 5) using 10 coefficients.
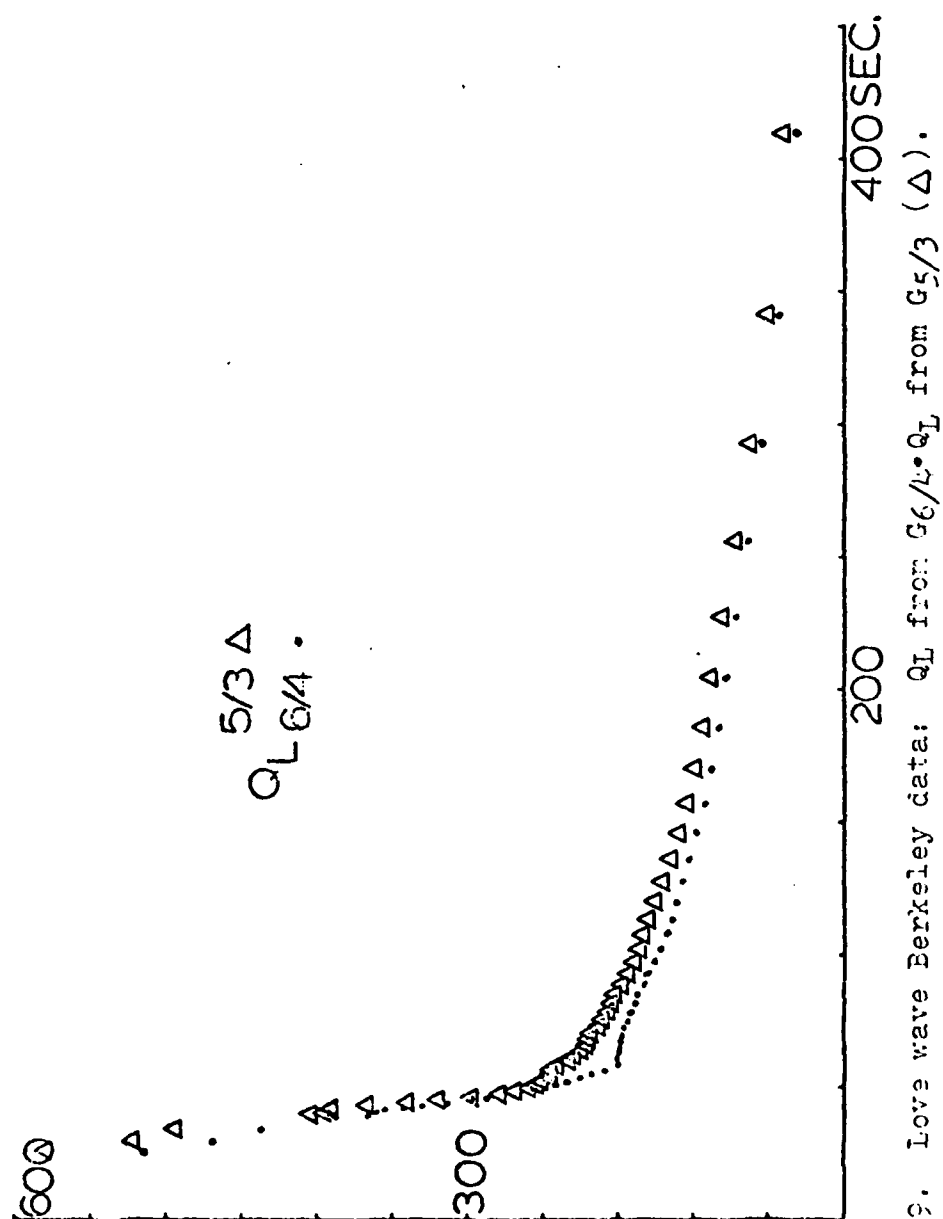
Fig. 9. Love wave Berkeley data: Q_L from $G6/4 \cdot Q_L$ from $G5/3$ ($\triangle$).
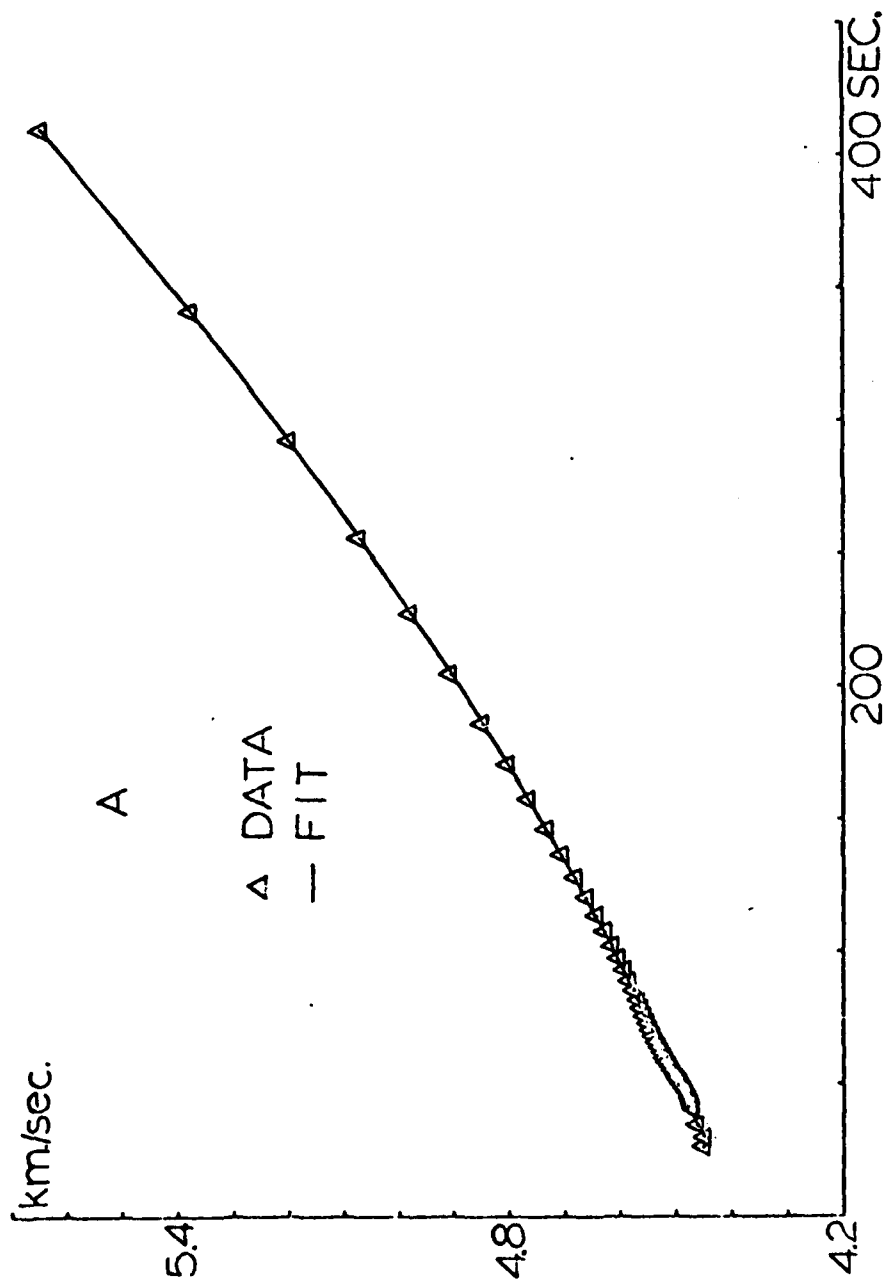
Fig. 10. Love wave inversion results with Berkeley data: A) phase
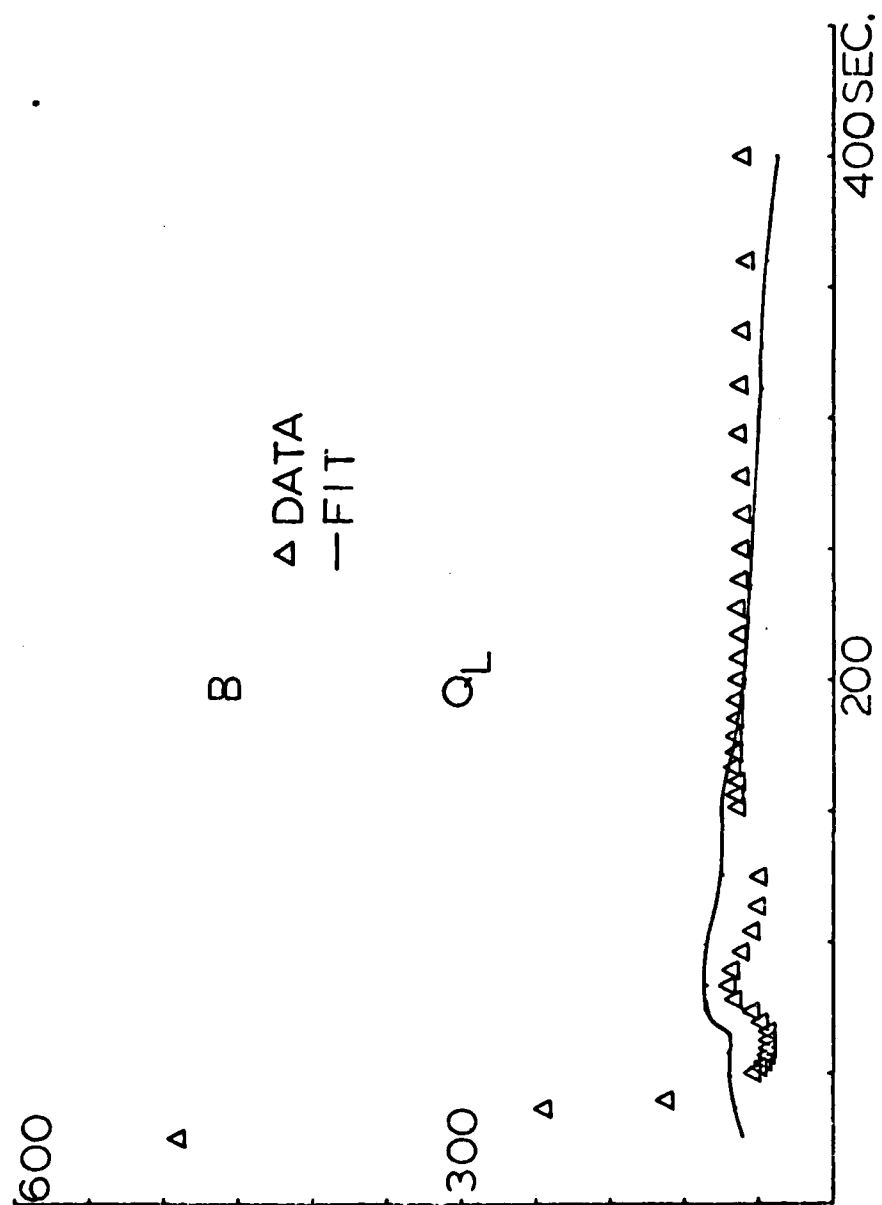velocity fit; B) phase Q fit. (corrected velocity data;
see Table 6 for uncorrected).
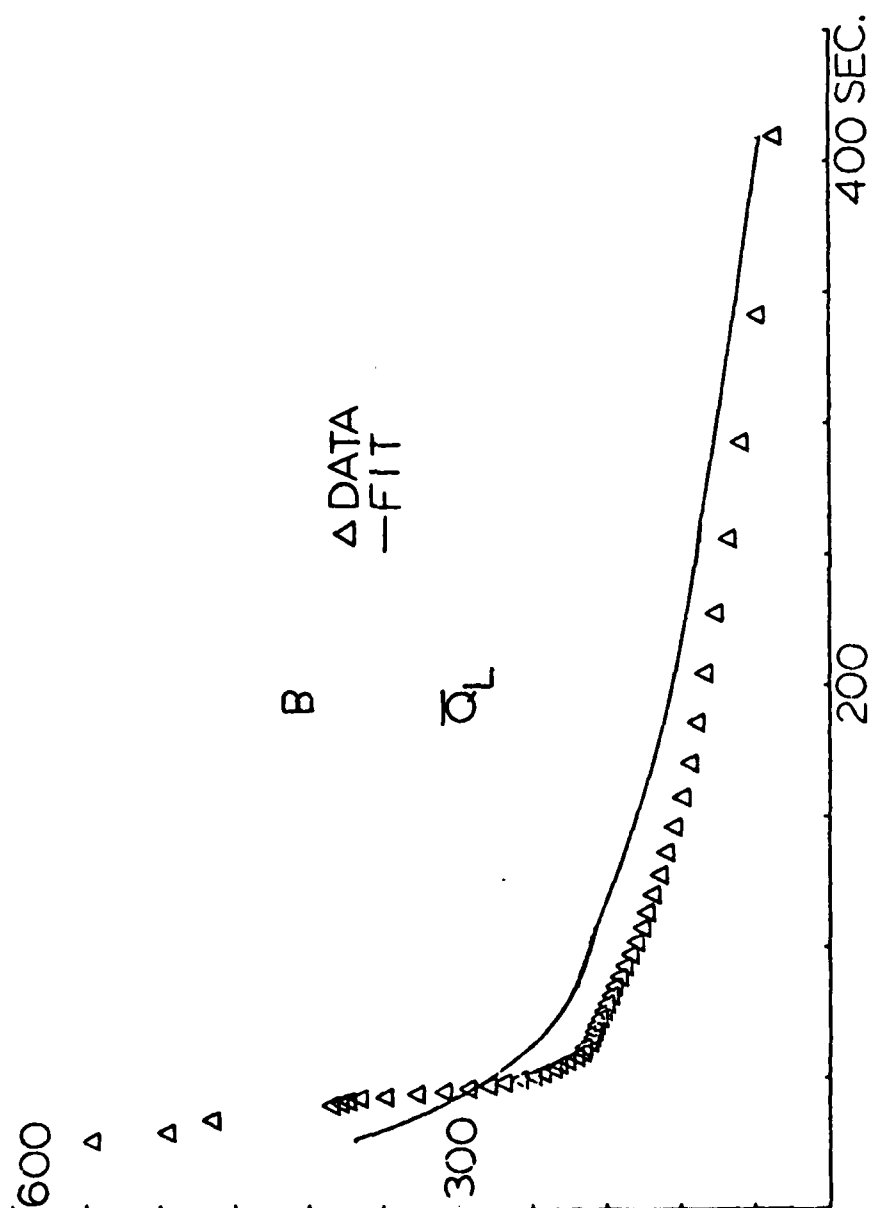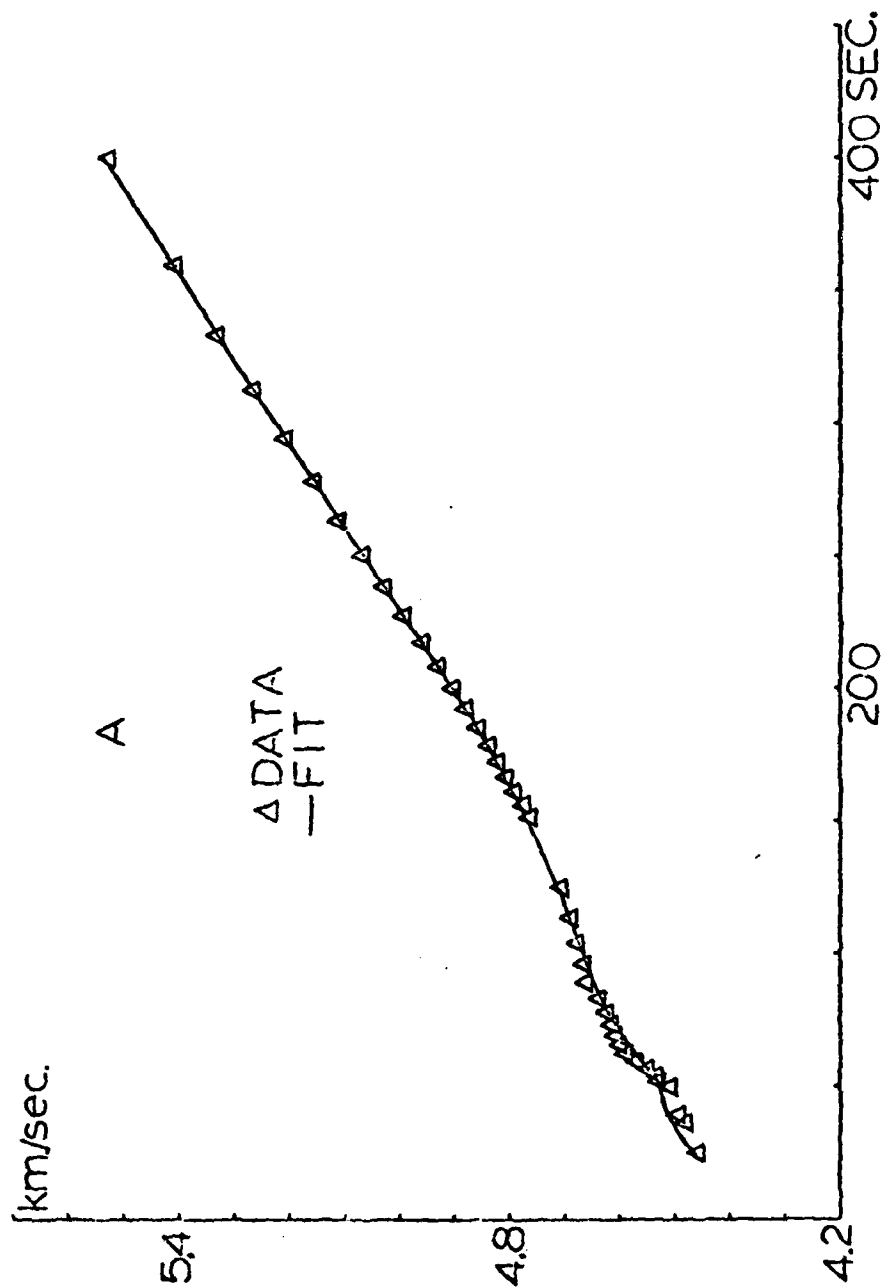
Fig. 11. Love wave inversion results with Anderson data: A) phase velocity fit; B) phase Q fit. (Corrected velocity data; see Table 6 for uncorrected.)
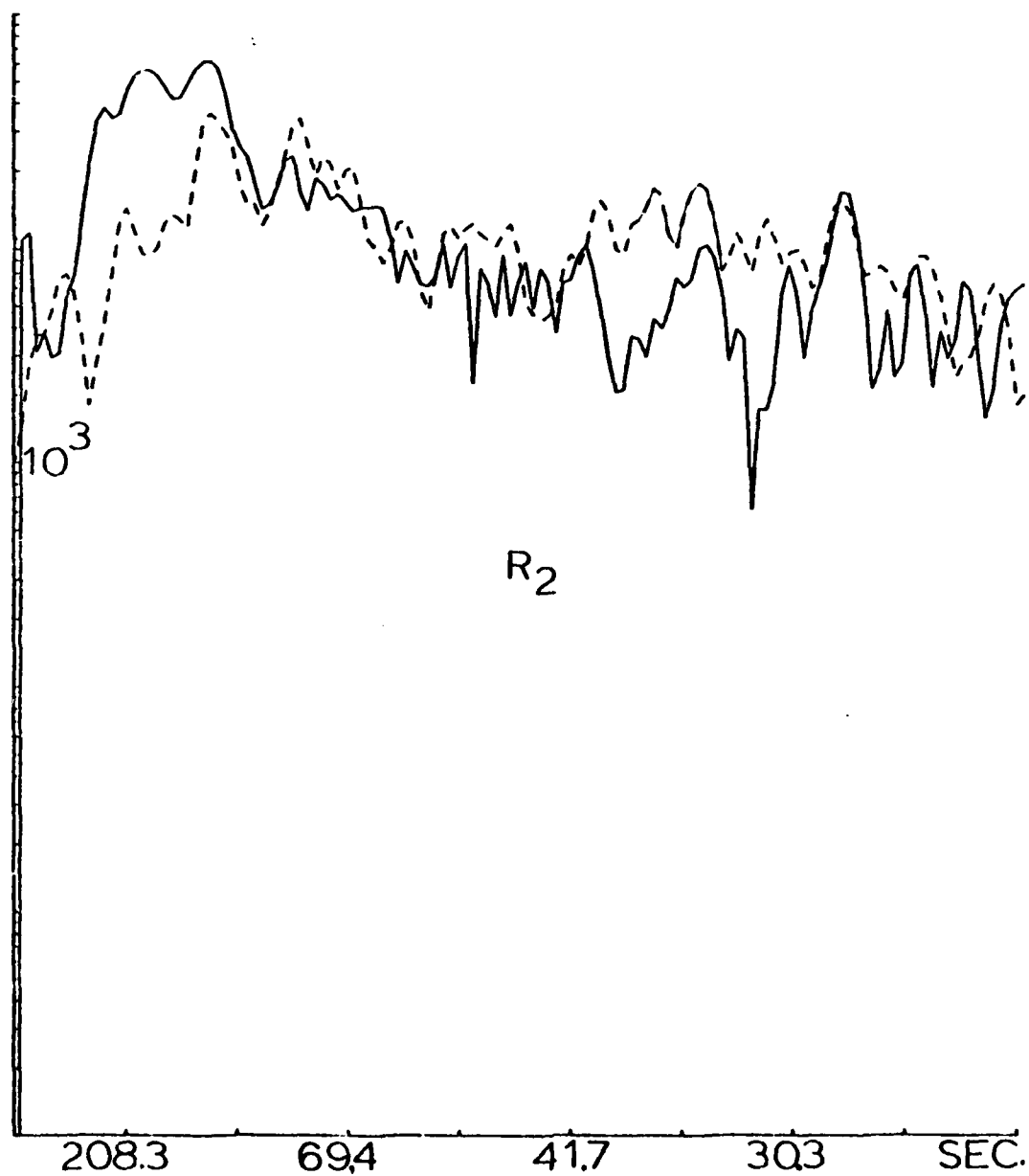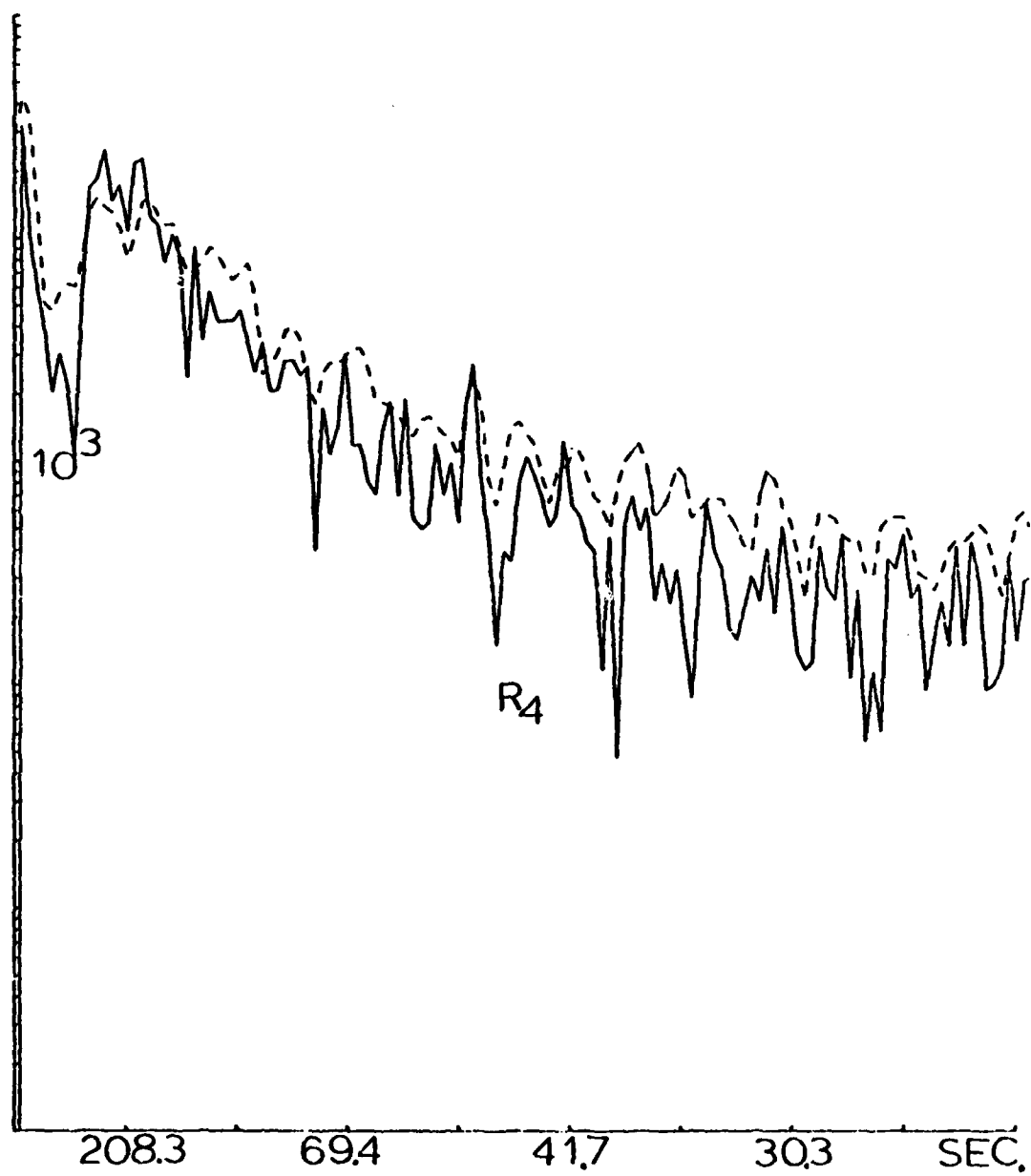
Fig. 12 a. Plots of the Rayleigh wave spectrums. Dashed
curve is a noise sample windowed leading the
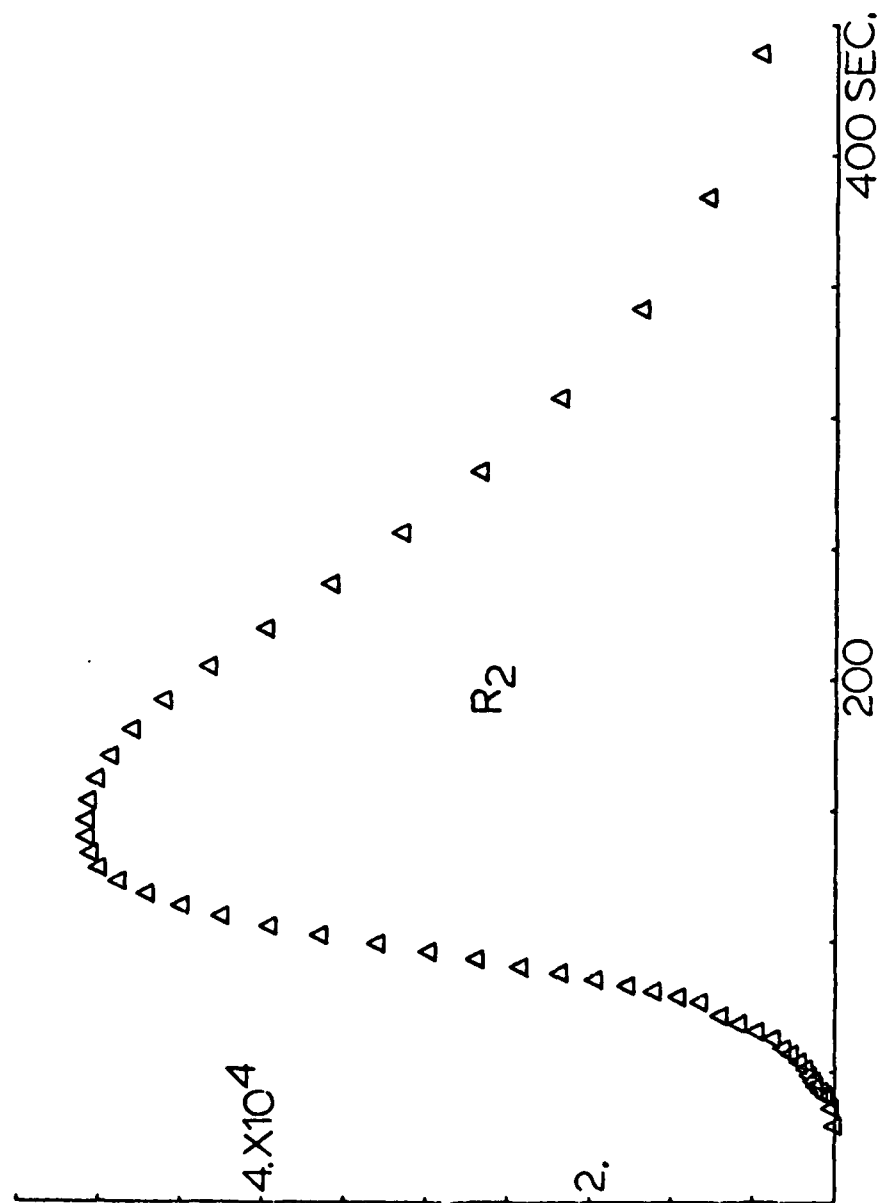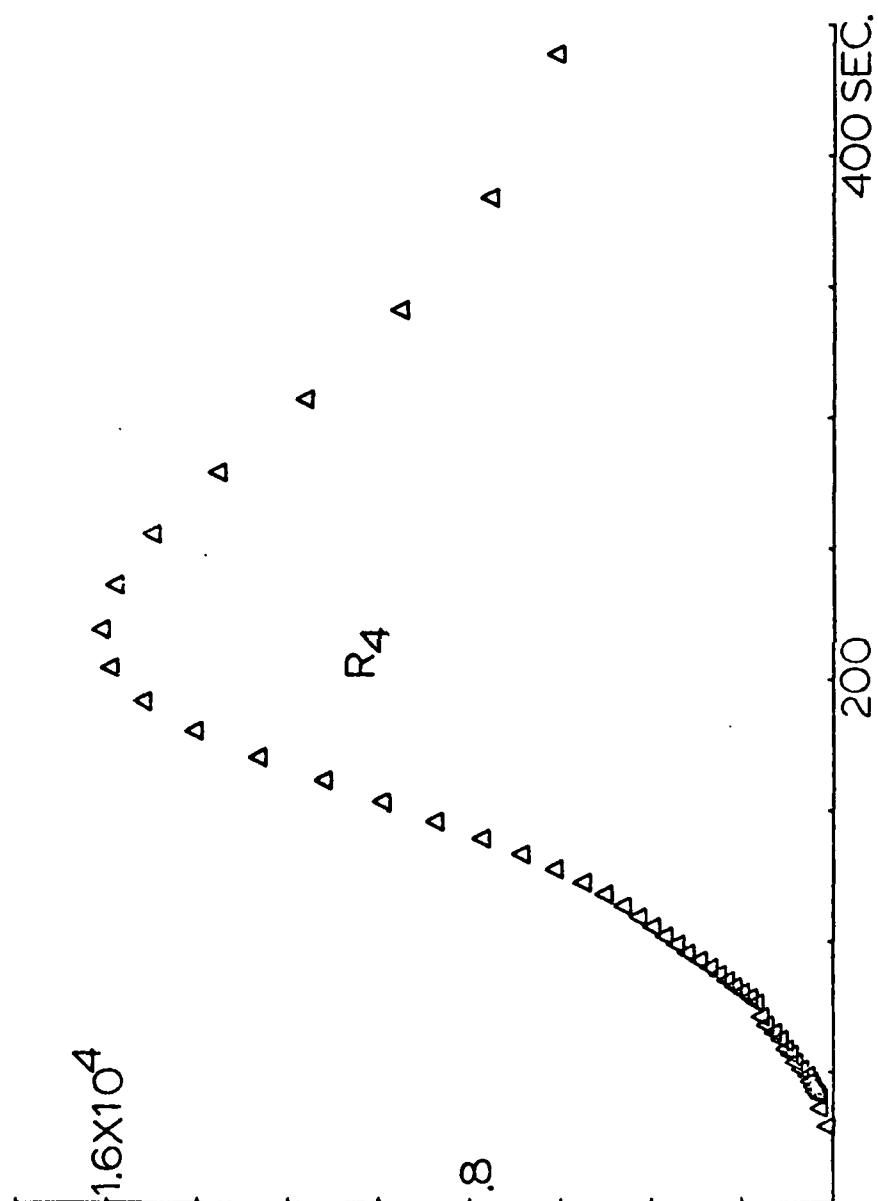wavetrain sampled.
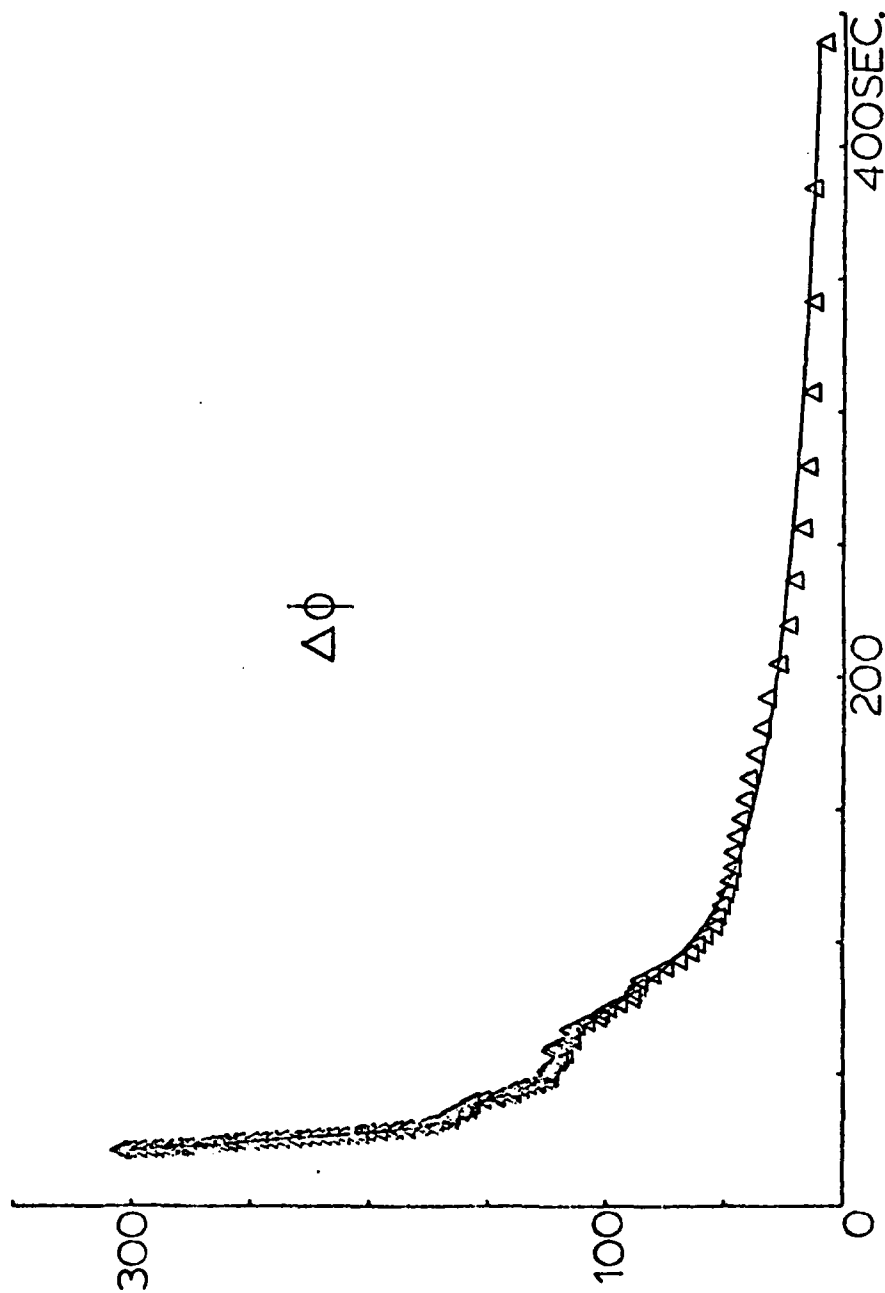
Fig. 12 b. Plots of the smoothed Rayleigh wave spectrums.

Fig. 13. Plot of the phase difference ($\Delta\phi$) between the Rayleigh waves R3 and R1. Triangles are data while curve is smoothed (Appendix 5) using 10 coefficients.
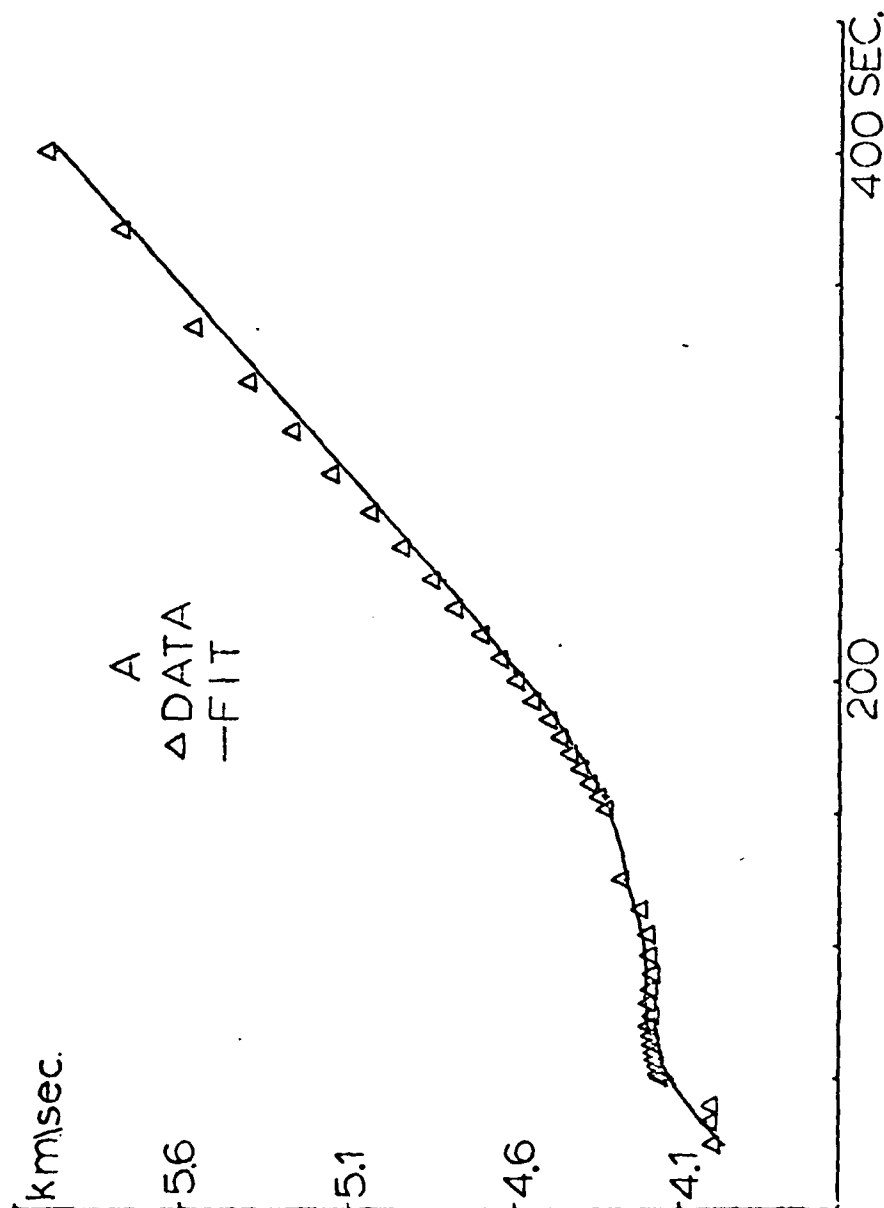
Fig. 14. Rayleigh wave inversion results with Berkeley data: A) phase velocity fit; B) phase Q fit.
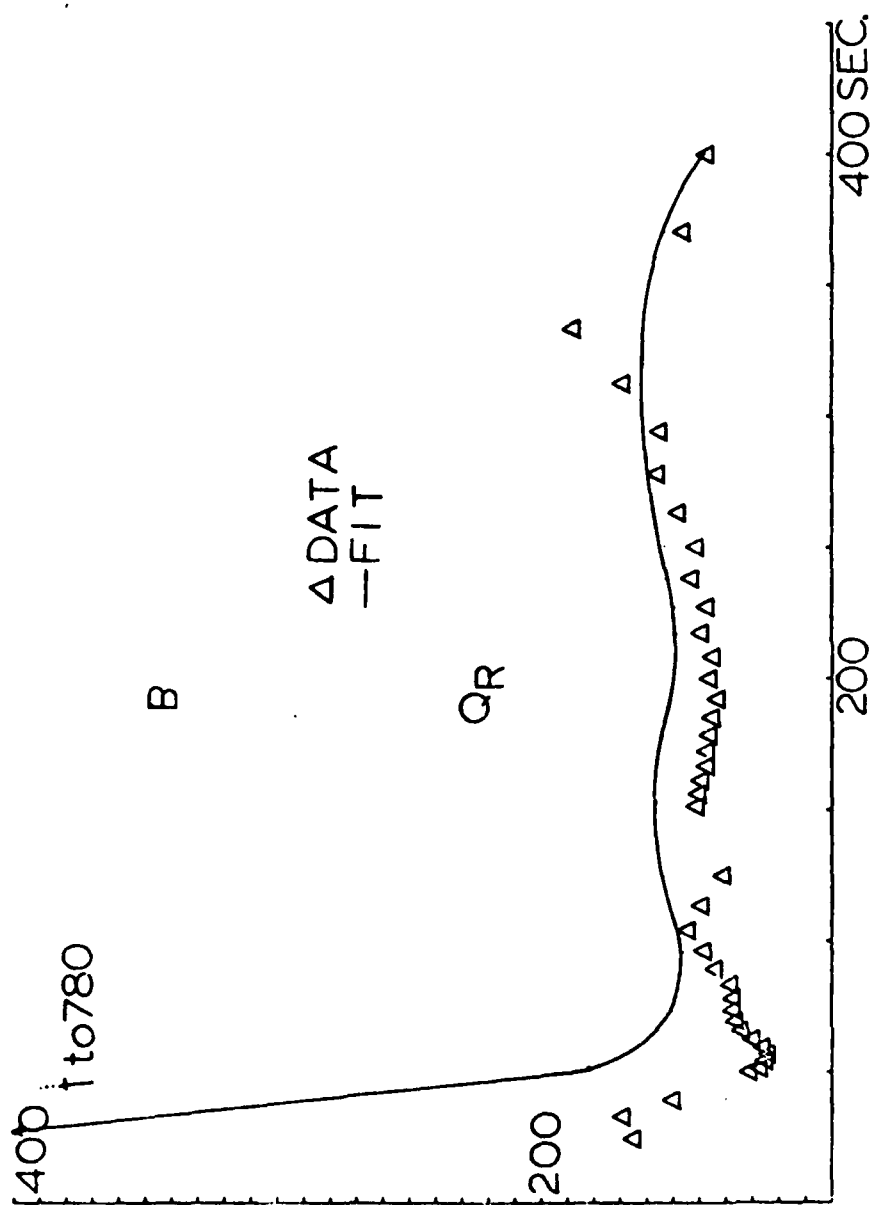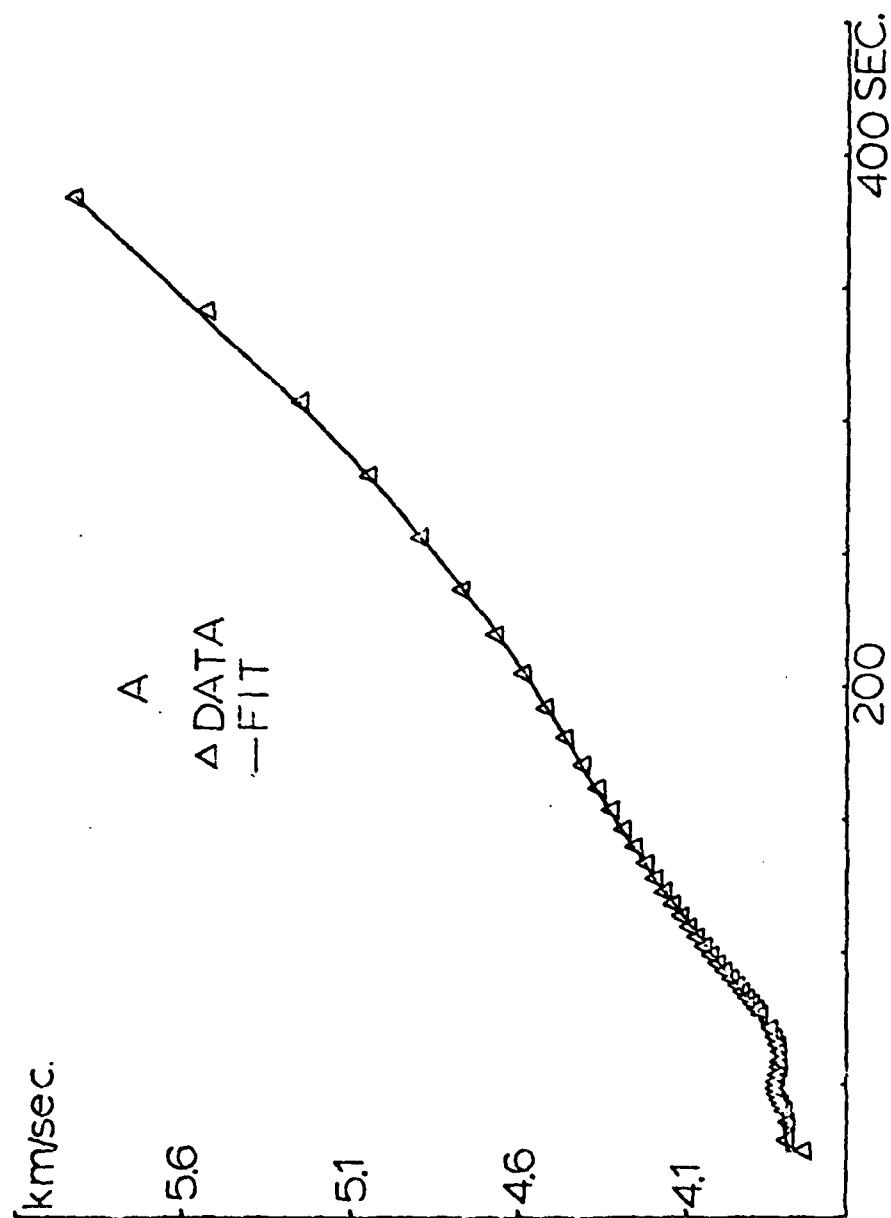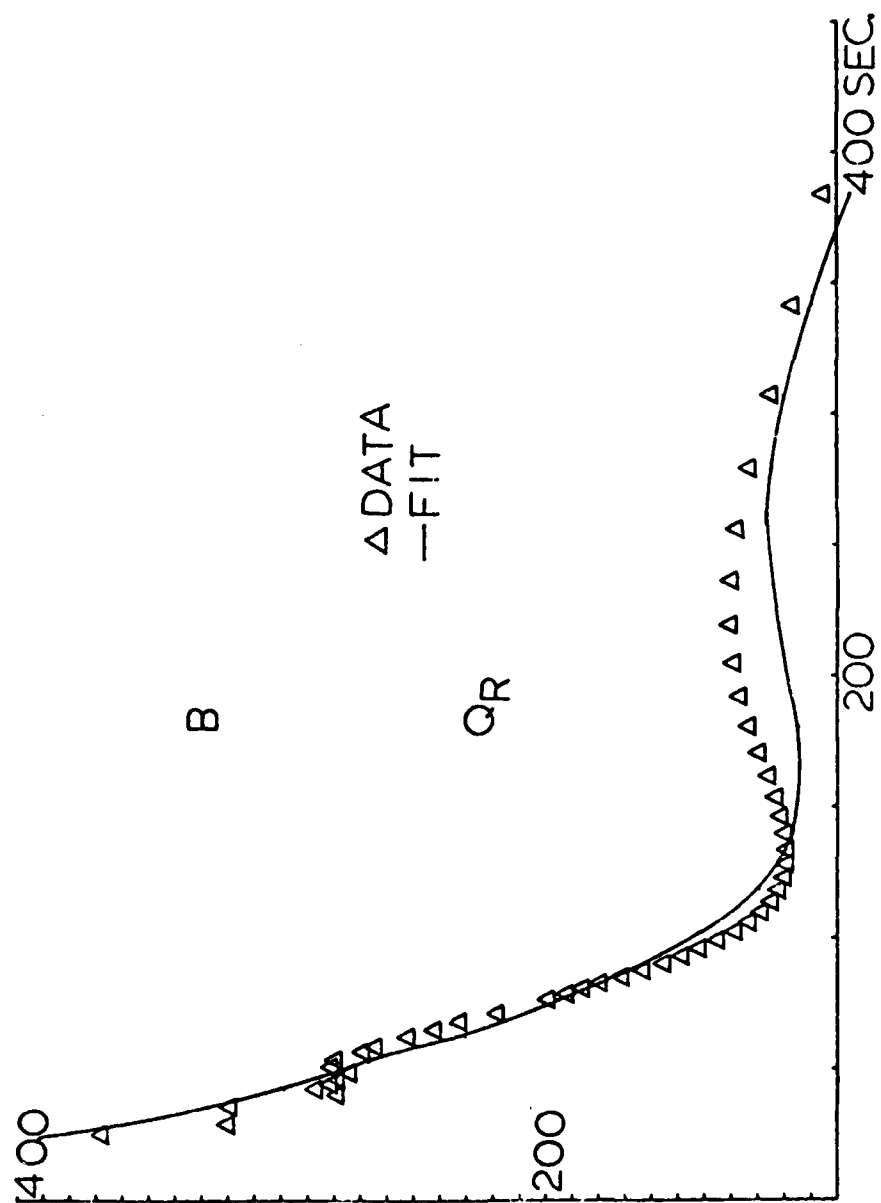
km/sec.

5.6

5.1

4.6

4.1

A

△ DATA
—FIT

200   400 SEC.

Fig. 15. Rayleigh wave inversion results with Anderson data:
A) phase velocity fit; B) phase Q fit.

B

Q_R

△DATA
—FIT

400 SEC
200
400
200

REFERENCES

Anderson, D. and Hart, R. The Q of the earth, in press.

Anderson, D., Ben-Menahem, A., and Archambeau, C.,
   1965. Attenuation of seismic energy in the upper
   mantle, J. Geophys. Res., 70, 1441-1448.

Ben-Menahem, A., and Toksoz, M.N., 1962. Source-
   mechanisms from spectra of long-period seismic
   surface waves. I. The Mongolian earthquake of
   December 4, 1957, J. Geophys. Res., 67, 1943.

Dorman, J., Ewing, M., and Oliver, J., 1960. Study
   of shear-velocity distribution in the upper mantle
   by mantle Rayleigh waves, Bull. Seism. Soc. Am.,
   50, 87-115.

Futterman, W., 1962. Dispersive body waves, J.
   Geophys. Res., 67, 5279-5291.

Gilbert, F. and Backus, G., 1966. Propagator matrices
   in elastic wave and vibration problem, Geophys.,
   31, 326-332.

Hart, R., Anderson D., and Kanamori, H. The effect
   of attenuation on gross earth models, in press.

Hart, R., Anderson, D. and Kanamori, H., 1976. Shear
   velocity and density of an attenuating earth,
   Earth Planet. Sci. Letters, 32, 25-34.

Herrin, E. and Goforth, T., 1977. Phase-matched
   filters: applications to the study of Rayleigh
   waves. Bull. Seism. Soc. Am., 67, 1259-1275.

Jackson, D. D., 1972. Interpretation of inaccurate,
   insufficient and inconsistent data, Geophys. J. R.
   Astr. Soc., 28, 97-109.

Jeffreys, H., 1965. Damping of S waves, Nature,
   208, 675.

Kanamori, H., and Anderson, D. Importance of physical
   dispersion in surface-wave and free-oscillation
   problems, in press.

Kanamori, H., 1970. Velocity and Q of mantle waves,
   Phys. Earth Planet. Int., 2, 259-275.

Knopoff, L., and Chang, F., 1977. The inversion of surface wave dispersion data with random errors, J. Geophys., 43, 299-309.

Knopoff, L. and Jackson, D.D., 1972. The analysis of undetermined and overdetermined systems, Dymanic Response of Structures, Herrmann and Perrone (ed.), Pergamon, New York.

Liu, H., Anderson, D., and Kanamori, H. Velocity dispersion due to anelasticity; implications for seismology and mantle composition. in press.

Lomnitz, C., 1975. Linear dissipation in solids, J. Appl. Phys. 28, 201-205.

Marquardt, D.W., 1963. An algorithm for least-squares estimation of nonlinear parameters, J. Soc. Indust. Appl. Math., 11, 431-441.

Pilant, W.L. and Knopoff, L., 1964. Observations of multiple seismic events, Bull. Seism. Soc. Am., 54, 13-39.

Press, F., Ben-Menahem, A., and Toksoz, N., 1961. Experimental determination of earthquake fault length and rupture velocity, J. Geophys. Res., 66, 3471-3485.

Schwab, F., and Knopoff, L., 1972. "Methods in Computational Physics." Academic Press, New York, New York.

Strictk, E., 1967. The determination of Q, dynamic viscosity and transient creep curves from wave propagation measurements, Geophys. J., 13, 197-218.

Sykes, L., Landisman, M., and Sato, Y., 1962. Mantle shear wave velocities determined from oceanic Love and Rayleigh wave dispersion, J. Geophys. Res., 67, 5257-52-71.

Tsai, Y. and Aki, K. Simultaneous determination of the seismic moment and attenuation of seismic surface waves, B.S.S.A., 59, 275-287, 1969.

APPENDIX 1

INVERSION OF SURFACE WAVE DATA FOR VELOCITY AND ANELASTICITY USING EXACT KERNELS

I.   INVERSION OF LOVE WAVE DATA FOR VELOCITY

AND ANELASTICITY USING EXACT KERNELS

by

Walter Silva

Department of Geology and Geophysics

University of California

Berkeley, California, U.S.A.

ABSTRACT

The general problem of inverting Love wave
dispersion and amplitude data to obtain a velocity
and Q_S structure is considered. A formulation is used
which incorporates attenuation into the Haskell-Thompson
matrix method in an exact manner and thus retains the
inherent non-linearity in the anelasticity. The
resulting exact inversion kernels allow simultaneous
inversion for velocity and intrinsic attenuation
parameters. The method is applied to synthetic data
which allows a comparison to be made with inexact
kernels. The results indicate that the use of inexact
kernels may introduce spurious oscillations into the
Q_S structure and that a simultaneous inversion can be
more stable than inverting for velocity alone.

INTRODUCTION

Surface waves provide an invaluable tool in the study of the earth's interior. Their use has mainly been in dispersion studies to infer such elastic parameters as velocity and density in structures ranging from soils to the lower mantle. However, in recent years there has been an increasing interest in the anelastic parameters of the earth. This type of investigation can supply valuable information concerning material properties, structures, and temperature distributions in the earth. Of most recent interest is the frequency dependence and coupling between intrinsic velocity and attenuation. With this in mind, it now becomes important to have more exact methods of inverting the data for both velocity and attenuation if any meaningful interpretation is to result from such investigations.

A formulation is presented here using an exact generalization of the Haskell-Thompson matrix method (Haskell, 1953; Silva, 1976b) to include anelasticity in inverting Love wave dispersion and attenuation data for both layer velocity and attenuation. Synthetic data are used to allow a comparison to be made between the exact formulation and the approximate linear theory of Anderson and Archambeau (1964). A somewhat unstable problem is considered in order to demonstrate

the differences and to represent more accurately actual inversions, since surface wave attenuation data are typically sparse and of limited accuracy and bandwidth.

FORMULATION

In a recent paper (Silva, 1976b) a theory was presented for introducing, in an exact manner, anelastic attenuation into a Haskell-Thompson formulation. This is applied here to Love waves. The earlier treatment considered plane P and SV waves propagated in a layered linear viscoelastic half-space. In particular, attenuating (or elastic) layers over an elastic half-space were considered. However, due to the boundary conditions, the component of attenuation parallel to the interface A_x (which describes the spatial decay of the surface wave) is constrained to be continuous along with the horizontal wave number P_x. This means that each layer, along with the half-space, must be attenuating.

Define P_x and A_x as

$$P_x = \frac{\omega}{c} \quad , \quad A_x = \frac{\omega}{c} \left\{ \frac{-1 + \sqrt{1 + Q_L^{-2}}}{1 + \sqrt{1 + Q_L^{-2}}} \right\}^{\frac{1}{2}} \tag{1}$$

with c the Love wave phase velocity and where A_x has been defined in this form to accommodate a Love wave

phase quality factor Q_L (Brune, 1962). The attenuation then has introduced another eigenvalue Q_L^{-1} to be determined as a function of period. In the application to surface waves, equation (18) of Silva (1976b) (considering now SH only) for the complex vertical component K_z of the complex wave number K must be modified to the following:

$$K_z = \left\{ K^2 - K_x^2 \right\}^{\frac{1}{2}} \qquad R\left\{K\right\} > R\left\{K_X\right\} \qquad (2)$$

$$= -i \left\{ K_x^2 - K^2 \right\}^{\frac{1}{2}} \qquad R\left\{K\right\} < R\left\{K_X\right\}$$

where

$$K^2 = K_x^2 + K_z^2 = \frac{\omega^2}{V_s^2} \; \frac{2}{1 + \sqrt{1 + Q_s^{-2}}} \left\{ 1 - \frac{i}{Q_s} \right\}$$

and

$$K_x = P_x - iA_x \quad , \quad K_z = P_z - iA_z$$

with V_s and Q_s the homogeneous shear wave velocity and specific attenuation factor, respectively. The characteristic equation is then obtained in the usual way (Haskell, 1953) and K_x found for each period using Mueller's method (Conte and Debor, 1972). In Figure 1 are shown C, Q_L, and U, the group velocity, for the crustal model of Table 1 which represents the error free data. Group velocity is calculated using a
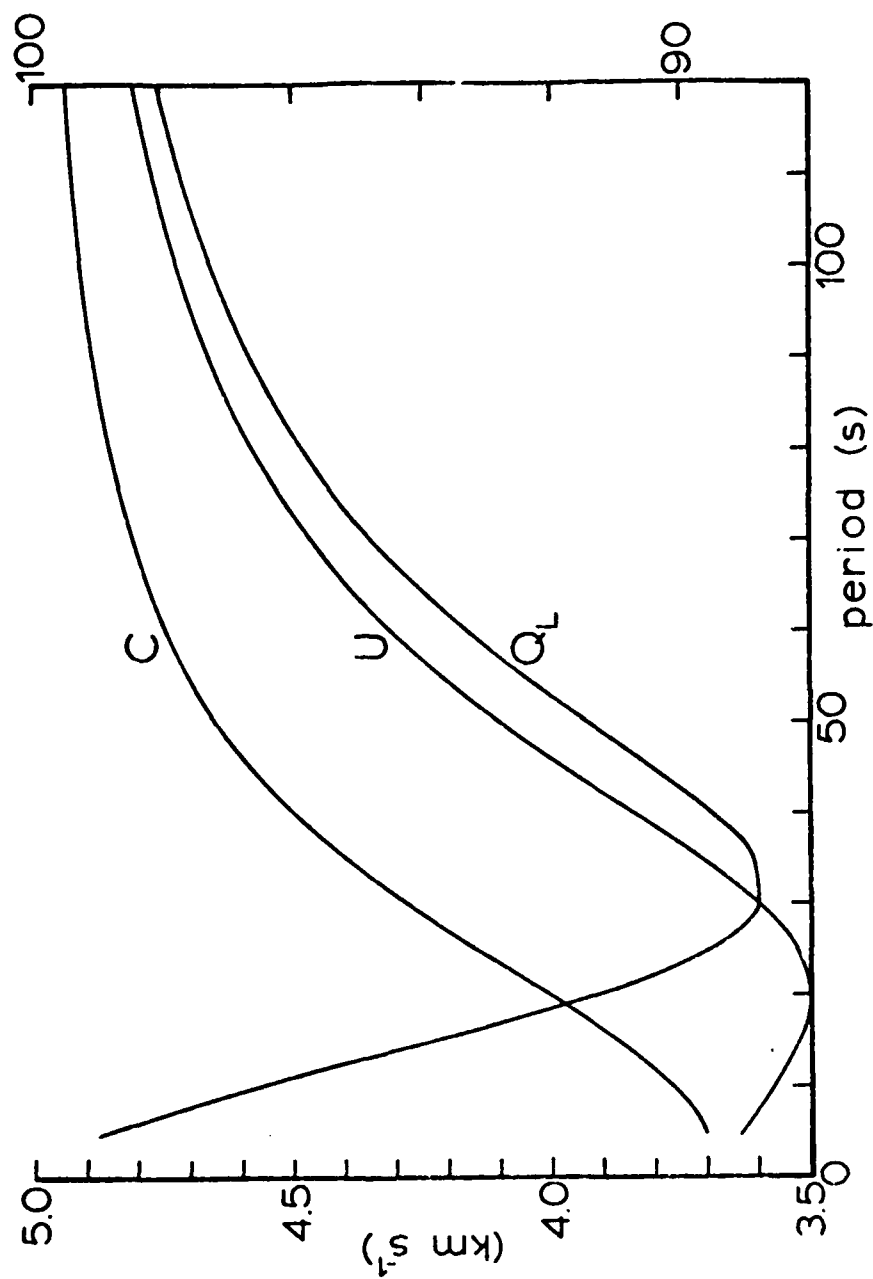
Fig. 1. Plot of phase velocity c, group velocity U, and quality factor Q_L for the crustal model of Talbe 1. (c, U in km/sec)

variational method applied to dissipative media
(Silva, 1976a).

INVERSION

Since the development above represents an exact
forward solution, the non-linearity of both the shear
velocity and intrinsic attenuation is retained. In
order then to invert the phase velocity and attenuation
data for V_S and Q_S a Taylor series approximation is
made, keeping only the linear terms, and iterations
performed. We then have:

$$\delta c \approx \frac{\partial c}{\partial V_S} \; \Delta V_S + \frac{\partial c}{\partial Q_S} \; \Delta Q_S$$

$$\delta Q_L \approx \frac{\partial Q_L}{\partial V_S} \; \Delta V_S + \frac{\partial Q_L}{\partial Q_S} \; \Delta Q_S$$

(3)

where δc and δQ_L represent the difference between the
observed phase velocity and Love wave attenuation
parameters at each period and those calculated from
an appropriately close starting model. The derivatives
are calculated in the following way: the first $\frac{\delta c}{\delta V_S}$,
is an analytical derivative using an extension of
Rayleigh's principle to dissipative media (Silva,
1976a), while the remaining are calculated numerically,
using a 10% parameter change. Plots of the derivative
versus period for each layer are shown in Figures 2
through 5. The plots contain a number of interesting

features. Figure 2 shows the derivative $\dfrac{\partial c}{\partial V_S}$ and should be compared with $\dfrac{\partial Q_L}{\partial Q_S}$ (Figure 5) which confirms the relation,

$$\frac{\partial c}{\partial V_S} \approx \frac{c}{V_S} \quad \frac{Q_S^2}{Q_L^2} \quad \frac{\partial Q_L}{\partial Q_S} \qquad (4)$$

which is derived as equation (A2) in Appendix 4. This is also the relation, applied rather to inverse Q, used in the linearized theory (Anderson and Archambeau, 1964). The most revealing plots are those of $\dfrac{\partial c}{\partial Q_S}$ (Figure 3) and $\dfrac{\partial Q_L}{\partial V_S}$ (Figure 4) which confirm equation (A3) of the Appendix 4:

$$\frac{\partial c}{\partial Q_S} \approx - \frac{c \quad V_S}{4 \, Q_S^2 \, Q_L^2} \quad \frac{\partial Q_L}{\partial V_S} \qquad (5)$$

In Appendix 4 it is argued that in equations such as (3) the term involving $\dfrac{\partial Q_L}{\partial V_S}$ is comparable to those involving $\dfrac{\partial c}{\partial V_S}$ and $\dfrac{\partial Q_L}{\partial Q_S}$. This demonstrates the large dependence of surface wave amplitudes on the velocity structure in plane layer models and strongly suggests that the derivative $\dfrac{\partial Q_L}{\partial V_S}$ will play an important part in any inversion scheme. Also note the lack of similarity of the curves in Figures 3 and 4 with those in Figures 2 and 5 which indicates that they contain a different distribution of information and thus their inclusion should add to the stability of the inversion process.

TESTS WITH SYNTHETIC DATA

The crustal model shown in Table 1 was used as
a layer over half-space in a previous work (Harkrider,
1968) to demonstrate the results of a variational
formulation for surface waves. The 40 km thick crust
was subdivided here into four identical 10 km thick
layers in order to allow the inversion process greater
freedom in parameter adjustment. Although this may
seem excessive in order to exaggerate the effect, one
should realize that the data here are error free and
the real model is known. The period range is 120 to 5
seconds with 5 second intervals and the non-geometrical
dispersion due to dissipation (Burton, 1977) is
neglected.

In order to compare the linearized inversion
theory (Anderson and Archambeau, 1964) with the exact
formulation, both inversions were carried out on the
same data (Figure 1) generated by the exact theory
using the crustal model of Table 1. Both inversions
used the method of singular value decomposition
(Lancsoz, 1961) with the non-linear appropriately
scaled (Wiggins, 1972) in order to produce a consistent
comparison. The results of the inversions are shown
in Table 2.

The first section, A, shows the results of the
linear theory (Anderson and Archambeau, 1964) using

the exact velocity structure. The inversion results
in a highly oscillating Q_S structure even with error
free data and an exact velocity structure. The
oscillations represent up to a 30% error, yet the
forward problem agrees with the exact Q_L in Figure 1
to well within 0.5%.

In section B is the result of simultaneously
inverting for V_S and Q_S using the exact treatment.
The Q_S structure was perturbed in an oscillating
manner towards the linear solution to determine
whether the iterations would move in this direction
or towards the actual model. It is important to stress
that the linear solution represents a global minimum
for that method and a local minimum for the exact
formulation. Considering the results in section B,
it appears that the overall oscillations in Q_S have
decreased and the velocity structure has been approx-
imately recovered. This is really quite satisfactory
because: 1) the inversion is extracting twice as many
parameters as for either Q_S or V_S alone and, 2) from
the derivative $\frac{\partial Q_L}{\partial V_S}$ (Figure 4) it is apparent that
phase and amplitude data are certainly not independent.
The stability here is due to the derivative $\frac{\partial Q_L}{\partial V_S}$ since
any attempt to invert with simply the derivatives
$\frac{\partial c}{\partial V_S}$, $\frac{\partial Q_L}{\partial Q_S}$ diverges wildly in both V_S and Q_S.

Section C shows a standard V_S-only inversion

using simply the analytical derivative $\frac{\partial c}{\partial V_s}$ (Figure
2). Since its final velocity model (smallest SSRC
for a suite of iterations) is not as close as the full
inversion of section B for the same starting velocity
model, the amplitude data actually adds resolution and
stability to the velocity inversion.

An obvious result that emerges from this study is
that attempting to resolve a number of layers with data
of limited bandwidth can result in an ill-conditioned
system. This fact, coupled with an approximate kernel,
leads to an oscillating solution which is far from the
exact model. The exact formulation leads to a result
which is closer to the actual model, but the con-
vergence is slow. One approach to this problem is
to use more sophisticated inversion schemes (Der
et al., 1970; Jackson, 1972; Wiggins, 1972) which
generally achieve better stability at the price of
decreased resolution.

CONCLUSION

An exact formulation is used in calculating the
dispersion and attenuation for Love waves in a layered
linear viscoelastic half-space. The exact method is
used to demonstrate the instability inherent in using
the approximate linear inversion kernel (Anderson and
Archambeau, 1964). Although the approximate theory
agrees well within 0.5% of the exact, in a forward

sense, the inversion can result in alternating high and low Q layers where none existed. The reason for this instability is found in the neglect of the derivative $\frac{\partial Q_L}{\partial V_S}$. It is thought that this result strongly favors simultaneous inversions for both velocity and attenuation of surface waves which may result in better resolution for both velocity and attenuation. The use of dispersion data only may be the source of discrepancies in the inversion of surface wave data (McEvilly, 1964) which are sometimes interpreted in terms of anisotropy. Studies currently in progress involve the simultaneous inversion of both Love and Rayleigh wave data using exact kernels and hopefully will further resolve this matter.

In applying this formulation to observational data two points must be emphasized. First the phase data must be corrected for anelastic dispersion as discussed by Kanamori and Anderson (1977). One approach is to correct all of the data to a convenient reference frequency before applying the inverse method. The second consideration is the effects on the velocity and Q_S structure due to errors in both phase and amplitude measurements. The most general conclusion is that the resolution will be reduced (Wiggins, 1972). However, since the relative errors in phase and amplitude measurements are very different, the coupling between the errors and the model parameter requires a

very detailed treatment (Der, 1972), and is not within

the scope of the present paper. In general though,

the magnitude of the $\dfrac{\partial\, Q_L}{\partial\, V_S}$ term mandates accurate

amplitude data if it is to contribute significant

information to the inversion process.

TABLE 1

A standard model for a crust over a mantle (Harkrider, 1968). Identical layers were introduced into the crust to permit greater freedom in the inversion process.

V_S(km/sec)	(cgs)	Q_S	thickness(km)
3.60	2.80	100	10
3.60	2.80	100	10
3.60	2.80	100	10
3.60	2.80	100	10
4.50	3.30	100	∞

TABLE 2

Results of inversion methods using data generated from model of Table 1: A) linear theory inversion of Q_s only; B) exact theory inversion for Q_s and V_s; C) inversion for V_s using only the derivative $\frac{\partial c}{\partial V_s}$. (SSRQ$_L$, sum square residuals Q_L; SSRC, sum square residuals c; NI, number of iterations.)

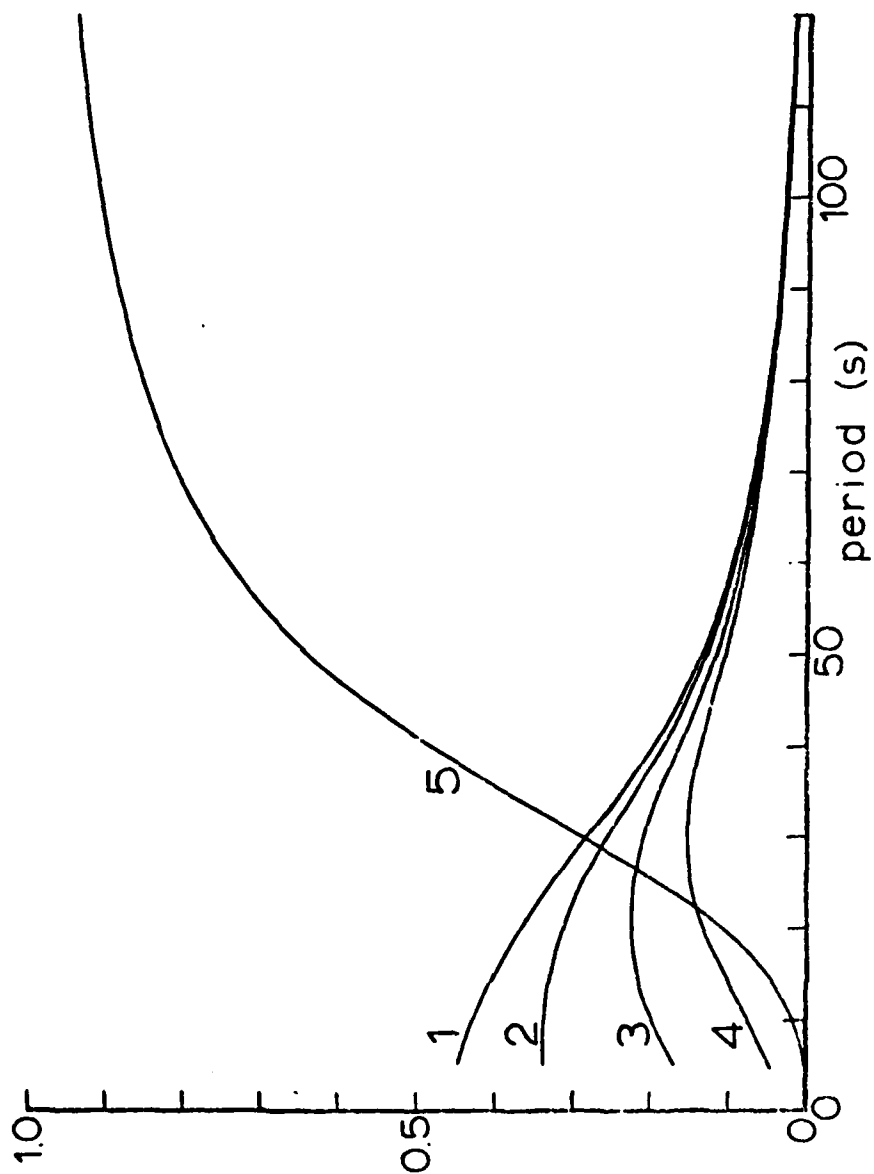|	Layer	Initial Q_s	V_s	SSRQ	SSRC	Final Q_s	V_s	SSRQ	SSRC	NI
A	1	100	3.60			122	3.60	$3.\times10^{-3}$	$2.\times10^{-12}$	0
	2	100	3.60			74	3.60			
	3	100	3.60			130	3.60			
	4	100	3.60			94	3.60			
	5	100	4.50			100	4.50			
B	1	110	3.20	.08	0.1	100	3.59	$9.\times10^{-10}$	$1.\times10^{-9}$	13
	2	90	3.20			98	3.63			
	3	110	3.20			101	3.57			
	4	90	3.20			100	3.62			
	5	100	4.50			100	4.50			
C	1	100	3.20	.07	0.1	100	3.53	$3.\times10^{-3}$	$1.\times10^{-4}$	11
	2	100	3.20			100	3.46			
	3	100	3.20			100	4.28			
	4	100	3.20			100	2.98			
	5	100	4.50			100	4.50			

Fig. 2. The derivatives $\frac{\partial c}{\partial V_s}$ for the crustal model. Layers are indicated with layer 5 the half-space.
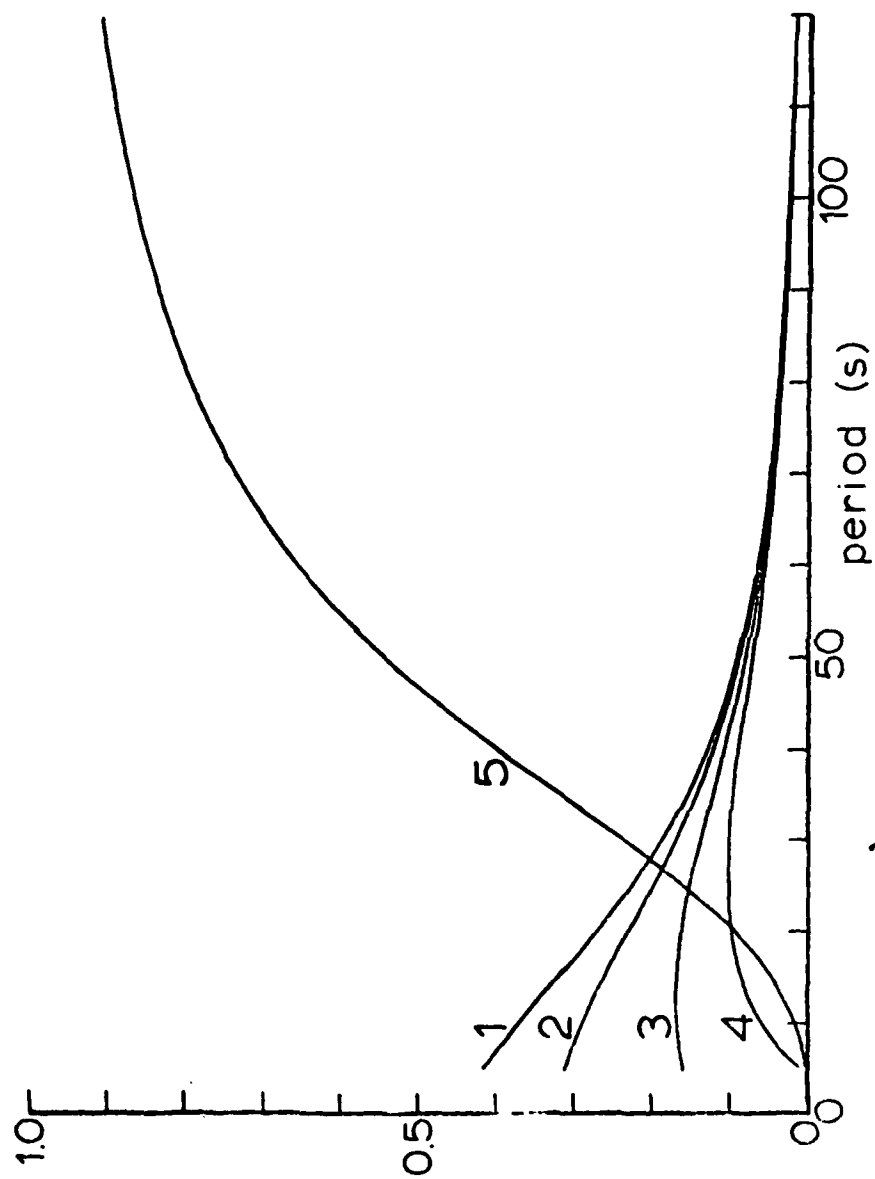
Fig. 3. The derivatives $\frac{\partial c}{\partial Q_S}$ for the crustal model. Layers are indicated with layer 5 the half-space.

Fig. 4. The derivatives $\frac{\partial Q_{\tau}}{\partial V_S} \frac{1}{V_S}$ for the crustal model. Layers are indicated with layer 5 the half-space.

Fig. 5. The derivatives $\frac{\partial Q_L}{\partial Q_s}$ for the crustal model. Layers are indicated with layer 5 the half-space.

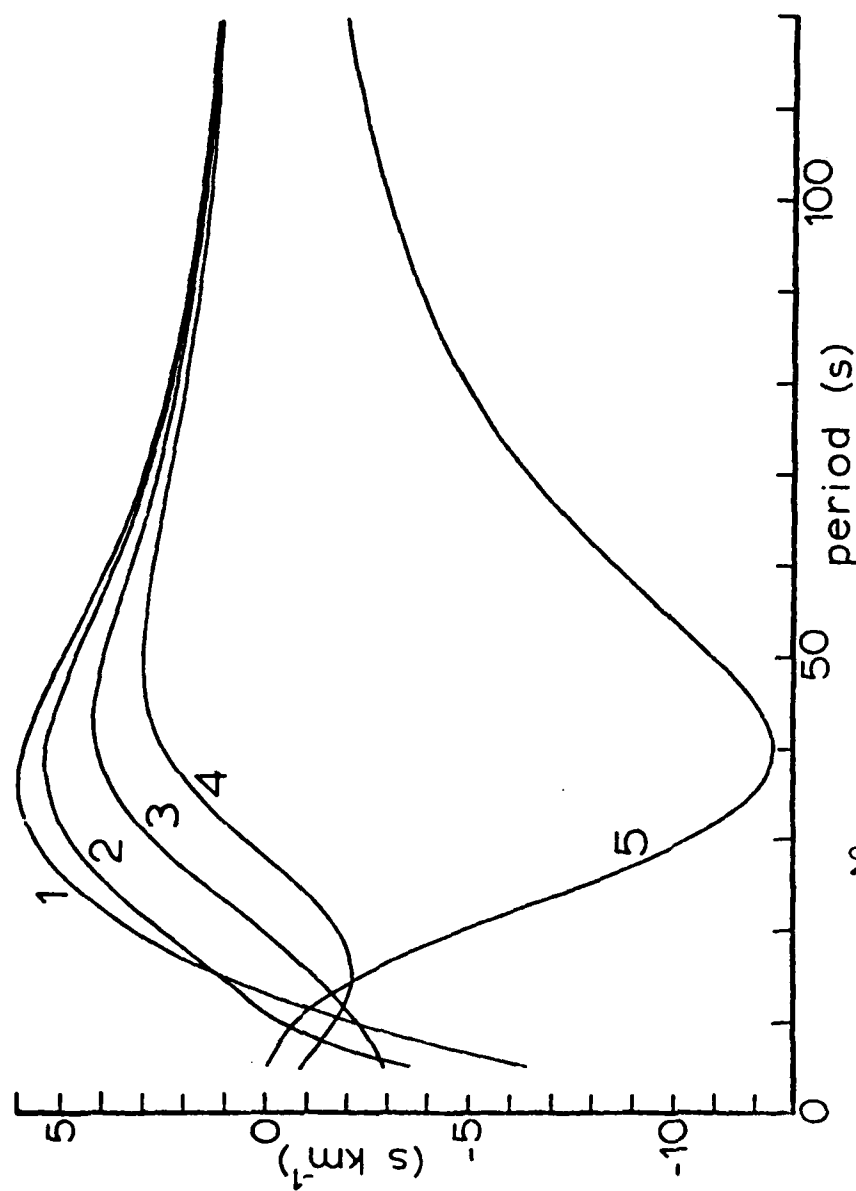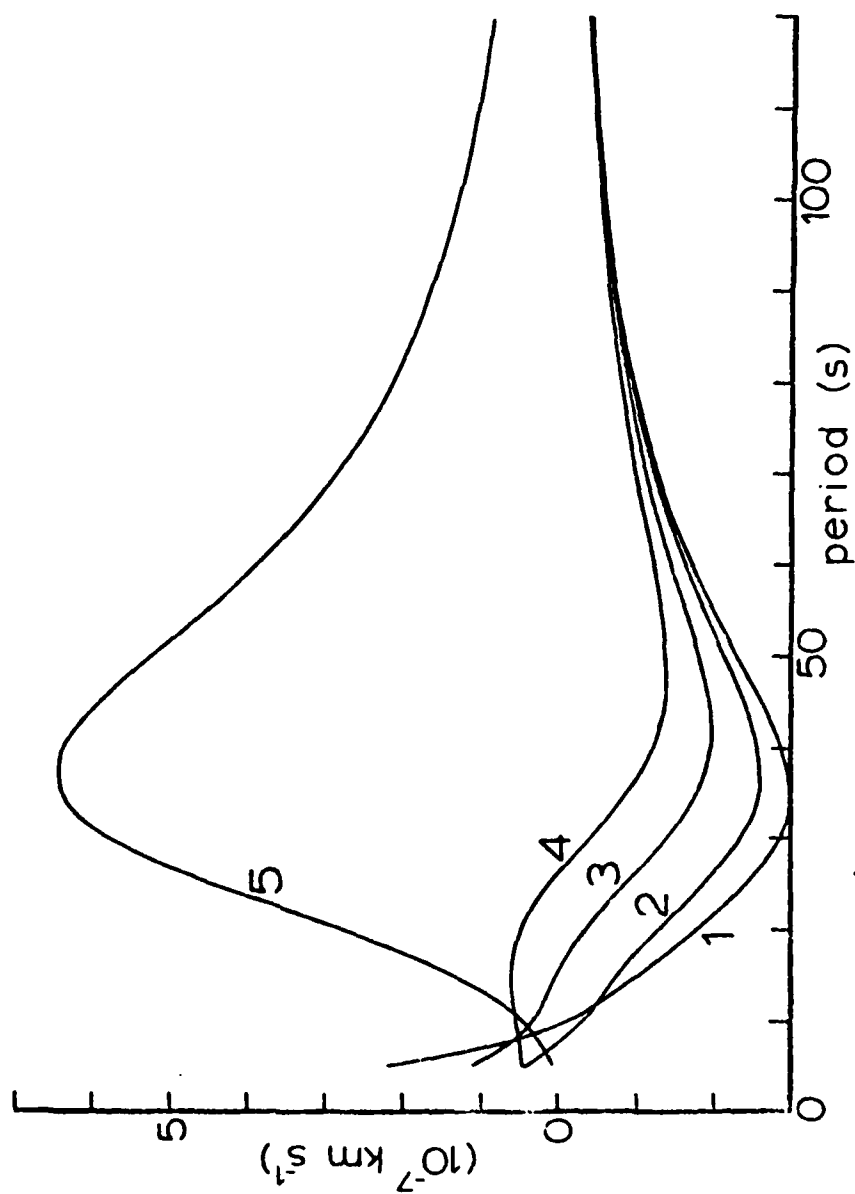# REFERENCES

Anderson, D.L. and Archambeau, C.B., 1964. The anelasticity of the Earth, J. Geophys. Res., 69, 2071-2084.

Brune, J.N., 1962. Attenuation of dispersed wave trains, Bull. Seism. Soc. Am., 52, 1, 109-112.

Burton, P.W., 1977. Inversions of high frequency Q^{-1} (f), Geophys. J.R. Astr. Soc., 48, 29-51.

Conte, S.D. and Debor, C. Elementary Numerical Analysis, 396pp., McGraw-Hill, 1965.

Der, Z., Masse, R., and Landisman, M., 1970. Effects of observational errors on the resolution of surface waves at intermediate distances, J. Geophys. Res., 75, 3399-3409.

Der, Z.A. and Landisman M., 1972. Theory for errors, resolution, and separation of unknown variables in inverse problems with application to the mantle and the crust in southern Africa and Scandinavia, Geophys. J. Roy. Astr. Soc., 27, 137-178.

Harkrider, D.G., 1968. The perturbation of Love wave spectra, Bull. Seism. Soc. A., 58, 3, 861-880.

Haskell, N.A., 1953. Dispersion of surface waves in multilayered media, Bull. Seism. Soc. A., 43, 17-36.

Jackson, D.D., 1972. Interpretation of inaccurate, insufficient and inconsistent data, Geophys, J.R. Astr. Soc., 28, 97-109.

Kanamori, H. and Anderson, D.L., 1977. Importance of physical dispersion in surface wave and free oscillation problems: review, Rev. Geophys. Space Phys., 15, 105-112.

Lancsoz, C. Linear Differential Operators, 564 pp., D. Van Nostrand, London, 1961.

McEvilly, T.V., 1964. Central U.S. crust-upper mantle structure from Love and Rayleigh wave phase velocity inversions, Bull. Seism. Soc. Am., 54, 6, 1997-2015.

Silva, W.S., 1976a. A variational formulation for
Love waves in a layered anelastic solid, Geophys.
J.R. Astr. Soc., 45, 445-450.

Silva, W.S., 1976b. Body waves in a layered anelastic
solid, Bull. Seism. Soc. A., 66, 5, 1539-1544.

Wiggins, R.A., 1972. The general linear inverse
problem: implication of surface waves and free
oscillations for earth structure, Rev. Geophys.
Space Phys., 10, 1, 251-285.

II. INVERSION OF RAYLEIGH WAVE DATA FOR VELOCITY AND ANELASTICITY USING EXACT KERNELS

The following treatment will be precisely that of the previous except Rayleigh waves will be considered. The formulation again is that of the Haskell-Thompson method extended to include anelastic attenuation (Silva, 1976b) and applied to Rayleigh waves. The phase quality factor (Q_R) is defined exactly as in section I. An additional quality factor Q_U is introduced here and is termed the group quality factor. It is defined by the following equation C Q_R = U Q_U (Brune, 1962). It was neglected in the Love wave treatment because for a constant Q_S structure Q_U for Love waves is frequency independent and $Q_U = Q_S$. This holds for Rayleigh waves only if $Q_S = Q_p$ = constant and then $Q_U = Q_p = Q_S$. The structure considered is identical to that of the previous treatment (Table 1) with a constant Q_p = 200 structure added for P-wave attenuation.

In Figure 1 is shown C, U, Q_U and Q_R for the crustal model and represents the error free data. The group velocity, U, is calculated using a variational method applied to dissipative media (Appendix 3). In Figure 2 is shown the modulus and phase of the surface displacement ratio $\frac{U_o}{W_o}$ for the attenuating model. The phase is not very different from the elastic (90°) and the elastic modulus is within 1% of the attenuating model.

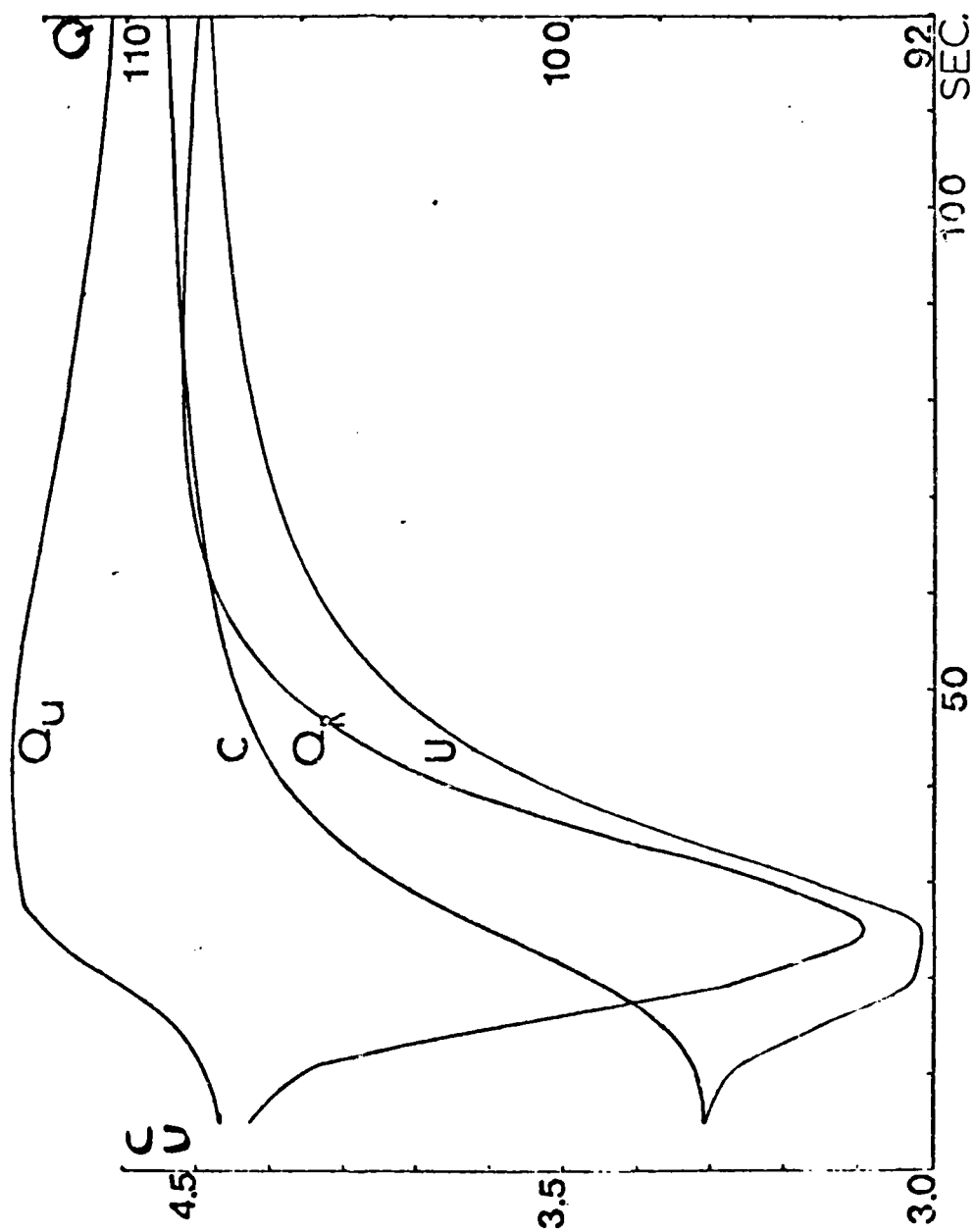Fig. 1. Plot of Rayleigh wave group quality factor Qu, phase velocity
C, phase quality factor QR, and group velocity U for crustal
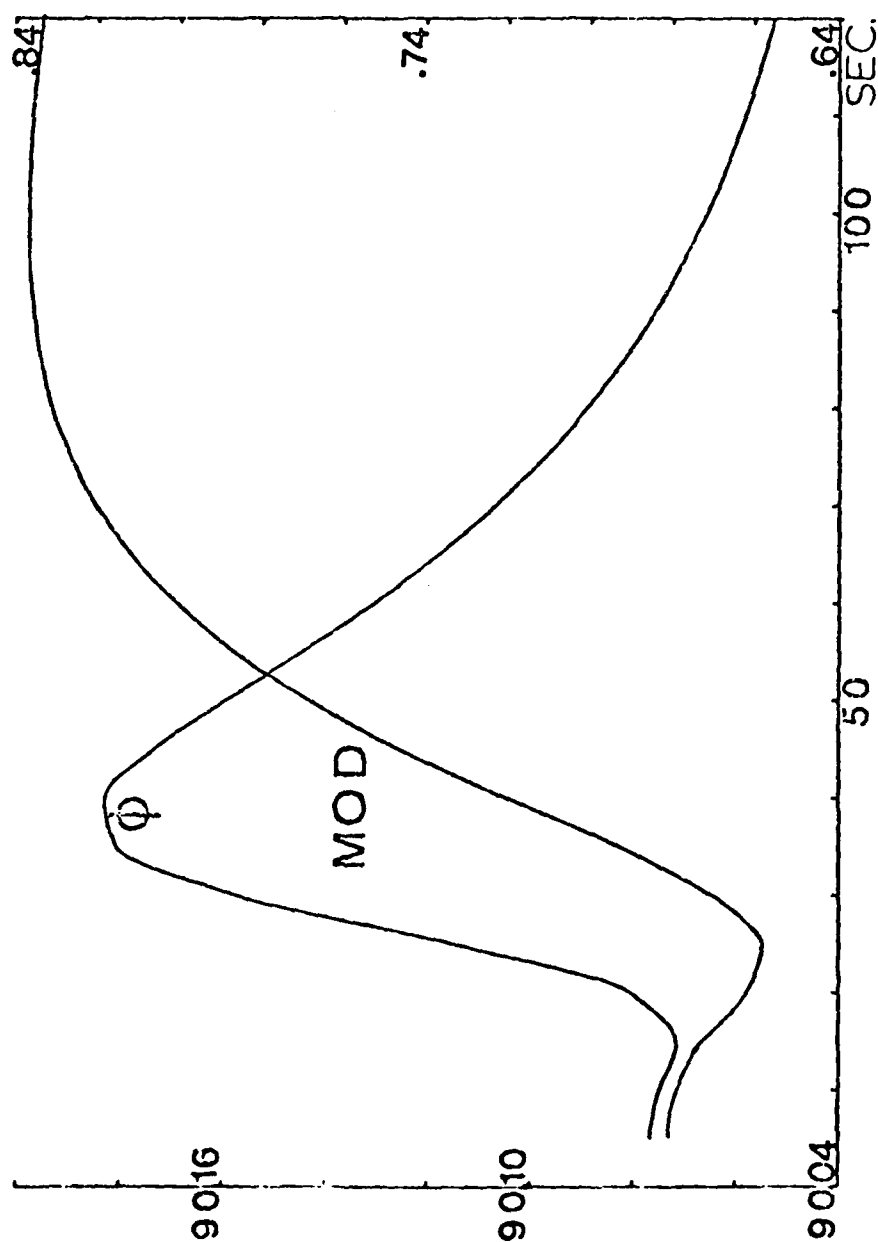model of Table 1. (C, U in km/sec)

Fig. 2. Plot of modulus and phase of surface displacement ratio (V_0/W_0) for the crustal model.

INVERSION

As in the Love wave inversion, the Taylor series
is truncated past the linear term with C and Q_R data
inverted for V_S and Q_S. The phase quality factor is
favored as an inversion parameter rather than Q_U since
its use is not contaminated by errors in determining
the group velocity. The derivatives are calculated
numerically using a 5% parameter change. A 10%
parameter change was found to be optimum in terms of
stability and speed of convergence; however, mode
tracking proved to be too difficult for this structure
and period range and therefore mandated a smaller
perturbation (plots are for a 10% change).

Considering now the plots of the derivatives
(Figures 3-14) we can note some interesting features
which give insight into the controlling features of
surface wave inversions. In Figure 3 is shown the
derivative $\frac{\partial c}{\partial v_s}$. The significant features are the
degree of independence of the curves and the presence
of peaks. Comparing these derivatives with those for
Love waves (section A, Figure 2) it is apparent that
the Rayleigh phase velocity has much more specific
information with respect to material shear velocity
for this structure and period range. This observation
is substantiated by comparing the shear velocity only
inversions for Love and for Rayleigh waves (Love;

section 1, Table 2; Rayleigh; Table 1).

Layer	Love	Exact Model	Rayleigh*
1	3.53 km/sec	3.60 km/sec	3.60 km/sec
2	3.46	3.60	3.60
3	4.28	3.60	3.60
4	2.98	3.60	3.60
5	4.50	4.50	4.50

It is quite obvious then that in this case the shape of the derivatives give an excellent indication of inversion effectiveness. A look at the next plot ($\frac{\partial c}{\partial v_p}$, Figure 4) indicates that considerable difficulty would be encountered in trying to extract the four layer P-wave velocities. Here a reduction in layering is in order and one can be guided in layer reduction by the curves. However, the magnitude is also of importance because the $\frac{\partial c}{\partial v_p}$ derivatives are competing with the $\frac{\partial c}{\partial v_s}$ derivatives and are roughly an order of magnitude smaller. This would result in putting most of the adjustment in the shear velocity structure and therefore excludes simultaneous determination of both P and SV velocity structures.

In Figure 5 is shown the first of the attenuation derivatives. As expected, it is small ($O(10^{-7})$) indicating a second order effect of attenuat . on phase velocity. An interesting feature is the

* Extracted from given tables.

appearance now of some double peaks and greatly in-

creased structure. However, the peaks here are less

separated than those of $\frac{\partial c}{\partial V_s}$ (Figure 3). Also,

comparing $\frac{\partial c}{\partial Q_s}$ (Figure 5) with $\frac{\partial Q_R}{\partial V_s}$ (Figure 9) it

is apparent that the relationship (Appendix 4)

$$\frac{\partial Q_R}{\partial V_s} = - \frac{4 \, Q_R^2 \, Q_s^2}{c \, V_s} \quad \frac{\partial c}{\partial Q_s}$$

holds.

The next plot, $\frac{\partial c}{\partial Q_p}$ (Figure 6), again shows the

lack of specificity of Rayleigh waves to P-wave

parameters. We may again invoke the previous relation-

ship and apply it to the P-wave parameters citing

$\frac{\partial Q_R}{\partial V_p}$ (Figure 10):

$$\frac{\partial Q_R}{\partial V_p} = - \frac{4 \, Q_R^2 \, Q_p^2}{c \, p} \quad \frac{\partial c}{\partial Q_p}$$

In Figure 7, $\frac{\partial Q_R}{\partial Q_s}$, we begin with the Q_R deriv-

atives. The similarity of this plot with $\frac{\partial c}{\partial V_s}$ (Figure

3) is predicted by the relation (Appendix 4)

$$\frac{\partial c}{\partial V_s} = \frac{c}{V_s} \quad \frac{Q_s^2}{Q_R^2} \quad \frac{\partial Q_R}{\partial Q_s}$$

and by an approximate theory of surface wave prop-

agation in anelastic media (Anderson and Archambeau,

1964; where now C and V_s are elastic velocities and results in a linear inversion for attenuation parameters). The shape of these $\frac{\partial Q_R}{\partial Q_s}$ curves indicates that with the correct velocity structure and correct Q_p structure, reasonable success should be expected in a Q_s inversion. The correct V_p, V_s, and Q_p structure is required in order that the correct Q_R is obtained in derivative calculations.

The next plot, $\frac{\partial Q_R}{\partial Q_p}$ (Figure 8), again shows relatively little structure and is indicative of P parameter insensitivity in Rayleigh waves. It can be compared with $\frac{\partial c}{\partial V_p}$ (Figure 4).

Figure 9 shows the derivative $\frac{\partial Q_R}{\partial V_s}$. Again, the double peak structure is present (as earlier compared with $\frac{\partial c}{\partial Q_s}$ in Figure 5) and we have increased structure at the cost of decreased independence. The final Q_R derivative, $\frac{\partial Q_R}{\partial V_p}$ (Figure 10), was earlier compared with $\frac{\partial c}{\partial Q_p}$ (Figure 6) and further shows little hope of a V_p inversion simultaneously with V_s, as $\frac{\partial Q_R}{\partial V_p}$ is an order of magnitude smaller than $\frac{\partial Q_R}{\partial V_s}$ and shows much less independence. This comparison is analogous to the $\frac{\partial c}{\partial V_s}$ and $\frac{\partial c}{\partial V_p}$ comparison. An interesting idea might be a mixed inversion. That is, use C for V_s and Q_R for V_p since $\frac{\partial Q_R}{\partial V_p}$ appears to be less linearly dependent than $\frac{\partial c}{\partial V_p}$ and $\frac{\partial Q_R}{\partial V_s}$ conversely appears to be more linearly dependent than $\frac{\partial c}{\partial V_s}$. Future work along these lines is needed.

The final plots (Figures 11-14) show the change
in modulus and phase of the surface displacement ratios
U_o/W_o for a change in V_S and Q_S. The derivatives show
that both the modulus and phase are much more sensitive
to the velocity structure than the Q_S structure for
this model. They also indicate that neither con-
tributes information independent of C or Q_R.

TESTS WITH SYNTHETIC DATA

As in the previous treatment of Love waves, the
40 km thick continental crust was subdivided into
four identical layers (section 1, Table 1). Both
the crust and uppermantle were assumed Poisson solids
for P-wave velocities which are kept fixed. Figure
1 shows the synthetic data (C and Q_R) with the same
period range and number of data as in the Love wave
inversion (120 to 5 seconds with 5 second intervals).

In Table 1 are shown the results of both the
linearized inversion (Anderson and Archambeau, 1964)
and the exact theory (both use singular value de-
composition with the non-linear appropriately scaled
(Wiggins, 1972)).

The first section, A, shows the results of the
linear inversion for Q_S using the exact velocity
structure. The Q_S structure is far from the true
structure (Q_S = 100 all layers) and the oscillations

are similar to linearized Love wave inversion (Table 2, section A). Since the error here, as much as 39%, is greater than the linearized Love wave inversion, part of the blame must be put on the approximate data kernels. That is, the partial derivatives used in the linearized Q_S inversion are numerically calculated for Rayleigh waves and are analytical derivatives for Love waves. The numerical derivatives in the linear Rayleigh formulation yield approximately a 5% error in the forward calculation. However, the error may be significantly larger for inverse operations. A simple calculation may serve to point this out as it indicates that small errors in inversions kernels can be magnified especially in large condition number systems.

Let;

$$D = (L + e)M = L(I + L^{-1}e)M$$

where D is some data vector, L some data kernel with error terms e, and M the model. Now if e is say 5% of L in some norm, then D will have an error of the same magnitude. On the other hand, inverting the system we have

$$M = (I + L^{-1}e)^{-1} L^{-1} D.$$

Now if we let $M' = L^{-1} D$ be the real model (error free) then

$$M = (I + L^{-1}e)^{-1} M'$$

or

$$M \approx (I - L^{-1}e)M', \quad \|L^{-1}e\| < 1$$

then the model we get (M) can differ from the true

model (M') by more than 5% even though L^{-1} is well

behaved (i.e., $\|L^{-1}e\| < 1$). This should discourage

non-iterative inversions with approximate kernels.

This error magnification is probably contributing

to the very poor inversion results of the linear

theory and should further underscore the need for

extreme caution in evaluating its results. However,

the comparison between the linear approximation and

the exact theory is not unjust because the error

certainly cannot account for all of the discrepancy

and the same numerical derivatives are used in the

exact formulation (future work will investigate the

effect of analytical derivatives).

In section B are shown the results of the exact

theory inversion for V_s and Q_s with an exact Q_p

structure (held constant). The results are quite

satisfactory as both the V_s and Q_s structures have

been recovered. Indeed, the results are superior

to the Love wave inversion as was expected from the

analysis of the derivative plots. The velocity only

inversion is shown in section C, shows good convergence,

and is far superior to the Love wave velocity inversion.

It appears then, that for this model the amplitude data

is not essential in the velocity inversion. Perhaps
a further perturbed starting structure would require
the amplitude data to stabilize the velocity inversion.
This was not attempted since more than a 10 percent
change is pushing the Taylor approximation and it
was desirable to keep the same starting models for
both Rayleigh and Love wave inversion.

In order to investigate the effect of Q_p on the
inversion, it was fixed at the wrong value (250) and
the V_s and Q_s inversion repeated. The results are
shown in section D and are somewhat surprising. One
might naively assume the effect of Q_p to be small
since it is twice Q_s. However, as section D shows,
fixing it at the wrong value (and with only a 25
percent discrepancy) has a disasterous effect on Q_s
and affects V_s through $\dfrac{\partial Q_R}{\partial V_s}$. In light of these
results, Q_p was allowed to float using the same
starting model as section D. The hope is that this
will release the inversion and allow it to converge
to a closer Q_s and V_s structure. The results are
shown in section E and indicate that this is indeed
the case as both the Q_s and V_s structures have essent-
ially been recovered while the crustal Q_p has moved
the correct way. An attempt at using the linear
theory for a simultaneous inversion for Q_s and Q_p
yielded extremely poor values for both and is not
shown.

CONCLUSION

Tests with synthetic data in inverting Rayleigh
wave phase and attenuation data for velocity and
anelasticity indicate a greater stability and reli-
ability for an exact formulation over the appropriate
linear formulation (Anderson and Archambeau, 1964).
In addition, when inverting for anelasticity Q_p has
a first order effect and must be considered as an
inversion parameter along with Q_s.

TABLE 1

Results of inversion methods using data generated
from model of Table 1 (Section A): A) linear theory
inversion for Q_s only; B) exact theory inversion for
Q_s and V_s; C) inversion for V_s using only the deriv-
ative $\frac{\partial c}{\partial V_s}$; D) inversion for V_s and Q_s with wrong Q_p;
E) inversion for V_s, Q_s, and Q_p. (SSRQ, sum square
residuals Q_R; SSRC, sum square residuals C; NI,
number of iterations in a suite of 20.)

		Initial					Final					
Layer	Q_p	Q_s	V_s	SSRQ	SSRC		Q_p	Q_s	V_s	SSRQ	SSRC	NI
A 1			3.60					88	3.60			
2			3.60					83	3.60			
3			3.60					120	3.60			0
4			3.60					61	3.60			
5			4.50					86	4.50			
B 1	200	110	3.20				200	100	3.60			
2	200	90	3.20				200	99	3.60			
3	200	110	3.20	$1.\times10^{-7}$	$7.\times10^{-2}$		200	100	3.60	$3.\times10^{-9}$	$2.\times10^{-10}$	7
4	200	90	3.20				200	99	3.60			
5	200	100	4.50				200	100	4.50			
C 1			3.20						3.60			
2			3.20						3.60			
3			3.20		$7.\times10^{-2}$				3.60		$2.\times10^{-10}$	6
4			3.20						3.60			
5			4.50						4.50			
D 1	250	110	3.20				250	98	3.61			
2	250	90	3.20				250	98	3.55			
3	250	110	3.20	$8.\times10^{-2}$	$7.\times10^{-2}$		250	104	3.69	$9.\times10^{-6}$	$3.\times10^{-6}$	6
4	250	90	3.20				250	90	3.54			
5	250	100	4.50				250	98	4.50			
E 1							228	99	3.60			
2							227	99	3.59			
3		Same as (D)					229	99	3.60	$1.\times10^{-8}$	$7.\times10^{-9}$	13
4							224	97	3.59			
5							274	98	4.50			

Fig. 3. The derivatives $\frac{\partial c}{\partial v_s}$ for the crustal model. Layers are indicated with layer 5 the half-space.
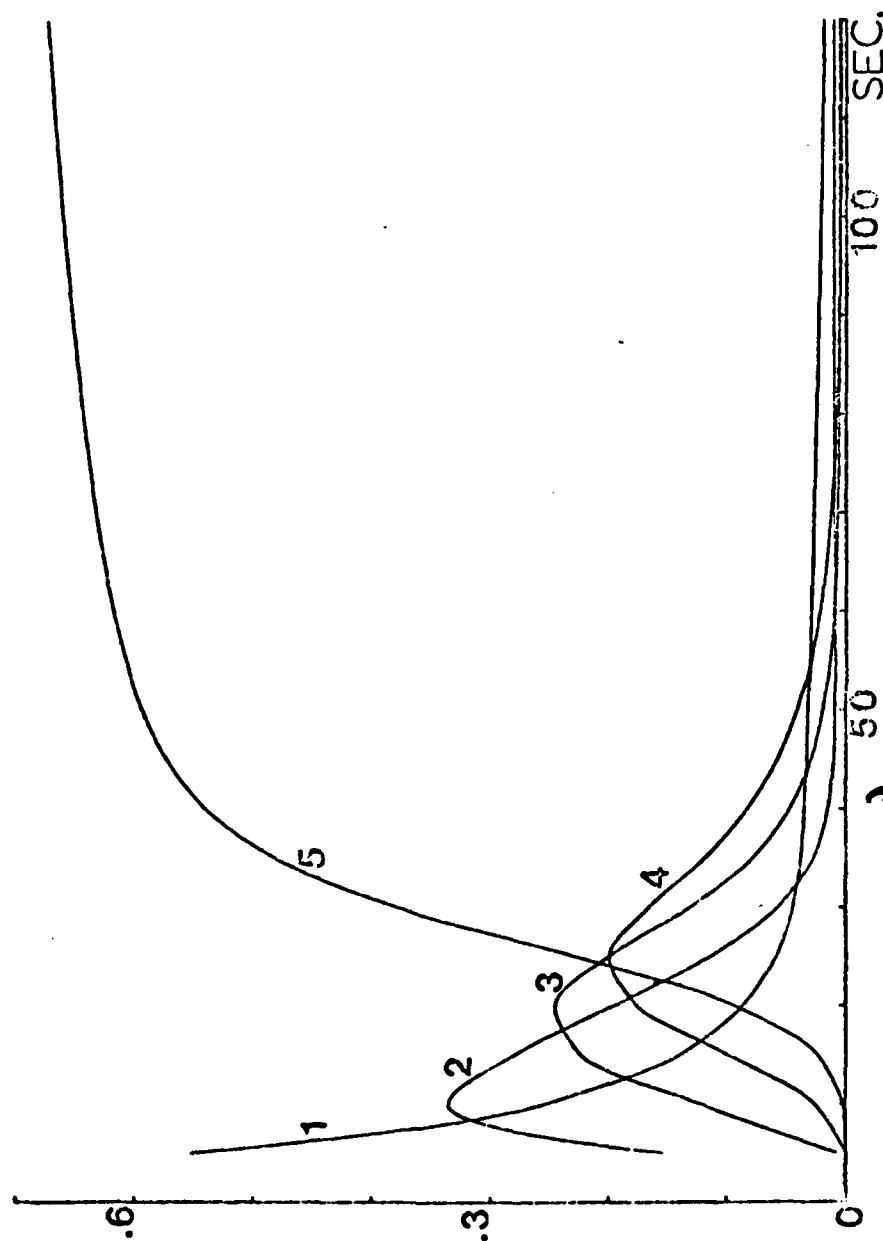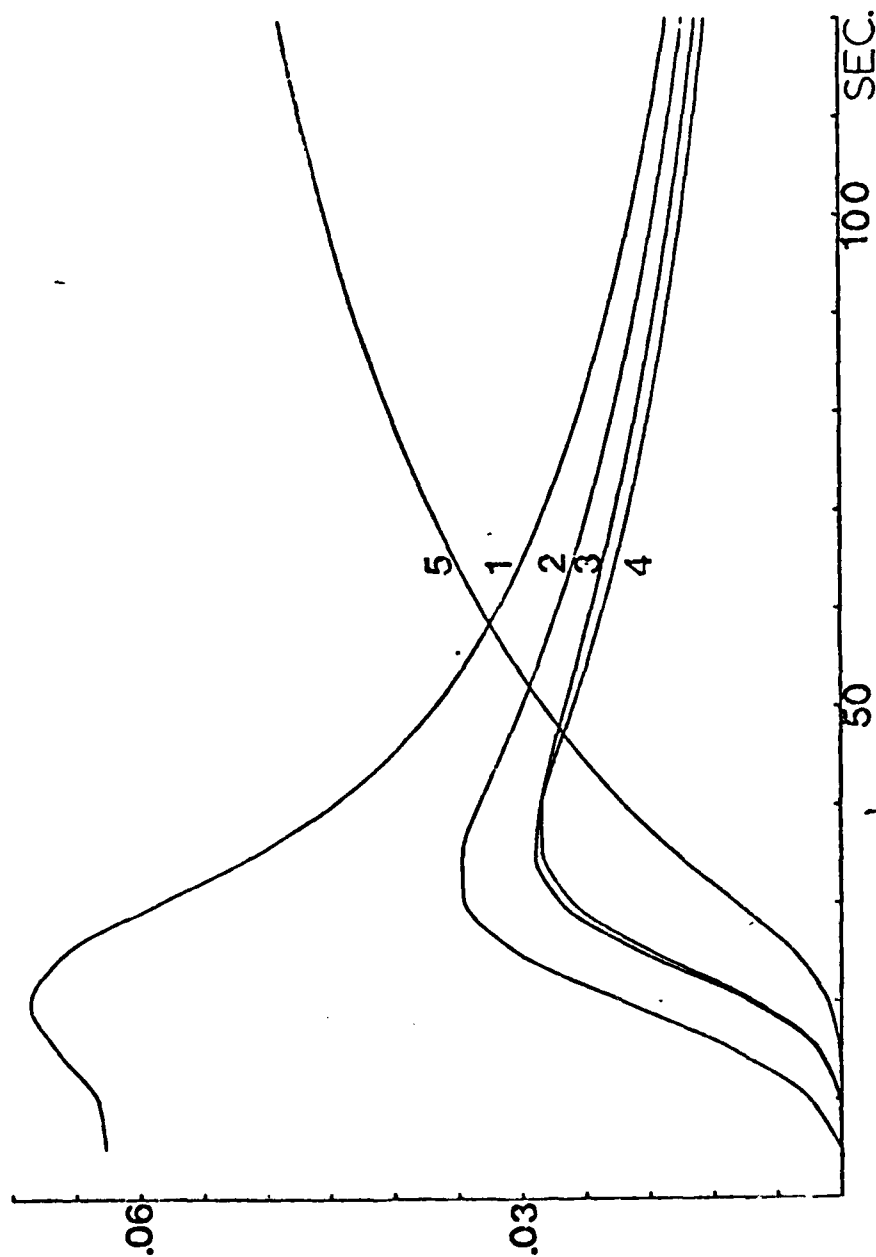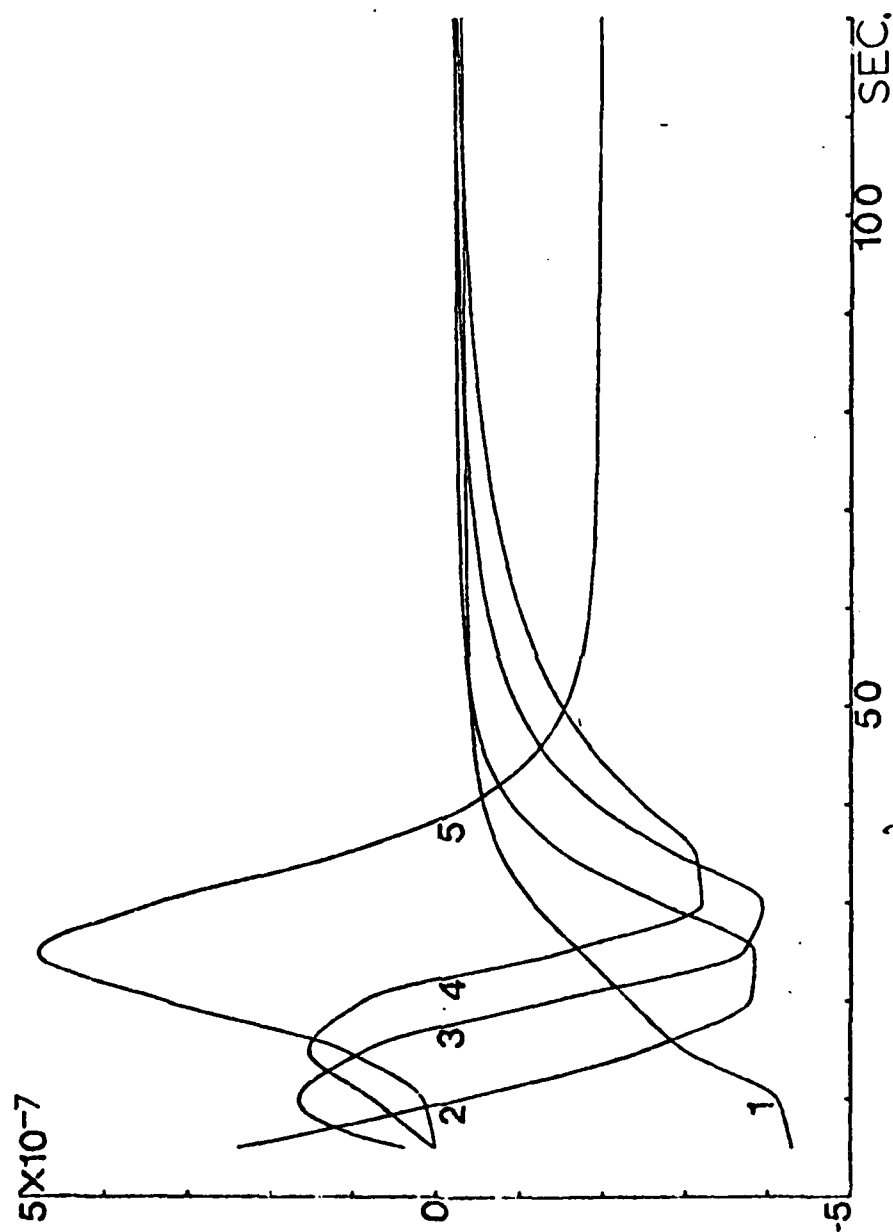
Fig. 4. The derivatives $\frac{\partial}{\partial V_P}$ for the crustal model. Layers are indicated with layer 5 the half-space.

Fig. 5. The derivatives $\frac{\partial c}{\partial \beta_s}$ for the crustal model. Layers are indicated with layer 5 the half-space.
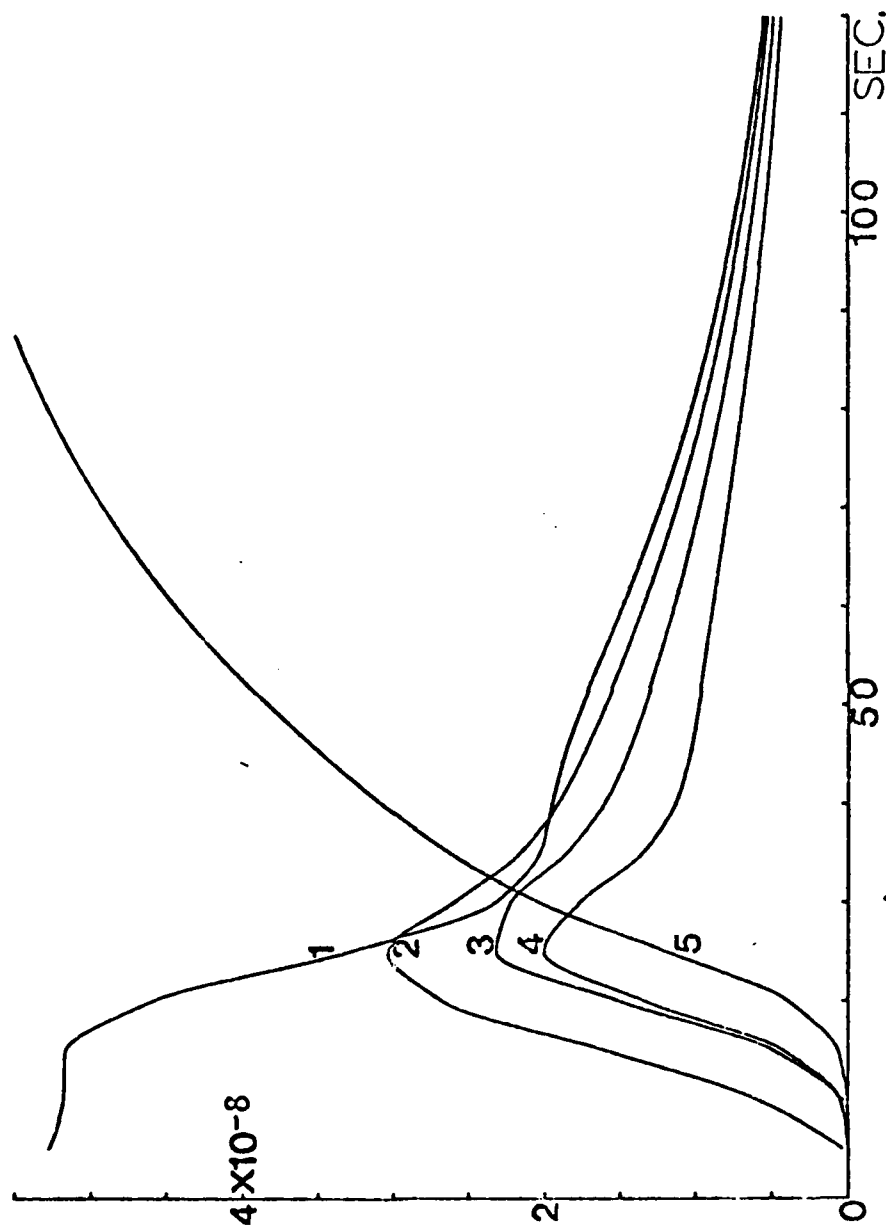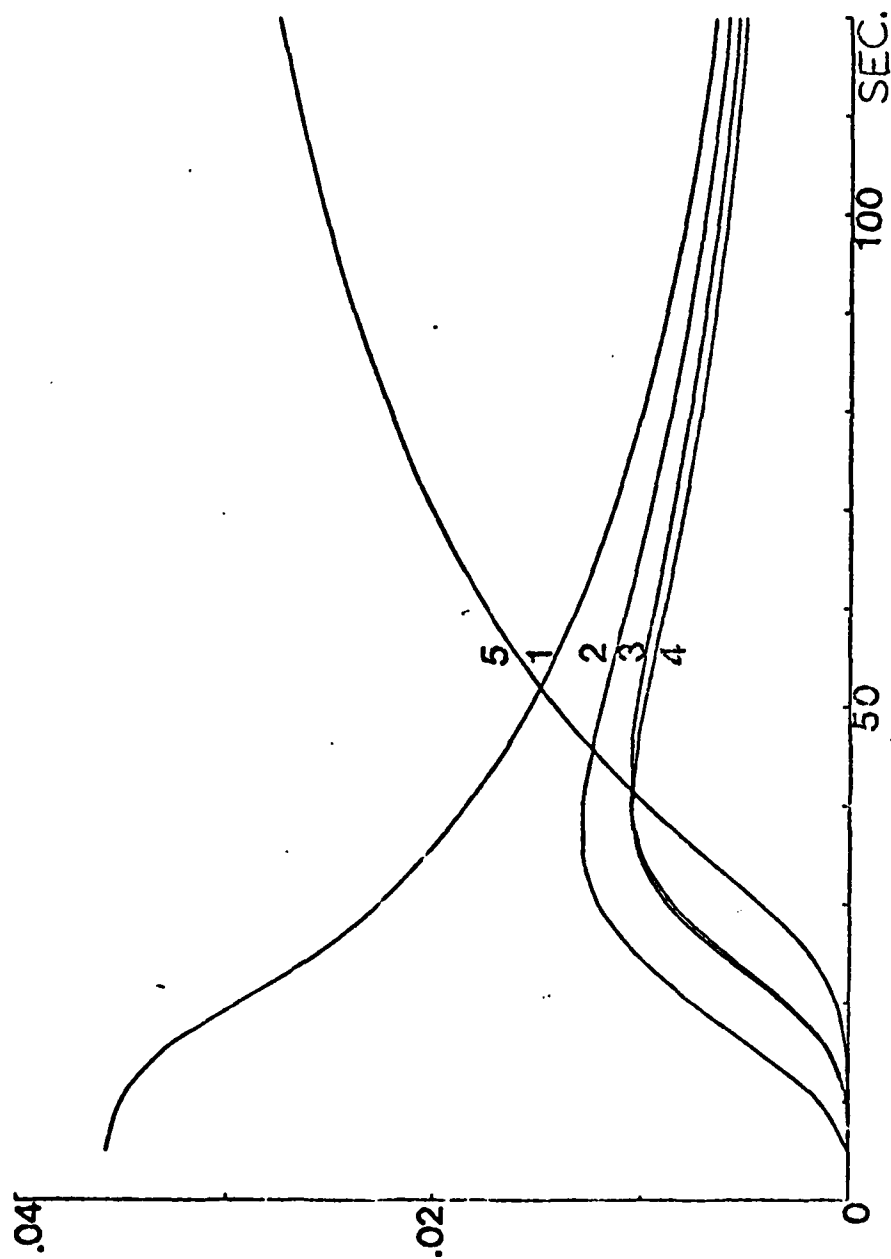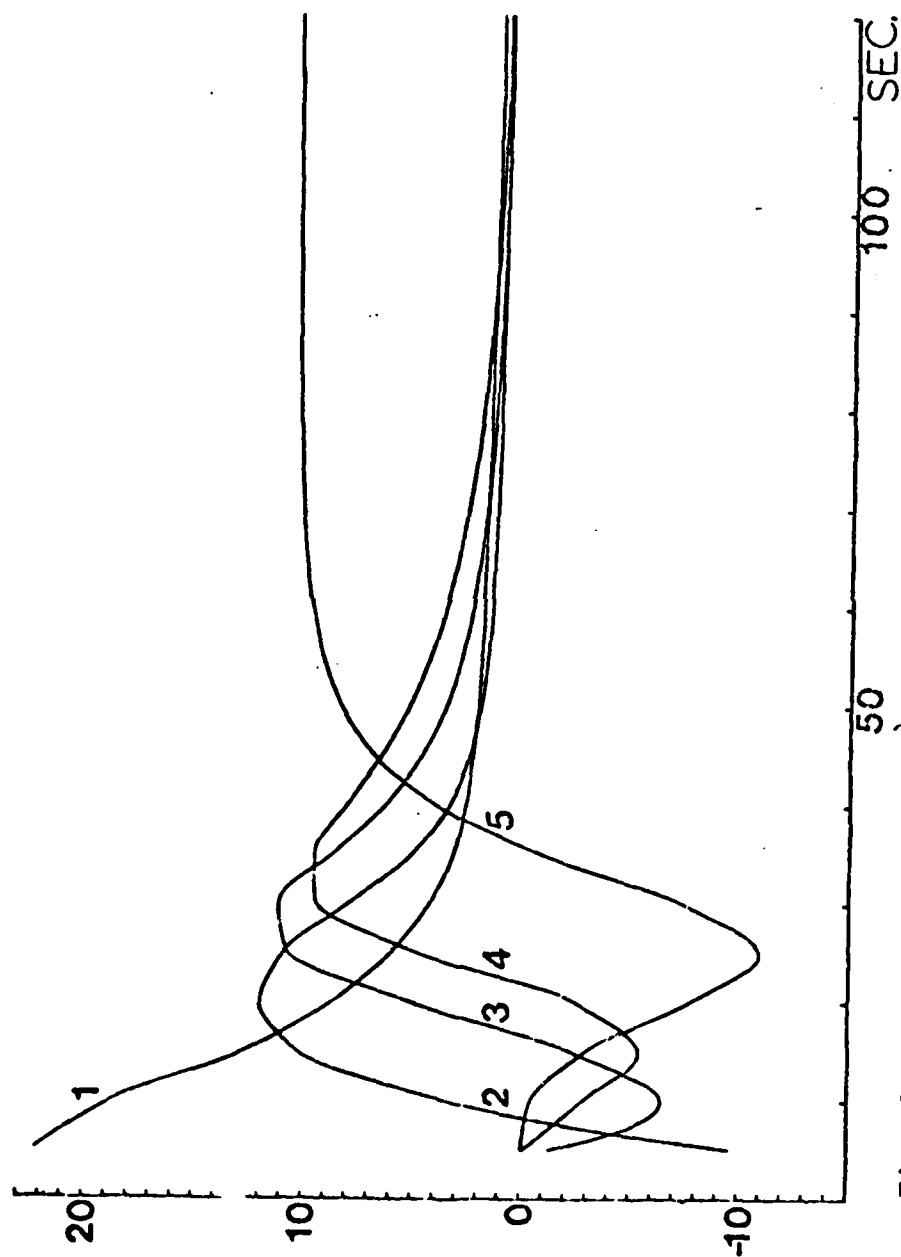
Fig. 6. The derivatives $\frac{\partial c}{\partial \beta_i}$ for the crustal model. Layers are indicated with layer 5 the half-space.

Fig. 7. The derivatives $\frac{\partial}{\partial}\frac{Q_R}{Q_s}$ for the crustal model. Layers are indicated with layer 5 the half-space.

Fig. 5. The derivatives $\frac{\partial}{\partial} \frac{Q_R}{Q_p}$ for the crustal model. Layers are indicated with layer 5 the half-space.

Fig. 9. The derivatives $\frac{\partial Q_R}{\partial V_S}$ for the crustal model. Layers are indicated with layer 5 the half-space.
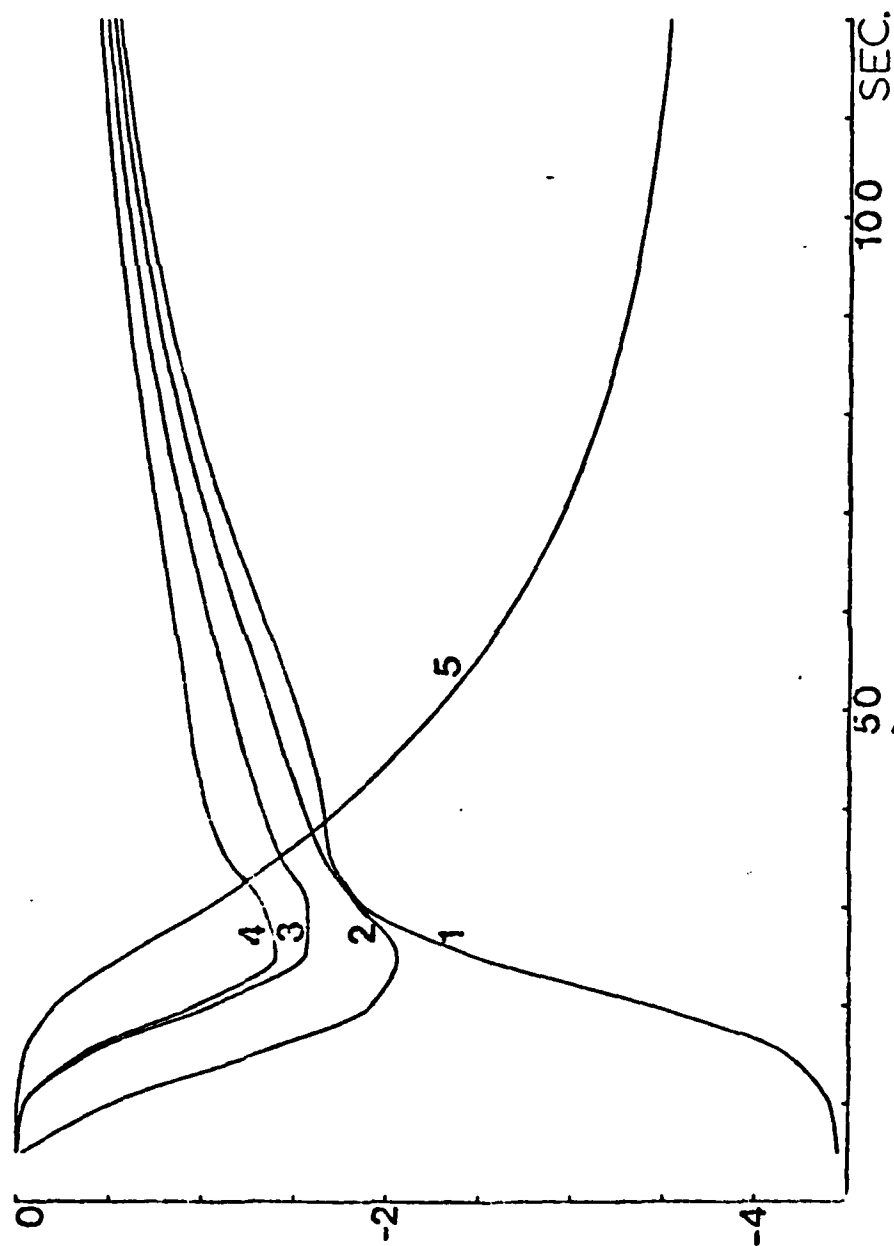
Fig. 10. The derivatives $\dfrac{\partial Q_R}{\partial V_P}$ for the crustal model. Layers are indicated with layer 5 the half-space.
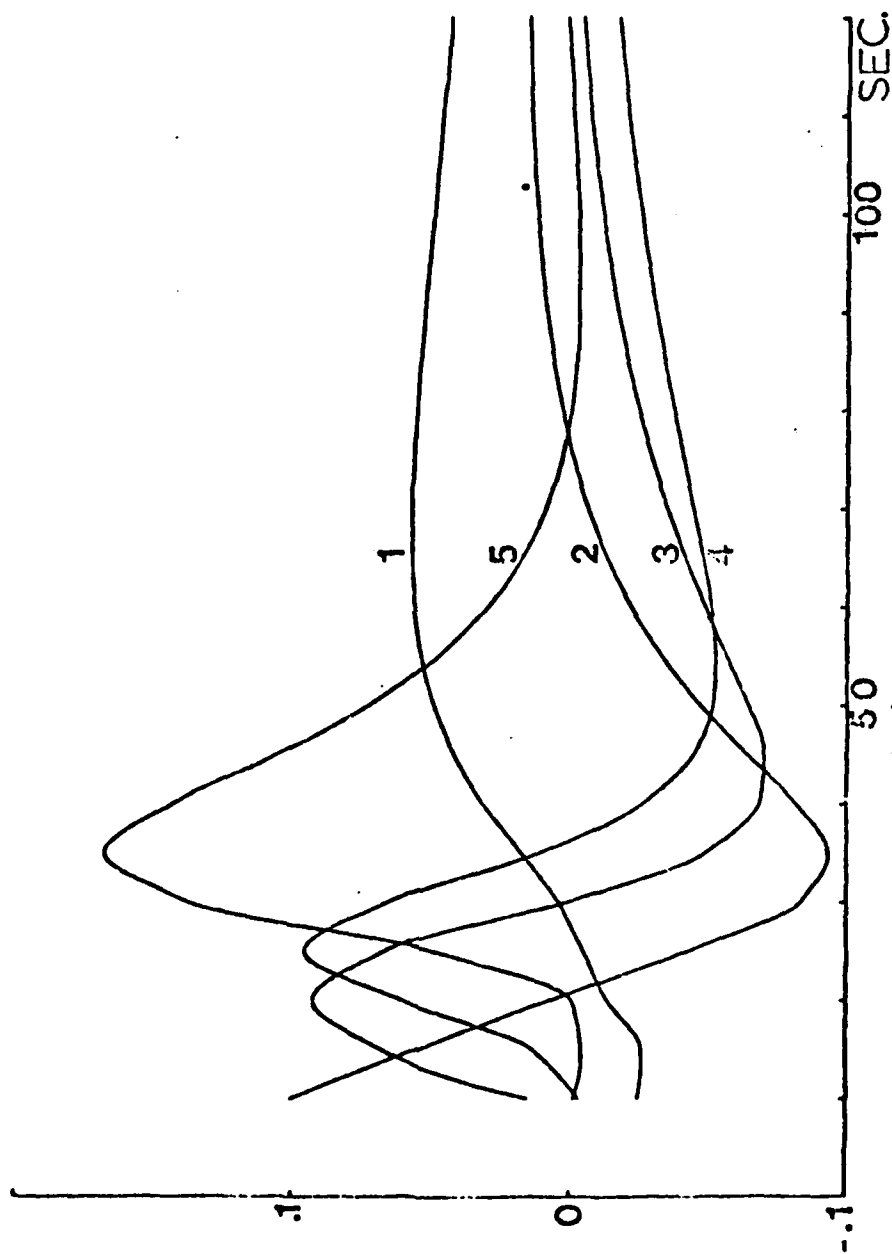
Fig. 11. The derivatives $\dfrac{\partial M}{\partial Vs}$ for the crustal model. Layers are indicated with layer 5 the half-space.
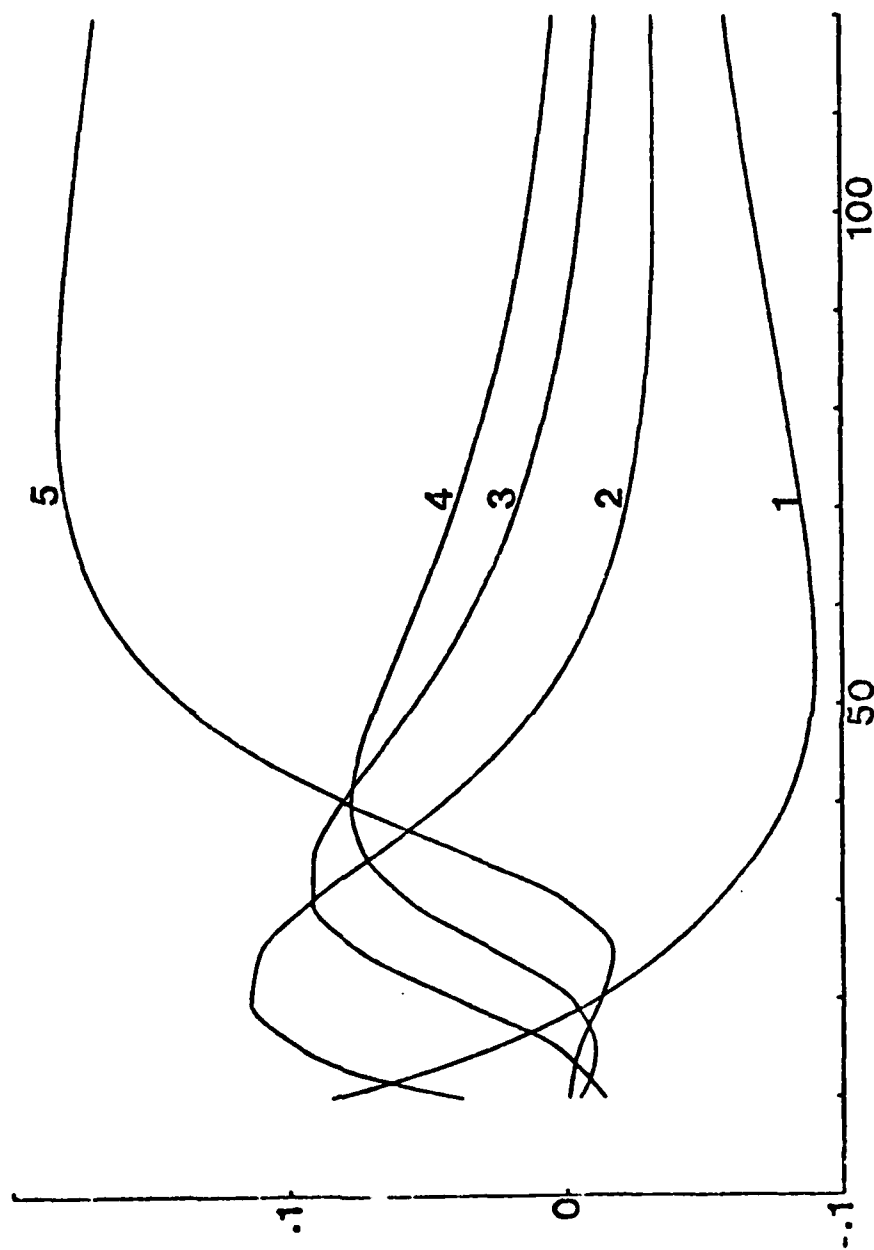
Fig. 12. The derivatives $\frac{\partial A}{\partial V_S}$ for the crustal model. Layers are indicated with layer 5 the half-space.
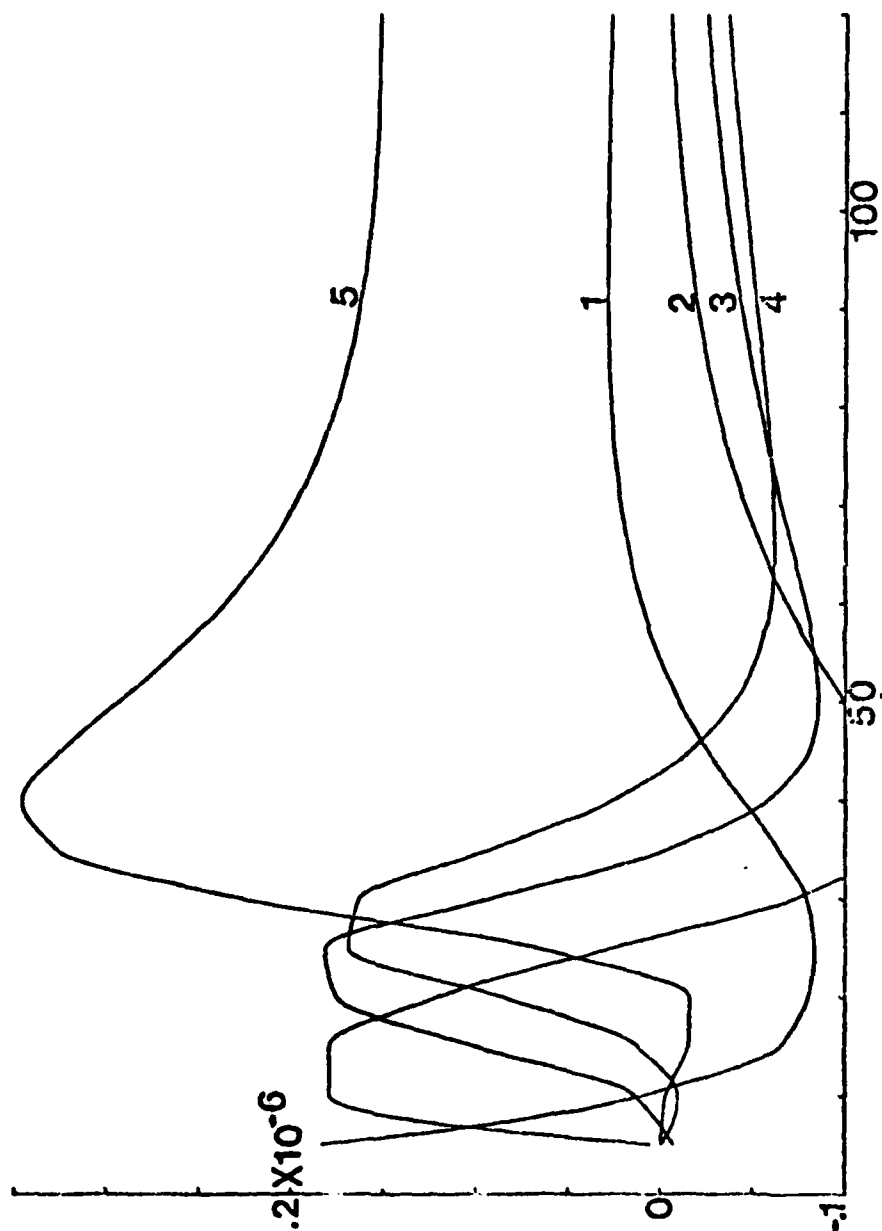
Fig. 13. The derivatives $\frac{\partial M}{\partial Q_s}$ for the crustal model. Layers are indicated with layer 5 the half-space.
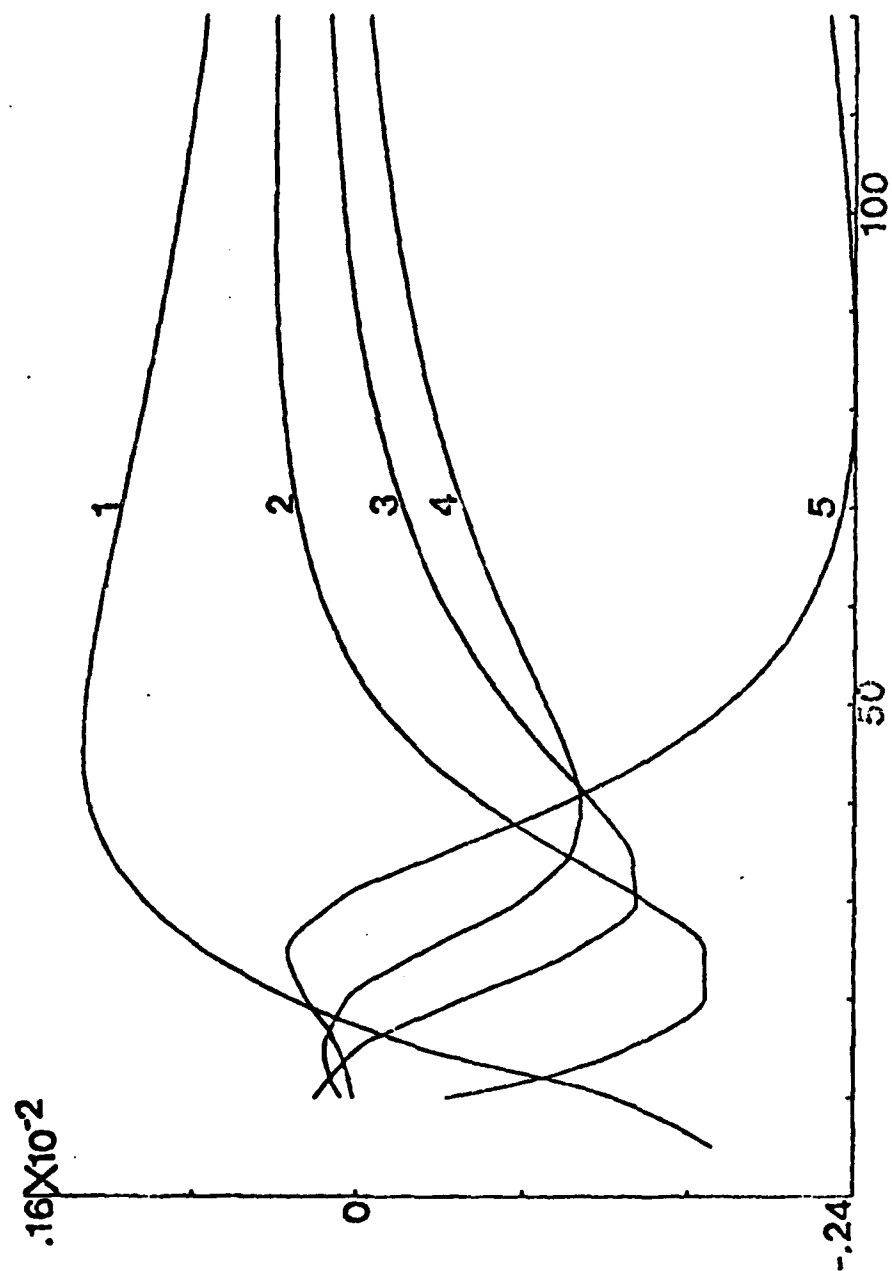
Fig. 14. The derivatives $\frac{\partial \phi}{\partial Q_i}$ for the crustal model. Layers are indicated with Layer 5 the half-space.

REFERENCES

Anderson, D.L. and Archambeau, C.B., 1964. The anelasticity of the Earth, J. Geophys. Res., 69, 2071-2084.

Brune, J.N., 1962. Attenuation of dispersed wave trains, Bull. Seism. Soc. Am., 52, 1, 109-112.

Silva, W.S., 1976b. Body waves in a layered anelastic solid, Bull. Seism. Soc. Am., 66, 5, 1539-1544.

Wiggins, R.A., 1972. The general linear inverse problem: implication of surface waves and free oscillations for earth structure, Rev. Geophys. Space Phys., 10, 1, 251-285.

APPENDIX 2

VARIATIONAL FORMULATION FOR LOVE WAVES

IN A LAYERED ANELASTIC SOLID

A Variational Formulation for Love Waves in a Layered Anelastic Solid

Walt Silva

Department of Geology and Geophysics, University of California, Berkeley, California, USA

Summary

A method is presented which allows the variational formulation for elastic surface waves to be extended to the case of dissipative media. With this formulation, correct to second order in the loss, Rayleigh's principle can be applied to perturbations of the Rayleigh quotient to yield group velocity without numerical differentiation. Other perturbations can be used to find the change in phase or group velocity due to changes in loss, density, or moduli.

Introduction

The use of Rayleigh's principle is of considerable importance in surface-wave calculations. As suggested by Meissner (1926) and Jeffreys (1959, 1961) and amended by Harkrider (1968) it has replaced numerical methods with an exact formulation for calculating group velocities. In addition, Rayleigh's principle may be used to calculate the effect on the velocity dispersion due to small perturbations in the elastic parameters. This type of information is, of course, most essential in solving inverse problems.

However, in its usual form, Rayleigh's principle is inadequate for dissipative systems since its use requires equating the time average kinetic and potential energies. This result follows from the virial theorem and imposes a vanishing Lagrangian for the system.

The purpose of the following development is to construct a Lagrangian for a non-conservative system which vanishes and then apply Rayleigh's principle to the resulting equation. This can be done by writing a Lagrangian for two systems operating simultaneously with one losing energy as the other gains energy, so that the total energy is conserved. An estimate of the error introduced in combining the systems is given in the Appendix.

The development will be for Love waves in order to simplify the equations. The extension to Rayleigh waves follows naturally.

Formulation

As a working example, we shall consider Love waves propagated along the

445

A

surface of a vertically heterogenous (layered) attenuating half space. The usual equation to be satisfied in each layer is

$$\mu_R \nabla^2 u + \frac{\mu_I}{\omega} \nabla^2 \dot{u} = \rho \ddot{u}$$ (1)

where u is the transverse particle displacement, ρ is the medium density, and μ_R and μ_I are the conservative and non-conservative Lamé parameters, respectively, which are in general frequency dependent (Borcherdt 1971; Silva 1976). We take as the solution to equation (1)

$$u = v(z) \exp(-A_x x) \cos(P_x x - \omega t)$$ (2)

where P_x is the spatial frequency such that the horizontal anelastic phase velocity c is given by $c = \omega/P_x$ and A_x is the horizontal attenuation factor. Application of the usual boundary conditions results in the continuity of both P_x and A_x. They then represent eigenvalues to be determined for propagating modes. The attenuation factor may be defined as

$$A_x = \frac{\omega}{c} \left[\frac{-1 + \sqrt{(1 + Q_L^{-2})}}{1 + \sqrt{(1 + Q_L^{-2})}} \right]^{\frac{1}{2}} \approx \frac{\omega}{2cQ_L}$$ (3)

where Q_L represents the effective quality factor for the spatial decay of the surface wave. Equation (3) can then be interpreted as the projection of the attenuation in the propagation direction. The shear quality factor Q_S is defined as

$$Q_S^{-1} = \frac{1}{2\pi} \frac{\Delta E}{E} \approx \frac{\mu_I}{\mu_R}$$ (4)

where ΔE is the energy lost and E the peak energy stored, both per cycle.

At this point we introduce the mirror image system which is taken to exist simultaneously with the original field. Since this field gains energy exactly as the first loses energy, we can write the field equation as

$$\mu_R \nabla^2 u^+ - \frac{\mu_I}{\omega} \nabla^2 \dot{u}^+ = \rho \ddot{u}^+$$ (5)

with the corresponding solution,

$$u = v(z) \exp(A_x x) \cos(P_x x - \omega t).$$ (6)

It is seen then that the only difference in the systems is in the sign of μ_I. This then affects only the sign of the attenuation constant and yields the same spatial frequencies as equation (2).

In order to construct a conservative Lagrangian density we make use of the following form (Morse & Feshbach 1953; Moisewitsch 1966).

$$\mathscr{L} = \rho \dot{u} \dot{u}^+ - \frac{1}{2} \frac{\mu_I}{\omega} \nabla^2 [u \dot{u}^+ - \dot{u} u^+] - \mu_R \left[\frac{\partial u}{\partial x} \frac{\partial u^+}{\partial x} + \frac{\partial u}{\partial z} \frac{\partial u^+}{\partial z} \right].$$ (7)

This yields an invariant Lagrangian, since u^+ increases in amplitude exactly as u decreases.

The corresponding Euler–Lagrange equations become:

$$\left.\begin{array}{l}
\dfrac{\partial \mathscr{L}}{\partial u} - \dfrac{d}{dt}\dfrac{\partial \mathscr{L}}{\partial \dot{u}} - \dfrac{d}{dx}\dfrac{\partial \mathscr{L}}{\partial u_x} - \dfrac{d}{dz}\dfrac{\partial \mathscr{L}}{\partial u_z} = 0 \\[4mm]
\dfrac{\partial \mathscr{L}}{\partial u^+} - \dfrac{d}{dt}\dfrac{\partial \mathscr{L}}{\partial \dot{u}^+} - \dfrac{d}{dx}\dfrac{\partial \mathscr{L}}{\partial u_x^+} - \dfrac{d}{dz}\dfrac{\partial \mathscr{L}}{\partial u_z^+} = 0
\end{array}\right\} . \tag{8}$$

Direct substitution of equation (7) into equation (8) yields equations (1) and (5). We now substitute the solutions (equations (2) and (6)) into equation (7) and then space-time integrate the Lagrangian density to yield the Lagrangian of the combined system. In the time and x integrations, where periodic solutions were assumed, the integrations result simply in averages.

Defining L as the Lagrangian of the combined system, we can write:

$$L = \omega^2 \int \rho v v^+ \, dz - (P_x^2 - A_x^2)\int \mu_R v v^+ \, dz - \int \mu_R v' v^{+\prime} \, dz . \tag{9}$$

The first term is interpreted as a time average kinetic energy and the remaining two terms as a time average potential energy. This allows the application of the virial theorem (Moisewitsch 1966) which states that for a conservative system which is quadratic in its potential energy the time average potential and kinetic energies are equal.

We may then put equation (9) onto the form of the Rayleigh quotient:

$$\omega^2 I_0 = (P_x^2 - A_x^2) I_1 + I_2 \tag{10}$$

with the energy integrals

$$I_0 = \int \rho v v^+ \, dz; \quad I_1 = \int \mu_R v v^+ \, dz; \quad I_2 = \int \mu_R v' v^{+\prime} \, dz.$$

Application of Rayleigh's principle

Rayleigh's principle states that for a given Rayleigh quotient, as in equation (10), any eigenvectors, correct to first order, will yield the eigenvalue appropriate to that mode correct to second order. This can be stated more precisely by considering the perturbation to equation (10) due to a small change in v and v^+.

$$\omega^2 \, \delta I_0 = (P_x^2 - A_x^2)\delta I_1 + \delta I_2 \tag{11}$$

where the perturbed energy integrals are given by:

$$\delta I_0 = \int \rho \delta(v v^+)\, dz; \quad \delta I_1 = \int \mu_R \delta(v v^+)\, dz; \quad \delta I_2 = \int \mu_R \delta(v' v^{+\prime})\, dz .$$

Making use of equation (11) the new eigenvalues correct to second order may be calculated.

$$(\omega + \delta\omega)^2 [I_0 + \delta I_0] = [(P_x + \delta P_x)^2 - (A_x + \delta A_x)^2]\cdot[I_1 + \delta I_1] + [I_2 + \delta I_2]. \tag{12}$$

Using equations (10) and (11) and neglecting second order in small quantities equation (12) becomes:

$$\omega \delta\omega I_0 = (P_x \delta P_x - A_x \delta A_x) I_1 . \tag{13}$$

and using $c = \omega/P_x$ for phase velocity, $U = \delta\omega/\delta P_x$ for group velocity, we can rewrite equation (13) in the following form:

$$U = \left[1 - \frac{A_x \delta A_x}{P_x \delta P_x}\right]\frac{I_1}{c I_0} . \tag{14}$$

At this point Rayleigh's principle may again be invoked and the elastic eigenvectors may be used in the calculation of the energy integrals.

In order to estimate the perturbation in $A_x(\delta A_x)$ due to a frequency perturbation, we use equation (3) and neglect the term containing $\delta Q_L/\delta\omega$. This is correct to at least second order in Q_L^{-1} since Q_L is a slowly varying function of frequency and the term has a coefficient of Q_L^{-2}. (It can, in fact, be estimated using a difference scheme since $Q_L(\omega)$ is known from the eigenvalues.)

With this approximation equation (14) becomes

$$U = \left[\frac{2}{1+\sqrt{(1+Q_L^{-2})}}\right]\frac{I_1}{cI_0} \tag{15}$$

which reduces to the usual elastic expression as $Q_L \to \infty$ and $v^+ \to v$. This expression, which is an approximation correct to at least second order in the loss, is thought to be preferable to numerical differentiation of the phase dispersion curve.

In order to calculate the effect on Q_L due to a small change in Q_S we must first find an expression for μ_R in terms of v_S and Q_S. This can be done by assuming a solution of equation (1) of the form

$$u = u_0 \exp\left(-i(\mathbf{K}.\mathbf{X}-\omega t)\right) \tag{16}$$

where $\mathbf{K} = \mathbf{P}-i\mathbf{A}$ (Borcherdt 1973). Substituting this into equation (1), and defining the shear velocity v_s as that of homogeneous waves ($\mathbf{P}$ parallel to $\mathbf{A}$) we can write:

$$\mu_R = \rho\frac{v_s^2}{2}\left[\frac{1+\sqrt{(1+Q_S^{-2})}}{1+Q_S^{-2}}\right]. \tag{17}$$

By substituting equation (17) into I_1 and I_2 we are able to explicitly calculate the change in the Love wave quality factor δQ_L due to a change δQ_S in the energy integrals. We can write the entire perturbed Rayleigh quotient at constant frequency as:

$$\omega^2[I_0+\delta I_0] = \{(P_x+\delta P_x)^2-(A_x+\delta A_x)^2\}.[I_1+\delta I_1+\delta_{QS}I_1]$$
$$+[I_2+\delta I_2+\delta_{QS}I_2] \tag{18}$$

where we have defined

$$\delta_{QS}I_1 = \int\rho\frac{v_s^2}{2}vv^+\delta\left[\frac{1+\sqrt{(1+Q_S^{-2})}}{1+Q_S^{-2}}\right]dz$$
$$\left.\begin{array}{c}\\\\\end{array}\right\} \tag{19}$$
$$\delta_{QS}I_2 = \int\rho\frac{v_s^2}{2}v'v^{+\prime}\delta\left[\frac{1+\sqrt{(1+Q_S^{-2})}}{1+Q_S^{-2}}\right]dz.$$

Using equations (10) and (11) and neglecting second-order terms in small quantities we can reduce equation (18) to:

$$0 = 2[P_x\delta P_x-A_x\delta A_x]I_1+[P_x^2-A_x^2]\delta_{QS}I_1+\delta_{QS}I_2. \tag{20}$$

Writing equation (3) as

$$A_x = P_x f(Q_L); f(Q_L) = \left[\frac{-1+\sqrt{(1+Q_L^{-2})}}{1+\sqrt{(1+Q_L^{-2})}}\right]^{1/2} \tag{21}$$

we can express the perturbation in A_x due to a change in Q_L:

$$\delta A_x = \delta P_x f(Q_L)+P_x\delta f(Q_L). \tag{22}$$

Neglecting the first term since it is at least second order in the loss we then have from equation (20):

$$\delta f(Q_L) = \frac{\delta A_x}{P_x} = \frac{1}{2P_xA_xI_1}[(P_x^2-A_x^2)\delta_{QS}I_1+\delta_{QS}I_2]. \tag{23}$$

and to the same order we have from equation (3)

$$\delta Q_L \approx -2 Q_L{}^2 \delta f(Q_L). \tag{24}$$

This formulation then allows estimates to be made on the change in the Love-wave quality factor or attenuation factor due to a small change in the shear quality factor. Further perturbations involving c_s and ρ can be made along similar lines (Harkrider 1968).

The extension to Rayleigh waves will, of course, be more tedious since equation (9) will now contain four integrals. In addition, equation (18) now must consider Q_p as well as Q_s. The situation is unpleasant though tractable and the group velocity is presently being programmed by the author.

Acknowledgments

References

Borcherdt, R., 1973. Energy and plane waves in linear viscoelastic media, *J. geophys. Res.*, **73**, 2442-2453

Borcherdt, R., 1971. *Inhomogenous body and surface waves in a generalized viscoelastic half-space*, PhD thesis, 308 pp., University of California, Berkeley.

Harkrider, D., 1968. The perturbation of Love wave spectra, *Bull seism Soc. Am.*, **58**, 861-880.

Jeffreys, H., 1961. Small corrections in the theory of surface waves, *Geophys. J. R. astr. Soc.*, **6**, 227-229.

Jeffreys, H., 1959. *The Earth*, 4th edition, University Press, Cambridge.

Kolsky, H., 1963. *Stress waves in solids*, Dover Publications Inc., New York.

Meissner, E., 1926. *Proc. 2nd Congr. Appl. Math., Zürich*, 3-11.

Moisewitsch, B. L., 1966. *Variational principles*, p. 20, Interscience Publishers, London.

Morse, P. M. & Feshbach, H., 1953. *Methods of theoretical Physics*, p. 298, McGraw-Hill, New York.

Silva, W., 1976. Body waves in a layered anelastic solid, *Bull. seism. Soc. Am.*, submitted.

Appendix

In order to estimate the error introduced by the formulation presented in this paper we shall consider a plane shear wave propagating along the x direction in a Voigt solid (Kolsky 1963).

The equation of motion can be written

$$\mu \frac{\partial^2 w}{\partial x^2} + \mu' \frac{\partial^2 \dot{w}}{\partial x^2} = \rho \ddot{w} \tag{1}$$

with the solution.

$$w = \exp(-Ax)\cos(\omega t - Px). \tag{2}$$

We may define the quality factor for this system as:

$$Q^{-1} = \frac{\mu'\omega}{\mu}.$$

(3)

Substituting equations (3) and (2) into (1) we arrive at:

$$P^2 - A^2 = \frac{\omega^2 \rho}{\mu(1 + Q^{-2})}.$$

(4)

On the other hand, if we had applied the Lagrangian formulation presented in this paper the results would have been:

$$P^2 - A^2 = \omega^2 \frac{\rho}{\mu}$$

(5)

which is correct to second order in the loss.

APPENDIX 3

DEVELOPMENT OF ENERGY INTEGRALS AND GROUP
VELOCITY FORMULATION FOR RAYLEIGH WAVES

Applying the formulation presented in Appendix 2 to Rayleigh waves and using elastic eigenvectors, the energy equation becomes

$$\omega^2 I_0 = \left(P_x^2 - \beta_k^2 \right) I_1 + 2 P_x I_2 + I_3 \quad ;$$

where

$$I_0 = \int \rho \left(\left| \frac{u_1}{w_0} \right|^2 + \left| \frac{u_3}{w_0} \right|^2 \right) dz$$

$$I_1 = \int \left[(\lambda_R + 2\mu_R) \left| \frac{u_1}{w_0} \right|^2 + \mu_R \left| \frac{u_3}{w_0} \right|^2 \right] dz$$

$$I_2 = R_e \left\{ \int \int \left[\lambda_R \left(\frac{u_1}{w_0} \right) \left(\frac{u_{3,3}}{w_0} \right)^+ + \mu_R \left(\frac{u_3}{w_0} \right) \left(\frac{u_{1,3}}{w_0} \right)^* \right] dz \right\} \sin \phi$$

$$I_3 = \int \left[(\lambda_R + 2\mu_R) \left| \frac{u_{3,3}}{w_0} \right|^2 + \mu_R \left| \frac{u_{1,3}}{w_0} \right|^2 \right] dz$$

with $\frac{U_1}{W_0}$ and $\frac{U_3}{W_0}$ the horizontal and vertical particle displacements normalized to the vertical surface displacement. The Lame parameter μ_R is defined in Appendix 2 with λ_R similarly derived and ϕ is the

phase difference between the vertical and horizontal attenuated displacements.

Performing the appropriate perturbations to obtain the group velocity the Rayleigh wave equation analogous to eq. (13) of Appendix 2 becomes

$$\frac{\omega\,\delta\omega}{P_x\,\delta P_x}\,I_o = \left(1 - \frac{A_x\,\delta A_x}{P_1\,\delta P_1}\right)I_1 + \frac{I_2}{P_x}\,.$$

The group velocity is then

$$U = \left(\frac{2}{1 + \sqrt{1 + Q_R^{-2}}}\,I_1 + \frac{I_2}{P_x}\right)(c\,I_o)^{-1}$$

Since the elastic eigenfunctions are used in the energy integrals the integrations can, in principle, be done analytically. However, due to the tedious algebra required it was decided to do the layer integrations numerically while doing only the half-space contribution analytically. The integration method adopted was that of Gauss-Legendre quadrature. The scheme uses the two point computation applied to successive points within each layer. Estimates of the accuracy are routinely obtained by checking the balance of the elastic energy equation. Typical figures are 4-6 function evaluations in a 10-20 km thick layer to achieve 10^{-2} percent accuracy. Liquid layers are included by using the liquid layer matrix D_m

(Chapter 1, Section 2) where appropriate and by setting $\bar{\mu} = 0$ in the energy integrals.

APPENDIX 4

ANALYSIS OF INVERSION DERIVATIVES

The purpose of the following development is to demonstrate, analytically, the relationships (magnitude and sign) which must exist between the inversion derivatives. The relationships follow from the complex surface wave velocity being an analytic function of the layer complex velocity.

Let

$$C = C_0 + \frac{iC_0}{2Q_L} , \quad V = V_0 + \frac{iV_0}{2Q_s} \tag{A1}$$

where C is the complex surface wave phase velocity and V is the complex shear wave velocity and both have an associated quality factor. The above expressions are actually low-loss approximations and are used for ease of computation.

At this point the Cauchy-Reimann conditions are applied and the partials $\partial\left(\frac{C_0}{2Q_L}\right)$, $\partial\left(\frac{V_0}{2Q_s}\right)$ are taken with respect to the quality factor only (velocity held constant). The first condition yields:

$$\frac{\partial C_0}{\partial V_0} = \frac{\partial\left(\frac{C_0}{2Q_L}\right)}{\partial\left(\frac{V_0}{2Q_s}\right)} = \frac{C_0}{V_0} \; \frac{Q_s^2}{Q_L^2} \; \frac{\partial Q_L}{\partial Q_s} \tag{A2}$$

Applying the second condition yields:

$$\frac{\partial \left(\frac{c_0}{2Q_L}\right)}{\partial V_0} = - \frac{\partial c_0}{\partial \left(\frac{V_0}{2Q_s}\right)}$$

resulting in

$$\frac{\partial Q_L}{\partial V_0} = - \frac{4 \, Q_L^2 \, Q_s^2}{c_0 \, V_0} \, \frac{\partial c_0}{\partial Q_s} \qquad (A3)$$

These relations are most useful in assessing the relative magnitudes of the elements of the Jacobian. Rewriting the Taylor approximation (eq. 3) with normalized parameters we have in matrix form:

$$
\begin{bmatrix} \frac{\delta Q_L}{Q_L} \\[2ex] \frac{\delta C_L}{C_L} \end{bmatrix}
=
\begin{bmatrix} \frac{Q_s}{Q_L} \frac{\partial Q_L}{\partial Q_s} & \frac{V_s}{Q_L} \frac{\partial Q_L}{\partial V_s} \\[2ex] \frac{Q_s}{C_L} \frac{\partial C_L}{\partial Q_s} & \frac{V_s}{C_L} \frac{\partial C_L}{\partial V_s} \end{bmatrix}
\begin{bmatrix} \frac{\delta Q_s}{Q_s} \\[2ex] \frac{\delta V_s}{V_s} \end{bmatrix}
\qquad (A4)
$$

Then, reducing the Jacobian to two derivatives using equations (A2) and (A3) results in the system:

$$
\begin{bmatrix} \frac{\delta Q_L}{Q_L} \\[2ex] \frac{\delta C_L}{C_L} \end{bmatrix}
=
\begin{bmatrix} \frac{Q_L}{Q_s} \frac{V_s}{C_L} \frac{\partial C_L}{\partial V_s} & \frac{V_s}{Q_L} \frac{\partial Q_L}{V_s} \\[2ex] - \frac{1}{4Q_L \, Q_s} \frac{V_s}{Q_L} \frac{\partial Q_L}{\partial V_s} & \frac{V_s}{C_L} \frac{\partial C_L}{V_s} \end{bmatrix}
\begin{bmatrix} \frac{\delta Q_s}{Q_s} \\[2ex] \frac{\delta V_s}{V_s} \end{bmatrix}
\qquad (A5)
$$

For the model in Table 1 and the corresponding partial derivatives (Figures 2-5) the elements 1,1, 1,2, and 2,2 of the coefficient matrix in equation (A5) are all of the same order of magnitude while element 2,1, due to the $Q_L^{-1} Q_S^{-1}$ factor, is several orders smaller. These results imply that element 1,2 is significant compared to elements 1,1 and 2,2 and cannot be neglected.

Note that equations (A2) and (A3) can be used as a check on the accuracy of numerical derivatives. It can also be easily shown that writing the Taylor series approximation for Q^{-1} in lieu of Q leads to precisely the same matrix equation as for Q (eq. A5). In other words, inverting for Q or inverse Q are formally equivalent.

APPENDIX 5

PHASE SMOOTHING

Consider the calculation of phase velocity using
the following formula (Toksöz and Ben-Menahem, 1963).

$$C(T) = \frac{\Delta x}{t(2) - t(1) + T(\Delta \phi + N)}$$

Where Δx is the path between stations and $t(1)$, $t(2)$
are times of subsequent Fourier windows. This required
the calculation of the phase difference ($\Delta \phi$) between
the two spectra. Since noise, including multiple
arrivals, is generally present $\Delta \phi$ may be poorly
behaved. It therefore, becomes necessary to devise
some suitable smoothing procedure. The idea is to
use some method which is easily controllable so the
smoothing is not excessive and useful information
lost. The method used here is that of simply fitting $\Delta \phi$
with a sine series and then retaining only those
coefficients which have the largest magnitudes. The
coefficients are then modified by the Lancsoz sigma
factors to reduce the associated Gibbs phenomena.

REFERENCES

Toksöz, M. and Ben-Menaham, A., 1963. Velocities of mantle Love and Rayleigh waves over multiple paths, Bull. Seism. Soc. Am. 53, 741-764.